Faculdade de Engenharia da Universidade do Porto

U.PORTO
FEUP **FACULDADE DE ENGENHARIA**
UNIVERSIDADE DO PORTO

Synthesis and characterization of PLLA microparticles loaded chitosan hydrogel to promote gingival repair
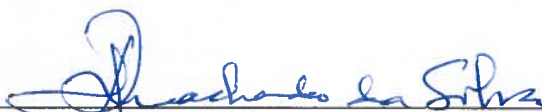
Marlene Ribeiro Rajão

junho de 2018

A Dissertação intitulada

"Synthesis and Characterization of PLLA Microparticles Loaded Chitosan Hydrogel to Promote Gingival Repair"

foi aprovada em provas realizadas em 28-06-2018

o júri

Presidente Prof. Doutor José Alberto Peixoto Machado da Silva
Professor Associado do Departamento de Engenharia Eletrotécnica e de Computadores da FEUP - U.Porto

Prof. Doutor José Domingos da Silva Santos
Professor Associado do Departamento de Engenharia Metalúrgica e de Materiais da FEUP - Uporto

Prof.ª Doutora Ana Colette Pereira de Castro Osório Maurício
Professora Associada c/Agregação da Instituto de Ciências Biomédicas Abel Salazar da U. Porto

O autor declara que a presente dissertação (ou relatório de projeto) é da sua exclusiva autoria e foi escrita sem qualquer apoio externo não explicitamente autorizado. Os resultados, ideias, parágrafos, ou outros extratos tomados de ou inspirados em trabalhos de outros autores, e demais referências bibliográficas usadas, são corretamente citados.

Autor – Marlene Ribeiro Rajão

Faculdade de Engenharia da Universidade do Porto

Faculdade de Engenharia da Universidade do Porto

U.PORTO

FEUP **FACULDADE DE ENGENHARIA**
UNIVERSIDADE DO PORTO

Synthesis and characterization of PLLA microparticles loaded chitosan hydrogel to promote gingival repair

Marlene Ribeiro Rajão

Versão 1

Dissertação realizada no âmbito do
Mestrado em Engenharia Biomédica

Orientador:
Professor Doutor José Domingos Santos

Coorientadores:
Doutor Vitor Sencadas
Professora Doutora Maria Ascenção Lopes

Junho 2018

Resumo

Atualmente, os produtos comercializados no mercado de aplicação oral para defeitos de recessão gengival são na sua maioria compostos por clorexidina e ácido hialurónico. Estes componentes apenas possuem propriedades anti-inflamatórias, antisséticas e anti-hemorrágicas, que somente aliviam os sintomas momentaneamente, pois são incapazes de tratar o problema a partir da sua causa: a perda de tecido gengival. Portanto, existe a necessidade de criar soluções alternativas que possam reparar a gengiva.

Quitosano é um polímero biocompatível, que está comprovado em diversos estudos que promove a regeneração de tecidos periodontais. Este pode ser sintetizado num hidrogel e combinado com outros componentes para criar hidrogéis à base de quitosano. Este material possui diversas propriedades vantajosas para promover a reparação de tecido gengival. Uma das quais é o fato de ser muco-adesivo, e assim, aloja-se na mucosa oral dos defeitos gengivais, e potencia a sua reparação até se degradar totalmente. A sua sensibilidade à temperatura é outra vantagem, já que só transita para um estado gelificado a temperaturas fisiológicas, próximo de 37ºC. Além disso, estes hidrogéis têm vindo a ser estudados como mecanismos de transporte para medicamentos, células e partículas poliméricas, que os auxiliam na reparação das lesões. Mais ainda, em meios ácidos, característicos de regiões lesadas, hidrogéis á base de quitosano facilitam a libertação dos componentes reparadores que transportam.

Ácido Poli Láctico (PLA) é um polímero aprovado pela Food and Drug Administration (FDA), continuamente usado em diversas aplicações biomédicas. A sua taxa de degradação lenta pode aprimorar a reparação progressiva do defeito gengival, por estimular o crescimento de fibroblastos gengivais humanos.

Portanto, fazendo a junção destes dois materiais, esta dissertação teve por objetivo a sintetização de um hidrogel á base de quitosano com micropartículas (MPs) de PLLA no seu interior, para promover a reparação gengival. Além disso, algumas propriedades das micropartículas PLLA assim como do hidrogel contendo PLLA foram caracterizadas. E ainda, testes *in vitro* da cultura de fibroblastos gengivais humanos com micropartículas PLLA foram efetuados.

Os resultados de SEM das micropartículas PLLA detetaram contaminação com tântalo. Portanto, o polímero foi purificado, retirando todos as meações de tântalo com sucesso. Ademais, as MPs apresentaram um tamanho de diâmetro uniforme de valor médio: $(1.718 \pm 1.89)\,\mu m$. A análise em FTIR concluiu que a sua cristalinidade é principalmente amorfa, contendo alguns cristais da forma α no seu interior. Em seguida, a análise DSC também verificou o estado principalmente amorfo das micropartículas PLLA. Por último, relativamente

aos resultados de TGA, a energia de ativação aparente foi obtida como sendo $197\ kJ/mol$. Este valor indica a energia que a microestrutura das micropartículas requer para desencadear o seu processo de degradação.

Posteriormente, amostras da matriz do hidrogel à base de quitosano – 0% MPs -, assim como com MPs no seu interior foram sintetizadas com sucesso. Os hidrogéis apresentaram elevada fluidez e podiam ser visivelmente distinguidos pela transparência das amostras 0% MPs e pela cor branca opaca das amostras com MPs no seu interior.

Após sintetização de amostras com diferentes concentrações de MPs, por SEM, a amostra com 1.5% (p/v) de MPs foi escolhida para ser posteriormente comparada com a amostra 0% MPs. A análise FTIR de ambas as amostras, confirmou a presença de grupos funcionais entre os agentes reticuladores e o quitosano. Os estudos de inchaço e degradação concluíram que na fase do inchaço, ambas as amostras – 0% MPs e 1.5% MPs - expandiram até ao seu volume máximo, tanto no teste hidrolítico como no enzimático. No teste hidrolítico da fase de degradação a pH 5, ambas as amostras mantiveram o seu volume máximo até ao término da experiência no dia 11. Contrariamente, no teste enzimático no mesmo valor de pH, as amostras perderam peso progressivamente até ao dia 11. Já a valores de pH de 7.3, ambas as amostras, tanto no teste hidrolítico ou enzimático, progressivamente degradaram, sendo que a maior taxa de perda de peso foi verificada no teste enzimático. Por último, testes reológicos concluíram que o material é um fluido pseudo-plástico não-Newtoniano. Além disso, demonstrou que as amostras 0% apresentam módulo elástico mais elevado, comparado às amostras 1.5% MPs. Ainda, a temperatura instantânea a que o gel transita de um estado líquido para um estado gelificado foi obtida como sendo aproximadamente aos 43°C.

Os testes *in vitro* da cultura de fibroblastos gengivais humanos com MPs PLLA foi descrita por diversos testes. O teste de MTT concluiu que as MPs são biocompatíveis com as células humanas. Relativamente aos resultados do teste de colagénio, foi observado um aumento da secreção de fibras de colagénio com o aumento da concentração de MPs. Por fim, o teste morfológico com os corantes fluorescentes DAPI e AlexaFluor, indicou que as células desenvolveram um maior rearranjo entre elas nas regiões ondes as MPs se aglomeraram.

Abstract

Nowadays, products sold on the market of oral application for gingival recession defects are mainly constituted of chlorohexidine and hyaluronan, which only possess anti-inflammatory, anti-septic and anti-haemorrhagic properties. These treatments solely alleviate the symptoms momently, since they are uncapable to treat the problem from its cause: the loss of gingival tissue. Therefore, there is a need for alternative solutions to repair the gingiva.

Chitosan is a biocompatible polymer, which has been stated to promote regeneration of periodontal tissues. It can be synthetized into a hydrogel and merged with other components to create chitosan-based hydrogels. This material possesses diverse advantageous properties to promote gingival tissue repair. One of which is its mucoadhesive property, that allows it to lodge in the oral mucosa of gingival defects, promoting its repair until its complete degradation. Its thermo-sensibility is another advantage, since it only transits to a gel state at physiological temperatures. Furthermore, these hydrogels have been studied as transportation mechanisms for drugs, cells and polymeric particles to assist in the repair of the lesions. Another feature is that in acidic mediums, characteristic of damaged regions, the chitosan-based hydrogel facilitates the release of the repairing promoting components that it is carrying.

Poly (Lactic Acid) (PLA) is an Food and Drug Administration (FDA) approved polymer, which is continuously used in diverse biomedical applications. Its slow degradation rate could enhance a progressive repair of a gingival defect, by stimulating human gingival fibroblast's growth.

Therefore, this dissertation aimed to synthetize a chitosan-based hydrogel loaded with neat Poly (L-Lactic Acid) (PLLA) microparticles for gingival repair. Some of the properties of the PLLA microparticles as well as the loaded hydrogel are characterized. Additionally, *in vitro* tests involving the culture of human gingival fibroblasts with PLLA microparticles were performed.

The SEM results of PLLA microparticles, detected contamination with tantalum. Henceforth, the polymer was purified, which successfully removed all the tantalum moieties. Moreover, the MPs presented an even diameter size of mean value: $(1.718 \pm 1.89)\mu m$. The FTIR analysis, concluded its primarily amorphous crystallinity, containing some α-form crystals within its structure. Additionally, DSC analysis also verified the mainly amorphous state of the PLLA microparticles. Relatively to the TGA results, the apparent activation energy was $197\ kJ/mol$. This value indicates the required energy that the microparticles need to absorb within their microstructure to trigger their degradation.

Afterwards, samples of chitosan-based hydrogel matrix – 0% MPs sample - and with PLLA MPs loaded in its interior were successfully synthetized. The hydrogels presented high fluidity and could be visually distinguished by the transparency of the 0% MPs samples and the opaque white colour of the MPs loaded hydrogels.

Thereafter, with SEM analysis, the sample with 1.5% (w/v) of loaded PLLA MPs was chosen to be further compared with the 0% MPs sample. FTIR analysis of both samples confirmed the presence of the functional groups between the reticulating agents and chitosan. The following swelling and degradation *in vitro* studies concluded that in the swelling phase, both samples swelled until its maximum, regardless of the pH value at which were immersed and the performed test - hydrolytic or enzymatic. In the degradation phase, at pH values of 5 -, in the hydrolytic test, the both samples maintained the maximum swelling until the termination of the study at day 11. Contrarily, in these pH values, in the enzymatic test, the samples significantly lost weight until complete degradation of the chitosan-based hydrogel matrix is verified at day 11. At pH values of 7.3, both samples in hydrolytic or enzymatic tests, progressively degraded, being the degradation rate of the enzymatic test higher. Lastly, rheological tests concluded that the material is a non-Newtonian pseudo-plastic fluid. Moreover, it demonstrated that the 0% MPs samples presented higher storage modulus, when compared to 1.5% MPs samples. Additionally, the instantaneous temperature at which both hydrogel samples transit from liquid to a gel like state was about 43ºC.

The PLLA microparticles trials *in vitro* with human gingival fibroblasts were reported. The MTT assay concluded that the MPs are biocompatible with the human cells. Concerning the collagen assay results, it was denoted that the augment of MPs concentration, accelerates the secretion of collagen fibres. At last, the morphology test with DAPI and Alexa Fluor fluorescent colourants, indicated that the cells develop inter rearrangement, which is higher in the spots that the microparticles agglomerate.

Agradecimentos

Em primeiro lugar, agradeço ao meu orientador, Professor José Domingos Santos, assim como aos meus coorientadores, Professora Maria Ascensão Lopes e Vitor Sencadas, por me terem guiado e auxiliado nas tarefas mais cruciais deste projeto, de modo a conseguir concretizá-las com sucesso.

Do mesmo modo, agradeço à Professora Maria Helena Fernandes e à Liliana Grenho por me terem acolhido tão bem durante os meses de trabalho no departamento de Farmacologia da Faculdade de Medicina Dentária. De seguida, um grande obrigado ao Professor Paulo Costa, pela sua disponibilidade em me auxiliar nos testes de caracterização efetuados na Faculdade de Farmácia.

Agradeço também às minhas colegas de laboratório, que de uma forma ou outra, ajudaram-me a manter sempre um espírito positivo e acompanharam-me da melhor forma durante todo este processo.

Por último, um obrigado muito especial á minha família, sobretudo os meus pais, assim como ao meu namorado e amigos mais chegados, pois a força que me forneceram constantemente foi uma âncora para conseguir alcançar o tão desejado diploma.

A todos o meu mais sincero obrigada!

Contents

x

List of Figures

List of Tables

Abbreviations, Acronyms and Symbols

Au – Gold

BT – Bilaminar Technique

C – Carbon

CO_2 – Carbon Dioxide

CEJ – Cementoenamel Junction

CPRT – Collagen Membrane

CTG – Connective Tissue Graft

DAPI – 4,6– diamidino–2-phenylindole

DLA – D-Lactide Acid

DMSO - Dimethylsulphoxide

DSC – Differential Scanning Calorimetry

DTG – Differential Degradation Curves of Thermogravimetric Analysis Graph

ECM – Extracellular Matrix

EDS – Energy Dispersive X-Ray Spectroscopy

FBS – Fetal Bovine Serum

FTIR – Fourier Transform Infrared Spectroscopy

FTIR-ATR - Fourier Transform Infrared Spectroscopy-Attenuated Total Reflectance

G' – Storage Modulus

G'' – Loss Modulus

GPTMS – (3-Glycedyloxypropryl) thimethoxysilane

GTR – Guided Tissue Regeneration

HEPES – (4-(2-hydroxyethyl)-1-(piperazineethanesulfonic acid)

hGFs – Human Gingival Fibroblasts

L_c – Crystalline Thickness

LLA – L-Lactide Acid

MEM – Minimum Essential Medium

MLA – Meso-Lactide Acid

MTT – 3-(4,5-di-methylthianol-2-yl)-2,5-diphenyl tetrazolium bromide

M_w - Molecular Weight

NMP – N-Methyl-2-Pyrrolidone

MPs - Microparticles

O – Oxygen

PBS – Phosphate Buffer Saline

Pd – Palladium

PDLA – Poly (D-Lactic Acid)

PLA – Poly - Lactic Acid

PLLA – Poly (L - Lactide Acid)

SCTG – Subepithelial Connective Tissue Graft

SEM – Scanning Electron Microscopy

Ta – Tantalum

T_c – Cold - Crystallization Transition Temperature

TCPS - Tissue Culture Polystyrene

TE – Tissue Engineering

T_g - Glass Transition Temperature

TGA – Thermogravimetric Analysis

T_m – Melt Transition Temperature

UV – Ultraviolet

α-MEM – Alpha Modified Minimum Essential Medium

β-GP - β-Glycerophosphate disodium salt hydrate

wt % - Weigh-Weight Percentage

X_c – Crystallinity

ΔH_m – Melting Enthalpy

ΔT – Cooling Process

Chapter 1

Introduction

1.1- Context

Worldwide, more than 60% of individuals suffer from gingival recession, which is mainly characterized by the disintegration of gingival soft tissue upon its inflammation. The immune system tries to tackle the bacteria lodged in the inflamed tissue, and to that means, it destroys the damaged tissue as well. This condition is designated as gingivitis and is the mildest one of the array of periodontal diseases, since it can be reversible. If left untreated, the immune system is unable to eradicate the bacteria and the disease developments to a more severe stage. At this phase, the inflammation progressively breaks down the periodontal support structure, that englobes connective tissue, periodontal ligaments and alveolar bone. Henceforth, this stage, designated as periodontitis, is irreversible, since the organism is unable to regenerate lost supportive tissues. Even more, without a foundation to anchor, teeth lose their stability and ultimately decay. In the European Countries, older population in the range of 65 to 74 years old have about a 20% to 50% probability to lose all their natural teeth. [1] [2] Thus, treating the condition at the first stage – gingivitis - is essential to inhibit periodontitis disease progression and regenerate the lost soft tissues.

The most standard held treatments performed nowadays for gingival recession involve surgical procedures. The main approach includes a portion of healthy tissue to be harvested from diverse oral sites. These include advanced gingival flaps from the healthy region adjacent to the damaged one, as well as grafts of palatal connective and epithelial tissues, or even free gingival healthy tissue. The excerpts are then sutured in the gingival defect area and normally, the results lead to an optimal repair of the treated legion. However, it has the disadvantage of a second surgical site being held on the own patient or in a donor, in case of allografts. Thus, this treatment increases the patient's and donor's discomfort. Moreover, consequent complications during recovery can occur, since the harvested site also needs to heal itself. [1] Therefore, an unnatural solution is required to diminish those chances.

Biocompatible polymers have been widely studied and tested for bone and cartilage regeneration in the orthopaedic area as well as in the periodontal area. However, just a small portion refers to polymers promoting alveolar processes repair, and an even smaller one develops solutions for only gingiva repair or regeneration. For tissue regeneration applications,

a polymer must be biocompatible, serializable and its degraded products cannot cause toxicity in the organism. Biodegradable polymers overcame the nonbiodegradable ones, for the fact that after the prior's implantation, a second surgical procedure is not required to remove the material. [3], [4], [5] My personal research concluded that Poly (Lactic Acid) was one of the most promising *in vitro* studied polymers that potentially could promote a significant human gingival fibroblast's proliferation in further *in vivo* experiments.

Poly (Lactic Acid) (PLA) has been widely applied in the biomedical field since the 1960's as sutures and implants. As reported, this material promotes human gingival fibroblast's proliferation *in vitro*. Recently, it was revealed that its L-form isomer – Poly (L-Lactide Acid) (PLLA) - with high molecular weight overcomes the excessively fast degradation kinetics of PLA. [6], [7], [8] Therefore, slowly degradable PLLA microparticles could enhance a progressive repair of the damaged region, by stimulating human gingival fibroblast's growth and subsequent tissue formation.

Hydrogels are biopolymers that can expand with water without disintegrating its structure. They can be initially synthetized from natural as well as synthetic sources. Then, they can be moulded into 3-dimensional scaffolds capable of mimicking tissues. However, since each gingival defect is unique by size and depth, the hydrogel's structure must differ for all. So, a room temperature gel able to solidify in *in vivo* temperatures, is a feasible formula to be developed for the treatment of all gingival depressions. Subsequently, with time, the motionless framework can stimulate adhesion and proliferation of cells in its interior. After some time, as it disintegrates, the proliferated cells in its bulk are now able to attach in the surrounding healthy tissues. [9]

In order to facilitate a hydrogel administration in gingival defects without surgery, a fairly long-standing approach can be employed. An injectable system allows a clean and easy administration of the developed composite only to the target area, without affecting the surrounding healthy tissues. This method is very comfortable for the patient and does not require the extra care that surgical scars would. [10]

Bearing in mind that few biomaterials possess all the characteristics to perform ideally on their one, the development of a composite to synergize the beneficial properties of multiple materials is required. [11] Henceforth, the objective of this work is to create a multifunctional injectable chitosan-based hydrogel loaded with neat Poly (L-Lactide Acid) microparticles. This manuscript mentions the current treatments held for gingival repair. Moreover, it englobes the study of the objective's basic concepts, as well as the synthetization and characterization of the composite and *in vitro* study of human gingival fibroblasts cultured with PLLA microparticles.

Chapter 2

State of the Art

2.1 – Literature Review

The study of synthetic materials for the repair of oral soft tissues has been conducted since two or three decades ago, to overcome the complications associated with the treatments carried out in that era. Some of those therapies are still performed nowadays, being autologous tissue harvest to be grafted in the defected region of the gingiva, the most common. However, this procedure implies the healing of the harvested region as well, which can decrease its efficiency in long term.

To overcome those disadvantages, hydrogels synthetized from chitosan have been recently studied for gingival repair and regeneration. Boynueğri *et al.* [12], reported its biocompatibility *in vivo* and its ability to promote primal tissue formation in periodontal intraosseous defects. Ji *et al.* [13], Pakzad *et al.* [14] and Miranda *et al.* [15] and further authors performed tests *in vitro* that came to validate the results stated by Boynueğri.

The mucoadhesive properties of the hydrogel were also evaluated, since it is pertinent to analyse its facility to adhere to the mucosal defected area along its progressive degradation. *In vivo* studies conducted by Monika Bansal *et al.* [16] showed excellent muco-adhesion of the chitosan hydrogel to the oral mucosa of periodontal pockets. Upon the next year, Gawish [17] also reported the bio-adhesion of a chitosan-based auto gel in the oral mucosa of chronic periodontitis lesions.

Hydrogels physiologically thermosensitive, only transform into a gel form at biological temperatures. This property is advantageous for a simple administration of the hydrogel in a fluid form into the periodontal pocket by injectable systems. Ruan *et al.* [18] reported the thermo-gelling temperature at 37ºC of a chitosan/β-GP, being liquid at lower temperatures. Previous studies also corroborate the results obtained by Ruan *et al.*. [13], [14], [16], [19]

Yu *et al.* [20] and Chang et al. [21] reported pH-sensitivity in some chitosan-based hydrogels loaded with drugs. At lower pH values – 5.5 to 6.5 –, which is usually detected in the lesion area, the drugs were most rapidly released and significantly decreased inflammation and promoted cell viability. Thus, this property is a great advantage, since it releases most rapidly drugs in the lesion area and at a slower rate as the lesion is progressively healed. Therefore,

these scaffolds are an excellent vehicle to deliver drugs, cells or microparticles into the defect area that potentialize the effect of the hydrogel alone. Most of the carried-out studies on this subject englobe loading drugs with anti-microbial, anti-biotic, anti-fungal or anti-inflammatory properties into the hydrogel to later be released in the lesion region. For instance, Mendes *et al.* [22] tested the release of miconazole – anti-fungal agent, whereas Bansal *et al.* [16], Pakzad *et al.* [14] and Ruan *et al.* [18] studied the hydrogel's ability to be a good vehicle for antibacterial drugs. Overall, the studies outcomes were promising, since the hydrogels could carry the drug and released it in the lesion area at effective concentrations to eliminate pathogenic bacteria during the defect's healing period.

In the most recent years, Shirosaki *et al* developed and optimized a promising chitosan-silicate hydrogel for periodontal lesions, due to its reported mucoadhesive, thermosensitive, and *in vitro* biocompatible and proliferation promoting properties. [23], [24], [25]

Commercially, there is a wide range of gingival gels, prescribed by the dental practitioners, that are mainly anti-inflammatory and anti-bacterial, such as the following: TePe®, Oddent®, Bexident®, Gengigel® and NBF Gel®. However, regeneration of the damaged tissue is not yet possible with these available products, since they are primarily composed by Chlorhexidine and/or Hyaluronan, which do not exhibit tissue regenerative properties. [26], [27], [28], [29], [30]

Thus, the base of this work is to synthetize a hydrogel with gingival tissue regenerative properties, combined with the anti-inflammatory and anti-bacterial actions as well. This is of extreme importance for patients suffering from chronic periodontitis with significant gingival tissue loss, which can lead to teeth decay. So, the developed product aims to minimize the continuous treatment product prescriptions, that only treat the subsequent symptoms of gingival tissue loss. Therefore, the developed strategy only requires a dose of regenerative product when the first symptoms of gingivitis emerge, to effectively repair the loss tissue, without further treatment.

Furthermore, synthetic Poly-Lactic Acid derived polymers had already been reported as biocompatible, as well as promotive of adhesion and viability of human gingival fibroblasts onto its membranes. This material is resorbable in the human body, without requiring a need for a second surgical intervention to be removed, which diminishes in this way, the chances of post treatment complications. Moreover, studies report that its repairing properties are similar to the conventional flaps surgically autografted from the patient's own healthy oral regions. Thus, its effect also decreases the patients discomfort during treatment, since only the lesioned site is manipulated during the procedure. [7],[31]

Additionally, since this material possesses a slow degradation rate, it is reported that it is stable up to 6 weeks after implementation on oral mucosa before any resorption commences. This membrane can be designed with pores and rough surface, which stimulate cell proliferation in its bulk, that will further progressively populate the healthy surrounding tissues during the membranes degradation. Complete membrane degradation is reported to be between 6 to 12 months, depending on its porosity and membrane thickness. [32], [33]

Some studies report asymptomatic swelling in some patients treated with a PLA based membrane, which is due to the inflammatory inducing properties of the material. However, it is intelligible that inflammation triggers regeneration, since the inflamed site promotes angiogenesis, which in return carry anti-inflammatory agents and nutrients in its blood stream that stimulate and assist new cell growth and tissue formation. [34]

Studies which report high root coverage percentage after the treatment of periodontal defects with a PLA based membrane is summed in Table 2.1.

Table 2.1 – Root coverage percentage at several months upon implementation of a Polylactic Acid – based membrane in gingival recession defects on humans.

Study (Author, (Year))	Membrane Material	Period after treatment (months)	Root Coverage (%)
Roccuzzo *et al.* (1996) [31]	Polylactic acid	6	82
Waterman *et al.* (1997) [32]	Polylactic acid	12	76
Trombelli *et al.* (1998) [35]	Polylactic acid	6	65
Matarasso *et al.* (1998) [36]	Polylactic acid	12 12	63 74
Muller *et al.* (2000) [33]	Polylactic acid	12	51
Amarante *et al.* (2000) [37]	Polylactic acid	6	56
Tatakis D. *et al.* (2000) [34]	Polylactic acid – based	6	80

Statistical analysis on the table's results on root coverage after 12 months, revealed an average of $(66 \pm 11.5)\%$. Thus, it can be supposed that the treatment of gingival defects with a PLA-based material is feasible and holds long-term positive treatment outcome.

Therefore, in this study, a new way of applying PLA-based biomaterials on gingival defects will be investigated. In order to improve its regenerative properties, the material is firstly synthetized into microparticles. Additionally, to decrease its inflammatory inducing properties, the microparticles will be loaded into a chitosan-based hydrogel, which is reported to neutralize the inflammatory action of PLA based materials. [6]

2.2- Basic Concepts

2.2.1 – Gingiva

The oral soft tissues englobe oral mucosa, tongue, soft palate, tonsillar area, uvula, lips and floor of mouth. Oral mucosa is composed by the following three areas: *Masticatory Mucosa*, *Specialized Mucosa*, and the *Mucous Membrane*. The first englobes the gingiva and the coverage of the palate, whereas the second consists in the dorsum of the tongue. The last hedges the remainder of the oral cavity. [1], [38]

This work focuses in an engineered hydrogel to repair gingiva, which is the part of oral mucosa that overlays the alveolar processes. The gingival tissue is the most important one in the orofacial region and the most challenging as well. [39]

2.2.1.1 – Gingiva's Anatomy

In anatomical terms, gingiva is divided into *marginal*, *attached* - Figure 2.1 - and *interdental* areas. [1]
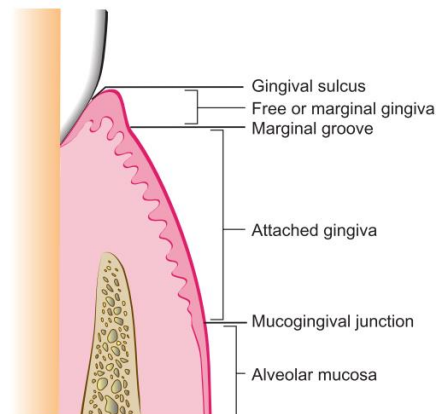
Figure 2.1 – Anatomical divisions of the gingiva [1]

As seen in Figure 2.1, the *marginal gingiva* surrounds the teeth like a wristlet and covers the gingival sulcus. This is an unattached soft tissue that presents a translucent pink colour, since it lacks fibres to connect it to the alveolar process. Therefore, it is a firm, but mobile tissue. Its normal width can vary in the range of 0,5 mm to 2,0 mm. This gingival section is delimited by the marginal grove, which separates it from the *attached gingiva*. [1], [39]

Relatively to the *attached gingiva*, it is the portion that shelters the teeth's roots and is tightly adherent to the underlying alveolar processes through fibres, which makes it appear stippled. Usually, its colour is opaque pink and can present some melanin pigmentation in certain areas. Moreover, this section of the gingiva is characterized by its higher firmness, dullness and resilience relatively to the *marginal* one. Its width is the distance between the bottom of the gingival sulcus and the mucogingival junction, which separates it from the alveolar mucosa. When healthy, the width of the *attached gingiva* differs in different areas of the mouth, ranging from 1.8 mm in the mandibula's first premolars to 4.5 mm in the incisor's maxilla region. [1], [39]

In relation to *interdental gingiva*, it is the section in which the gingival tissue occupies the space between adjacent teeth. This portion of the gingiva can present a pyramidal or concave shape, depending on various factors, such as the presence or absence of a contact point between the adjacent teeth. This factor moulds the *interdental gingiva* into a concave shape when the contact point is absent. In the case of its presence, the acquired shape depends on the distance between the contact point and the alveolar process higher point in the area. When the mentioned distance is high, the interdental gingiva shape tends to be pyramidal, since it has enough space to develop a pointed shape. Whereas a short distance moulds it into a concave

shape with the central portion formed by the attached gingiva. An additional factor which also influences the *interdental gingiva* profile is some absence of gingival tissue, caused by gingival recession. In this case, with the continuous loss of gingival tissue, the *interdental gingiva* progressively loses the central portion formed by the attached gingiva, acquiring a pyramidal shape, without a sharp central portion. [1]

2.2.1.2 – Gingiva's Histology

The gingiva is microscopically divided into the gingival epithelium and gingival connective tissue. [1] The first overlays the second in every gingival anatomical structure mentioned previously. The histological features are specific for each section. [39]

Gingival epithelium is defined as a continuous lining of stratified squamous tissue, being the keratinocyte, the main cell type. Additionally, the gingival epithelium includes Langerhans cells, Merkel cells and melanocytes. The priors are modified monocytes derived from the bone marrow and belong to the phagocyte system, whereas the second are tactile preceptors, since possess nerve endings. The last, as the name suggests, synthesizes melanin, conferring different colours to the gingiva. [1]

In morphological terms, the gingival epithelium is divided into three different areas: outer epithelium, sulcular epithelium and junctional epithelium, which overlay the marginal and attached gingiva, the sulcus and the cementoenamel junction – CEJ -, respectively. [39] Whereas microscopically, gingival epithelium is classified into the following tissues: keratinized, nonkeratinized and parakeratinized epithelia, being the latter two ones considered in an intermediate stage of keratinization. In Figure 2.2, nonkeratinized tissue is the least organized relatively to the remain, being its surface layer, the least defined as well. The keratinized tissue is the only one that possess a granular layer as well as a completely keratinized surface layer – horny layer – which is similar to that of the skin. [1]
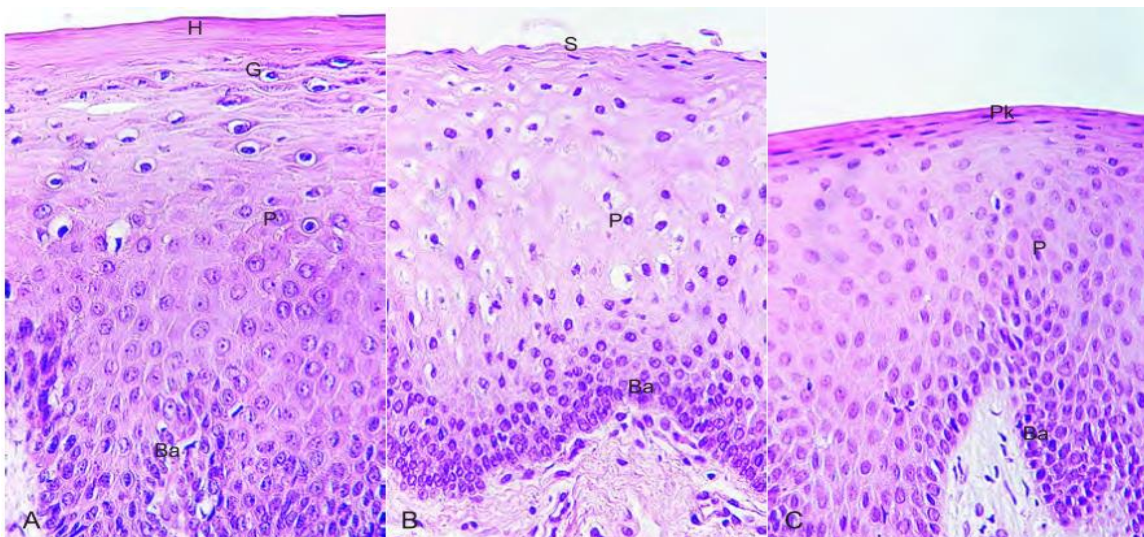
Figure 2.2 – Gingival epithelium in microscopical division. A) Keratinized tissue. B) Nonkeratinized tissue. C) Parakeratinized tissue. Horny layer (H). Granular layer (G) [1]

By coupling the classifications stated, the outer epithelium is primarily composed of keratinized and parakeratinized tissue, or it may exhibit a combination of both, whereas sulcular and junctional epithelium consist of nonkeratinized stratified squamous epithelium. Moreover, blending gingival anatomical structures with each respective histological tissue, it results that *attached gingiva* mainly consists of parakeratinized tissue, whereas *marginal gingiva* only consists of parakeratinized epithelium. Therefore, these tissues are slightly different from each other in a histological view, although both belong to the outer epithelium. Finally, the *interdental gingiva*, which is localized in the sulcular and junctional epithelium only consists of nonkeratinized tissue. [1], [39]

The gingival connective tissue or *lamina propria* is the underlying gingival section which is directly attached to the alveolar process. It consists of two layers: a *papillary area* and a *reticular layer*. The prior is subjacent to the epithelium and contains the papillary projections, whereas the latter is adjoined with the periosteum of the alveolar process. Microscopically, it is composed by about 60% of collagen fibres, 35% of matrix, 5% of gingival fibroblasts, vessels and nerves. Therefore, this tissue possesses a cellular and an extracellular compartment which contains fibres and ground substance. The latter fills the space between the fibres and cells, being highly concentrated with proteoglycans and glycoproteins, such as fibronectin and laminin. The fibronectin acts as a bond between the fibroblasts and the fibres, so that it helps in the mediation of cell adhesion and migration. Laminin attaches the lamina to the epithelial cells. The predominant cell in the gingival connective tissue is the gingival fibroblast. These cells are primordial from the mesenchyme and contribute to the development, maintenance and repair of this tissue. As other fibroblasts types in the human body, gingival fibroblasts synthetize collagen, elastic fibres, glycoproteins and glycosaminoglycans, which when present are indicators of good cell viability. [1]

In this work, the gingival fibroblasts are the cells studied *in vitro* due to their role in the repair of gingival connective tissue, which is progressively lost in periodontal diseases.

2.2.2 - Periodontal Diseases

Periodontal diseases englobe all the conditions of the tissues surrounding and supporting the teeth – periodontium. The periodontium can be affected by two classes of periodontal diseases: gingivitis and periodontitis. The primer is defined as inflammation of the soft tissue compartments of the gingiva, which includes the epithelium and connective tissue, without occurring tissue reduction. However, if the condition is left untreated, it can develop to periodontitis, were inflammation surpasses the soft tissues, entering the alveolar processes, which support the teeth. In order to attack the inflammation, the immune system breaks down its mechanical structures. Thus, reduction of supporting tissue as well as bone can occur, which subsequently leads to teeth loss. [40], [41]

2.2.2.1 – Incidence

Since 1990, oral health did not improve, instead, it dramatically aggravated. In fact, formerly, the number of people who suffered with an untreated oral condition was 2.5 billion,

whereas in 2015, that number rose to 3.5 billion. This is justified by demographic changes, such as population growth as well as the increase of the average life expectancy. Explicitly to severe periodontitis, the number of prevalent cases rose from 307 million in 1990 to 538 million in 2015, whereas incidence statistic was maintained with 6 million people suffering from the condition in the same lifespan. [42], [43]

2.2.2.2 – Risk Factors

In the 1960's, it was though that all individuals had the same probability of developing periodontal disease. However, as the years went by, scientists started to connect genetic, environmental and lifestyle factors, unique for each individual, which considerably increased their susceptibility to develop periodontal diseases. [44]

Genetics can play a role in the manifestation of periodontal diseases, since rare syndromes can affect phagocytosis, the epithelial and connective tissues, and even teeth.

Tobacco and alcohol are two lifestyle risk factors for chronic periodontitis, which can be modifiable in order to prevent such condition. It is stated that smokers are much more likely to develop periodontal diseases than non-smokers, as well as relatively suffer from more severe loss of tooth and its supporting structures. Also, the augment of number of packs smoked increases the prevalence as well as severity of the disease - Figure 2.3. Moreover, since nicotine is vasoconstrictive, the compromised microvascular response leads to reduced oxygenation in the periodontal pocket, which can lead to the proliferation of anaerobic bacteria. Therefore, due to the lack of immune response from the cytokines in the bloodstream, the treatments and other surgical interventions are ineffective for the control of the disease, since the healing does not occur post treatment. [40], [41], [44]
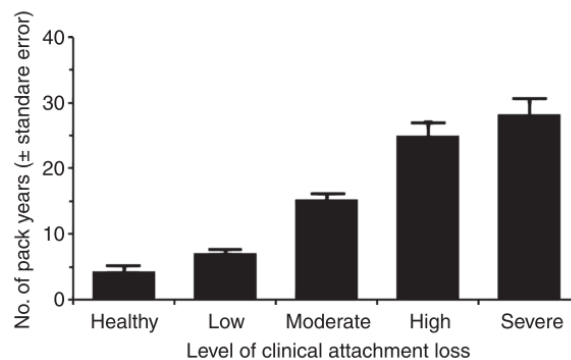
Figure 2.3 – Graph showing the relation between the number of years that individuals smoke and the severity of periodontitis they suffer from [44]

A compromised immune system resulted from conditions such as leukaemia, HIV and leucocyte disorders, leads to a higher susceptibility to develop periodontal diseases, since the body's immune system does not function in an efficient way to combat possible pathogens that develop in the human organism, including in the oral cavity. [40]

Good nutrition is also an important factor to prevent periodontal diseases, especially if the intake of vitamins C and D and calcium is within the recommended value. A study, conducted by Nishida, *et al.*, concluded that especially women, with a low intake of calcium had more

severe periodontitis than men. Moreover, vitamin C deficiency leads to decrease formation and maintenance of collagen and subsequently increase of periodontal inflammation, haemorrhage and tooth loss. [40], [44]

Diseases such as osteoporosis and diabetes increase the susceptibility of developing periodontal diseases. Osteoporosis is justified due to the characterized reduction of the bone's density through the skeletal system, including the jaw bone and alveolar processes. Relatively to the latter, several studies show that people with type 1 diabetes at all ages and adults with type 2 that control the disease do not present an increased risk for periodontal diseases over healthy people. Instead, those with poorly controlled diabetes, which worsen their glycaemic levels are associated with higher chance of developing severe forms of periodontitis. Moreover, the prevalence and severity of periodontitis increases in those individuals which suffer from long-term diabetes. [40], [41], [44]

2.2.2.3 – Pathogenesis

The oral cavity contains microflora, which lives in symbiosis with the host. A single person can present 150 species from the 800 identified as aerobic and anaerobic bacteria of the mouth. These organisms grow and attach on tooth surfaces, near the *marginal gingiva*, developing colonies. Its accumulating clusters form the dental plaque, characterized by densely packed deeper layers and mobile surface layers. [40], [41]

The pathogenesis of the disease stars with an unbalance between the microbial flora from the biofilm and the immune system of the host. Also, some studies suggest that when the number of anaerobic bacteria increases, the dental plaque matures to a state of periodontal disease. Additionally, among the identified species, certain are reported to be suppose pathogens, such as *Porphyromonas gingivalis*, *Tannerella forsythensis* and *Treponema denticola*. The primer is associated with severe periodontitis, however, other types of periodontitis cannot be excluded based on specific bacteria that a patient presents. [40], [41]

The epithelial tissue is a barrier against pathogens, since it releases Langerhans cells, which transport the microbial pathogen to the lymphoid tissue, where lymphocytes are present. Following, neutrophils, granulocytes and lymphocytes infiltrate the periodontal lesioned tissues, where neutrophils try to kill bacteria. However, since the microbial biofilm detains constantly growing number of bacteria, the neutrophils are unable to effectively eliminate all pathogens. The cytokines keep emitting signals to the neutrophils and lymphocytes to attack the ongoing inflammation, which becomes chronic destroying healthy tissue and bone. Thus, this severe state leads to alveolar bone reabsorption, degradation of ligament fibres and matrixes, as well as the development of granulose tissue in its place. This condition is continuous until tooth exfoliation or the inflamed area and granular tissue are treated. [41]

2.2.2.4 – Stages

Figure 2.4 presents the stages of periodontal disease. Gingivitis is the first and only stage of periodontal diseases that can be reversible by non-invasive treatments. It is characterized by the inflammation of the soft tissues that comprise the gingiva, primarily affecting the *marginal gingiva* section, since it is the one in contact with the microbial biofilm. This condition

precedes periodontitis, since, if left untreated, a periodontal pocket starts to form and is filled with microorganisms, that trigger an ignition process resembling the one verified on the gingiva. However, in this case, the inflammation takes place in the supporting structures of the teeth, like the alveolar processes and fibre ligaments, which start to deteriorate, leading to an irreversible repair of the lost tissues. [40], [41]
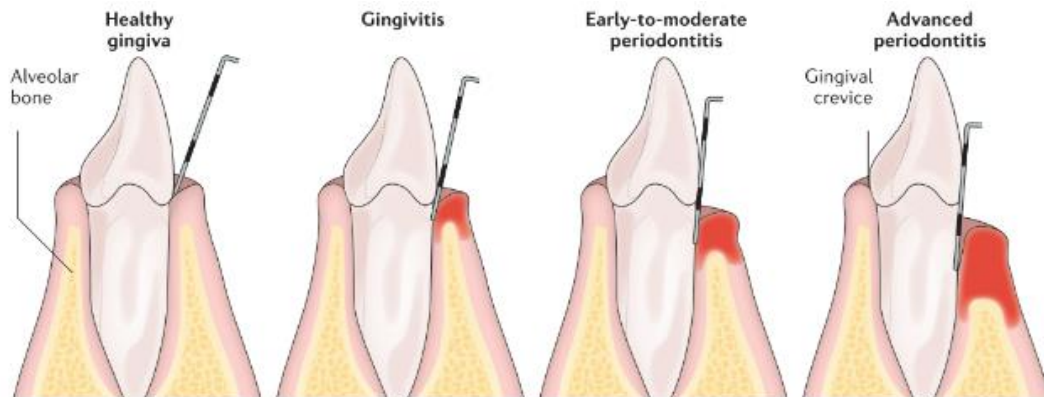
Figure 2.4 – Healthy gingiva and tissues affected by progressive stages of periodontal disease [41]

There are various types of periodontitis, being chronic, aggressive and severe periodontitis, the mainly studied ones. As the name indicates, chronic periodontitis is characterized by the chronic inflammation of the alveolar processes. In this stage, clinical attachment loss does not exceed 4mm. Aggressive periodontitis precedes the chronic type and can be presented in a local or generalized manner. Usually, this condition manifests in the early stages of life -from puberty until the fourth decade. There are no specific biomarkers that distinguish this type from the primer. Therefore, these are different conditions that develop from the same spectrum, although aggressive type has more probability to be manifested due to a genetic condition. Severe periodontitis differs from the latter by the greater loss of clinical attachment – more than 5 mm. [1], [41]

Certain periodontal diseases are caused by dental implants, when the immune system triggers a foreign body reaction towards them. One of such is peri-implant mucositis, which is characterized by the inflammation of gingiva around an implant. Comparable to periodontitis, peri-implantitis is the similar condition that occurs at the alveolar processes around the implant. As the name indicates, it is characterized as a local inflammation around the implant that affects the deeper supporting structures, leading to their deterioration, which ultimately leads to the removal of the implant. [41] Thus, after reflecting on the phases of the disease, we realize that it is important to detect and treat it in the early stages, when the situation is reversible.

2.2.2.5 – Current Medical Treatments

An individual suffering from any form of gingivitis is reversibly treated by the removal of dental plaque and calculus – debridement – at a dentist's clinic. Relatively to periodontitis, the treatment involves deep cleaning of the periodontal pocket - root planning – in addition to debridement. These non-surgical therapies can result in a positive outcome, if the patient takes

the preventive measurements at home, which primarily includes toothbrushing. In addition to mechanical removal of the plaque, drugs in the form of powders, gels, chips or fibres can be locally applied. These antibiotics and/or antimicrobials can be used up to 3 weeks post treatment in order to create a barrier in the target area, so it has time to repair itself. However, in certain cases, surgical therapy is required for the control of the inflammation to obtain comparably better outcomes. Open fap debridement is the most performed of those techniques. The procedure involves the surgically elevation of a section of gingiva, adjacent to the lesion area, to be sutured over the area with gingival recession. [41]

Novel therapies implicate tissue engineering methods for guided tissue regeneration. Certain examples include genes, proteins and cells incorporated in scaffolds manufactured from polymeric biodegradable materials in order to mimic the lost tissue. Guided tissue regeneration is currently only focused on bone regeneration. This technique involves the placement of a membrane between the alveolar processes and gingiva, with the purpose of stimulating bone regeneration, induced by the polymer's properties. [41] The ultimate goal of these studies is so that regeneration occurs along with the progressive degradation of the material, resulting in complete filling of new regenerated tissue in the space previously occupied by the implanted scaffold.

The state of the art presented in this work reports a positive stimulation from PLA materials to promote gingiva regeneration. Alongside, the search for a therapy that is minimally invasive, comfortable and manageable for the patient is still in course. Moreover, the manufacture of a polymer with the perfect properties to stimulate tissue regeneration still isn't over. Additionally, the scarcity of polymers to stimulate gingiva regeneration must be changed. Therefore, for those reasons, the properties of the biodegradable, nontoxic, biocompatible PLA material will be studied to evaluate its feasibility to promote gingiva regeneration.

2.2.3 - Poly (Lactic Acid)

Poly (Lactic Acid) (PLA) is an aliphatic biodegradable material with the following molecular formula: $[(C_3H_4O_2)_n]$. This polymer has been widely studied and consequently implemented in the biomedical field as sutures and prosthesis, since the late 1960's. It can be derived from renewable sources, such as sugar from corn starch, potato, sugar cane, beets and much more. The primer mentioned source is the most frequently used as raw material to produce the polyester's monomer – lactic acid $[(C_3H_6O_3)]$. To synthetize PLA, the latter covalently bonds by its adjacent functional groups – carboxyl [COOH] and hydroxyl [OH] -, when in high number of n repeated units – as its represented in the PLA's molecular formula. The carbon in the monomers composition is originated from the atmosphere, and then photosynthesized into the glucose contained in the renewable mentioned resources. Thus, PLA's biodegradable products possess very low toxicity for the environment as well for the human body, since the lactic acid and oligomers ultimately degrade to carbon dioxide and water. Therefore, PLA is advantageous for environmental, industrial, biomedical and pharmaceutical applications. [6], [45], [46]

2.2.3.1 – Synthesis

The production of PLA from corn's starch starts with the fermentation of its sugar, such as glucose or dextrose, by enzymatic hydrolysis. Afterwards, bacteria synthetize lactic acid, by fermenting the sugar– Figure 2.5. [45], [46]
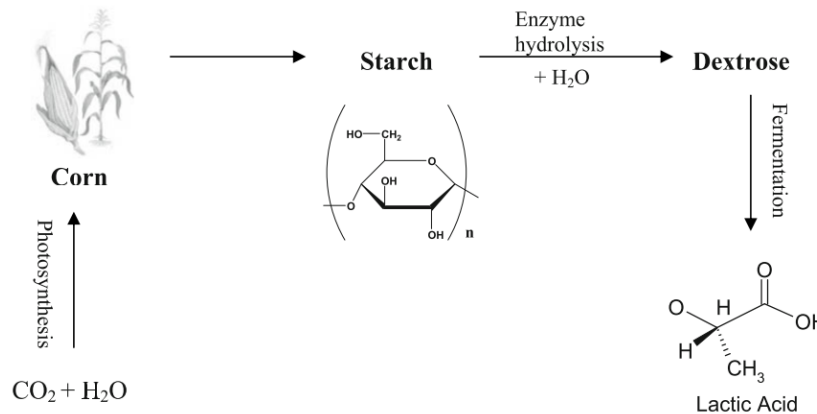
Figure 2.5 – Production of lactic acid from corn [46]

Taking into account its derivatives, lactic acid molecule is optically active and has two enantiomers: levo – (L-lactic acid) and dextro – (D-lactic acid), which possess identical physical properties, however rotate in opposite directions when exposed to polarized light. Namely, L-form rotates the plane of polarized light in an anti-clockwise manner, whereas D-form rotates it in a clockwise sense.

Natural bacterial fermentation generally yields a mixture of the two stereoisomers with 99.5% of L and 0.5% of D. [46] However, in industrial manufacture, the two main processes to synthetize PLA from lactic acid are polycondensation and ring opening polymerization (ROP). The primer is the standard, which consists of water extraction, produced by the condensation reaction with a solvent. This is carried out under high vacuum and temperatures. In the end, the obtained product has a tendency to have low to intermediate molecular weight - $M_w = [2 \times 10^3; \ 2 \times 10^4] \ g/mol$, due to poor removal of water and impurities. [46]

On the other hand, the latter involves the polymerization of the lactic acid's cyclic dimers - lactide acids –, which produce three different forms from lactic acid: L-lactide (LLA), D-lactide (DLA) and meso-lactide (MLA). Comparatively to the first method, this one is carried out under milder conditions and the obtained polymer possesses higher molecular weight - $M_w > 1 \times 10^6 \ g/mol$. Thus, with this technique, the final polymer can be constituted of 100% L-lactic, 100% D-lactic or a blend of both in different proportions, when produced by L-lactide, D-lactide or meso-lactide, respectively. [45], [46]

Therefore, PLA with different ratios of L-form and D-form can be obtained by synthetic manufacturing, which blends the two stereoisomers in distinctive proportions to obtain the materials with the desired properties.

2.2.3.2 – Medical Applications

PLA is a FDA approved polymer and does not present toxicity. Also, this polymer is effective, sterilisable and biocompatible. [6], [45]

In wound management, PLA and its copolymers have been applied as surgical sutures, healing dental extraction wounds and preventing postoperative bacterial adhesions. [47]

Orthopaedic devices such as plates, pins, screws and wires for bone fixation are also being developed from PLA to replace the commonly used metal – titanium -, since a second surgical procedure is needed to remove the latter. These are applications that require long-term retention of mechanical strength. Thus, in a study, PLA's properties were improved through the control of the L/D ratio during its production. PLA with the stereoisomer ratios of L/D - 85/15 - was synthetized and used to manufacture screws and fixation plates. The mandibular PLA plates showed positive results, since it did not require additional support in order to withstand the tension of the bone fracture. Currently, companies commercialize the aforementioned medical devices from PLLA with an intermediate molecular weight $(M_w > 7.0 \times 10^4 \, Da)$, in order to have a product with high strength and to be as similar as possible to actual bone. [6], [45], [47]

Tissue engineering meshes for guided bone regeneration made from PLLA have been studied and applied, due to the fact that oriented fibres possess piezoelectric properties. When the mechanical stress imposed by the bone is sensed by the biopolymer, its piezoelectricity creates voltage in the material, which subsequently promotes bone regeneration. However, since this material has poor mechanical properties, it is blended with other composts in order to combine piezoelectricity with improved physical characteristics. Additionally, in order to accompany the time for the tissue to regenerate, the material's degradation rate must be appropriate– Figure 2.6. [45], [47]
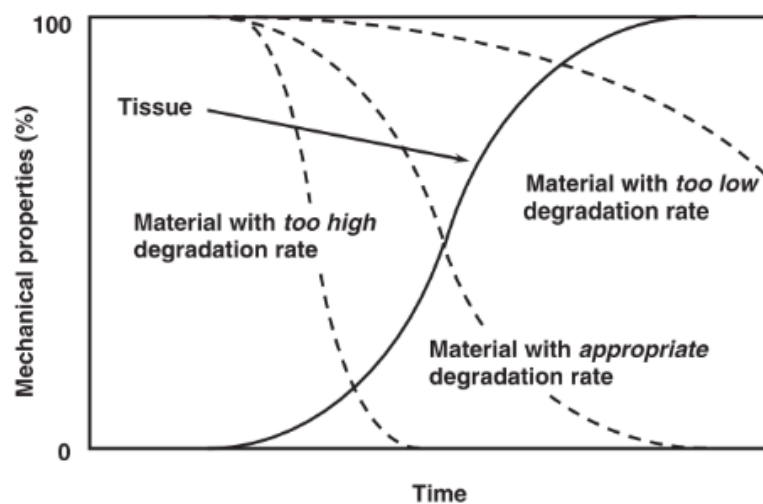
Figure 2.6 – Materials with various degradation rates versus tissue's regeneration time [45]

2.2.3.3 – Neat Poly (L-Lactic Acid) Microparticles

In this work, neat Poly (L-Lactic Acid) – Figure 2.7 - was the polymer in study. Thus, the proportion of the two stereoisomers in this material is 1:0 of L-form and D-form, respectively. PLLA was chosen over PDLA since the L-form with high molecular weight overcomes the excessively fast degradation kinetics of PLA. [8], [45]
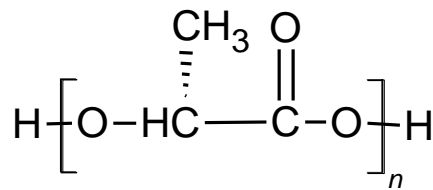
Figure 2.7 - Chemical Structure of PLLA monomer

Biomaterials with certain composition and structure can transmit specific signs to cells. Therefore, it is important to acknowledge the properties of a biopolymer and the way that it can influence cellular behaviour. [11]

2.2.3.3.1 - Properties

A polymer's size can affect its interaction when in direct contact with cells. Since natural tissues are constituted by a structure at a nanometer scale, a micromaterial has excellent physiochemical characteristics that can mimic surface properties of cell, stimulating cell growth and guiding tissue regeneration. By downsizing the material, the surface area, surface roughness and surface area to volume ratio increases, which can lead to higher performance due to superior physiochemical properties. [11]

The physical properties of a polymer include mechanical, thermal, permeability, optical, surface and electrical estates. The last two properties are specific to materials with orientation, such as fibres or films. [45]

A material's mechanical properties depend on various factors, such as molecular weight, structure's organization, orientation, crystallinity (X_C), and crystalline thickness (L_C), being orientation the most impactful in ordered structures. [45] However, that is not the case in this work, as previously mentioned. Thus, the most important mechanical factors of the polymer in study become molecular weight, crystallinity and crystalline thickness.

Polymer's molecular weight influences its degradation, since it is reported that PLLA with higher molecular weight possesses a lower rate of hydrolysis. Additionally, the erosion rate of branched PLLA monolayers is dependent on its average molecular weight as well. Moreover the crystalline phase transition also depends on the specimen's molecular weight, where it is much faster when the molecular weight is low. [48]

The crystallization of PLLA can occur in three forms: α, β and γ, being α the most common polymorph. [49]

The thermal properties are important to determine the thermal processing and withdrawn temperature, as well as the temperature range of a material to crystallize. Among them, melting temperature (T_m) and glass transition temperature (T_g) are the most relevant parameters for this purpose. [45]

The permeability of PLLA towards water, oxygen and carbon dioxide are important in biomedical applications, since the material needs to exchange gases when in direct contact

with the human organism's tissues, such as gingival tissue. Additionally, it is reported that the permeability of gases decreases with crystallinity. [45]

The optical properties study the ultraviolet (UV) light transmittance of the materials. PLLA does not transmit UV-C light, however, it is transparent to almost all UV-B and UV-A lights. [45] Therefore, this is a good method of sterilization for the material, since the light travels through the material, sterilizing it all the way through.

2.2.4 – Hydrogels

Hydrogels are polymeric networks crosslinked through physical, ionic or covalent bonds. They are well known for their ability to inflate with water, from 10-20% up to thousands of times their dry weight, instead of dissolving in a degradable manner. The water is attained due to two main reasons. The primer is the elevated thermodynamic affinity that these matrixes gain when in contact with solvents. The second is justified by the polymeric backbone, which is loaded by hydrophilic functional groups. Thus, water has a high affinity towards the material. Relatively to the non-dissolution property, it is due to the mentioned sturdy crosslinks that maintain its chains coupled. [9], [50], [51]

These networks can belong in two categories, when classified by the type of crosslink bonds – Figure 2.8. Chemical hydrogels possess covalently-crossed links between the polymer chains, that confers them permanent junctions. Whereas physical hydrogels are held together by molecular entanglements or physical interactions, such as hydrogen bonds and ionic or hydrophobic interactions, which imparts them with transient junctions. [9], [51]
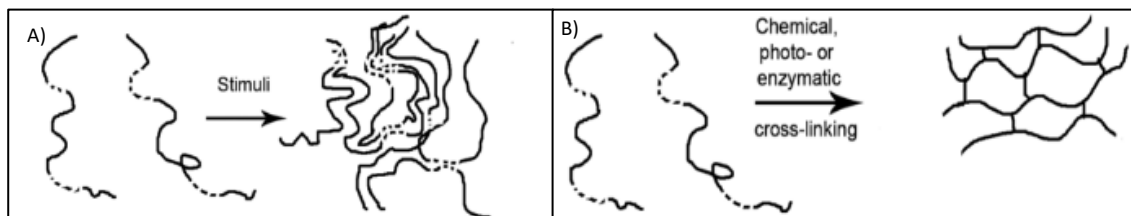
Figure 2.8 – Synthesis of hydrogels depend on its crosslink stimuli. A) Physical Hydrogels. B) Chemical Hydrogels. Full lines and dotted lines are hydrophilic and hydrophobic portions, respectively. [52]

In terms of the hydrogel's origin, it can be split into two categories as well: natural or synthetic. Natural hydrogels are manufactured from direct sources, such as collagen, fibrin and matrigel. Moreover, they can be derived from natural fonts, either chitosan from chitin or alginate from seaweed. A combination of the above sources is also a possibility. Whereas synthetic hydrogels can be produced from poly (ethylene glycol), diacrylate, poly (acryl amide), poly (vinyl alcohol) for example. Natural hydrogels possess advantages relatively to the synthetic ones, due to their bioactivity, which confers them native adhesion stimulation. Contrarily, synthetic hydrogels are inert due to being constituted by synthetic carbons. So,

these do not contain any molecules or endogenous factors to promote cell proliferation and differentiation. [9]

Different structured hydrogels can be produced by varying the kind and density of the links as well as the concentration and structure of the employed monomer, which reflects on its properties. Therefore, various equilibrium's establishment can occur with the liquid and temperature of the surroundings, so that, the mechanical strength and shape of the material interrelate with the properties of the ambiance whereby they contact. [9], [51]

2.2.4.1 – Tissue Engineering Applications

In order to be used in clinical applications, a hydrogel must present specific characteristics. One of which is that it is in a liquid state at room temperature and transforms into a gel at body temperature in a short period of time. Another property is that its constituent material needs to be biocompatible and bioresorbable. Lastly, its pH value must be equal to a physiological one, to allow the incorporation of cells or bioactive agents. [23]

The primary applications of hydrogels are performed by builds of their three-dimensional scaffolds. These structures can mimic an extracellular matrix, due to its resemblance to the natural one in physical and chemical properties, such as stiffness and hydrophilicity. [9], [11]

Techniques like *in vivo* tissue regeneration can be performed by incorporating autologous cells from a patient to the hydrogel structure. The cells are contained within the scaffold's pores, which are large enough to accommodate them and allow their development. The growth occurs in *in vitro* settings. Such conditions allow a bridge between the *in vitro* experiments and the *in vivo* environment, without any complications that culture mediums might fetch. By this means, the polymeric matrix promotes cells proliferation and differentiation, providing the cells, the specific space to engineer the intended tissue amongst the ECM like structure, until it is finally ready to be implanted in the patient. [9]

Hydrogels that degrade and release growth factors are applied as drug delivery systems to locally regenerate a damaged tissue. The process consists of forming larger pores by their dissolution, while releasing the growth factors and allowing cells to adhere within its structure. This occurs, since the hydrogel as the ability to covalently incorporate cell membrane receptor ligands, that stimulate adhesion, spreading and growth of those cells inside the progressively larger pores. [9]

This material is advantageous for TE applications due to several characteristics and properties. It provides a protective environment for growing cells or fragile drugs. It is also a good transport system for nutrients to cells and excretions from cells. Additionally, it can solidify at body temperature, thus, maintaining the drugs in the target region. However, it also possesses disadvantages, such as complexity to handle and sterilize and weak mechanical properties. Additionally, it is difficult to crosslink with drugs and cells, in *in vitro* conditions, to create the prefabricated stable matrix, with the purpose of being complete before administration. [9]

In the oral cavity, hydrogels have mucoadhesive properties since create hydrogen bonds with the mucosal surface. Thus, this system is advantageous to deliver loaded drugs in the mobilized oral lesion area in which is administrated. [22]

2.2.4.2 – Hydrogel Reagents Used in This Work

The PLLA microparticles will be incorporated into a modified chitosan hydrogel. Chitosan is the polymer of choice to synthetize the inflatable network due to two reasons. One of which is that a composite of PLA-chitosan neutralizes the inflammatory action that PLA alone induces to the cells, at the time of its degradation. The other is that chitosan, by being hydrophilic, decreases the water-barrier properties created by PLLA. [6], [45]

Chitosan is a polysaccharide that is partially deacetylated ($\geq$ 70% of deacetylation) from chitin, which is obtained from the exoskeleton of crustaceous. Thus, this copolymer is composed by D-glucosamine, which contains hydroxyl (OH) groups and a certain proportion of amino (NH_2) groups, depending on the deacetylation percentage - Figure 2.9. [53], [54]
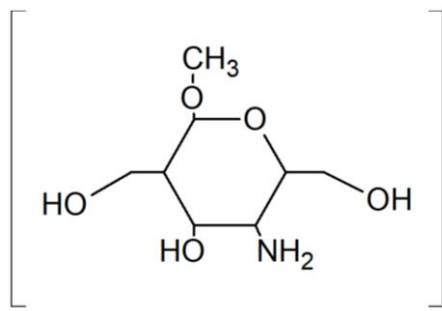
Figure 2.9 – Chemical structure of chitosan [55]

This material has been used in a vast range of medical applications as wound dressings, dental implants, bone cement, artificial skin, corneal contact lens, and encapsulating materials. This is possible due to its biocompatible properties that can promote cell proliferation and tissue development, such as: low-toxicity, no antigenicity, biodegradability, antibacterial action and wound-healing activity. Moreover, it can be synthetized into a hydrogel for additional medical and pharmaceutical applications. [54], [56], [25]

The presence of positively charged amino groups in the polymer's structure grants its antimicrobial characteristics at physiological pH conditions. Moreover, chitosan is naturally mucoadhesive due to being hydrophilic, which makes it adhere to fluids, such as saliva. These properties are important for buccal healing, since the material needs to stay in contact with the mucosal membrane as well as repel bacteria, in order to promote a continuous repair of the damaged area without infection. [16], [53], [54], [57]

In order to synthetize hydrogel for use in biomedical applications, chitosan needs to be crosslinked with another biomaterial, to improve its mechanical resistance and chemical stability, otherwise, it dissolves in acidic conditions at pH below 6. Several studies indicate that it is important to crosslink chitosan with a non-ionic polymer in order to retain the positive charge of the amino groups. [56], [58]

Organosiloxanes stimulate cell proliferation and gene expression. Additionally, in literature, these silicates are used as bonding agents. γ −glycidoxypropyltrimethoxysilane (GPTMS) contains epoxy groups that react with the amine groups of chitosan, forming hydroxyl groups, which bonds the biopolymers in a covalently chemical linkage. The more GPTMS added to the solution, the shorter is its gelation time, which is advantageous for applications in vivo.

The synthesis of chitosan-GPTMS hybrids has been reported to exhibit excellent cytocompatibility and promote proliferation in human MG63 osteosarcoma cells, as well as human bone marrow osteoblasts. Specifically, this composite demonstrated higher biocompatibility when compared with chitosan alone. Furthermore, it is also reported that GPTMS inhibits the hydrogel's degradation when immersed in phosphate-buffered solution (PBS). Thus, this reagent acts as a crosslinking agent of chitosan to form a stable hydrogel with short gelation time and hindered degradation. [23], [25], [59], [60]

However, since the chitosan needs to be dissolved in acetic acid, the solution is too acidic to be applied in a physiological environment. Thus, a neutralizing agent is necessary to increase the pH. In previous studies, it is reported that a chitosan/β- Glycerophosphate disodium salt hydrate (β-GP) hydrogel composite demonstrated good cytocompatibility with chondrocytes and human bone marrow mesenchymal stem cells (hBMSCs). Moreover, this reagent may also decrease the gelation time of the hydrogel, since its negatively charged molecules - HPO_4^- or PO_4^{2-} - electrostatically attract to the positively charged amine and amide free groups of chitosan. Taking these outcomes into consideration, in this work, β-GP is employed to set the hydrogel's pH at 7.3 and also decrease its gelation time. [25]

2.2.5 – Injectable Systems

Injectable systems comprise the ease of use advantages as well as being a minimally invasive treatment that does not affect healthy regions of the tissue, since it is only directed to the damaged area. Thus, this unpainful drug delivery system is more comfortable for the patient, without requiring surgical intervention, which could take a negative effect on the healing process.

Hydrogels can be easily administrated by this system. Moreover, thermodynamic hydrogels, only solidify *in situ*, within the damaged regions – Figure 2.10. Hence, the hydrogel does not move to another location and can progressively release the loaded growth factors, cells, proteins or biodegradable polymers to promote tissue regeneration within that area.
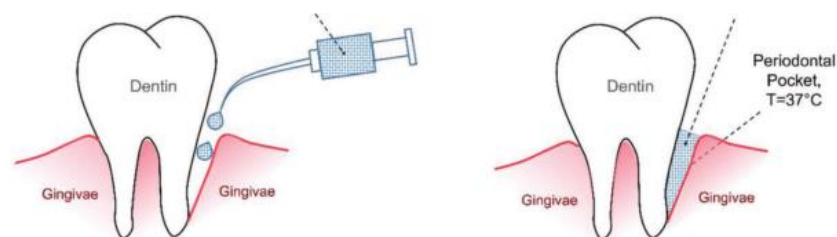
Figure 2.10 – Illustration of the sol-gel transition of the hydrogel after being administrated in the periodontal pocket. [61]

A characteristic of the synthetized hydrogel in this work is to possess a fluid consistency when exposed to temperatures below the physiological ones, and transit rapidly to a gel form right after injected in periodontal pockets.

In the current market, there are a couple of injectable hydrogels for the treatment of periodontal diseases. [9], [10], [62] Table 3.1 shows the polymeric products being administrated through an injectable system and its application.

Table 2.2 – Injectable hydrogels on market for treatment of periodontal diseases. NMP is N-methyl-2-pyrrolidone – an organic solvent. [62]

Product	Constituents	Administration System	*In situ* consistency	Treatment results
Atridox®	- 36.7% PLA - 63.3% NMP - 10% Doxycycline antibiotic	Multifunctional system - Two syringes injected simultaneously: - Doxycycline - PLA and NMP mixture	- Solid in pocket morphology - Wax-like consistency upon contact with gingival crevicular fluid	- Pocket depth reduction (1.3 mm) - Clinical attachment level increase (0.8 mm)
Atrisorb®	- 4% Doxycycline antibiotic - PLA - NMP	One injectable syringe	- Absorbable membrane	- Regeneration of damaged periodontal tissue

Chapter 3

Materials and Methods

3.1 – Materials Production

3.1.1 - PLLA Microparticle's Production

PLLA was obtained from Corbion Purac's company. The product is designated as PURASORB® PL 18, being an homopolymer of L-lactide with the molecular formula - $(C_6H_8O_4)_n$ - and respective chemical name – poly [(3S-cis) - 3,6 – dimethyl - 1,4 – dioxane - 2,5-dione]. It possesses an intrinsic viscosity and average intermediate molecular weight of $[\eta] = 1.8$ dl/g and $M_w = [2.17 - 2.25] \times 10^5 \, g/mol$, respectively. The manufactured polymer's appearance is white to light tan and is moulded in granules. Its finality is for use on medical device applications as well as polymer processing techniques. [63], [64]

The subsequent synthesis of PLLA microparticles was through the spray drying technique.

3.1.1.1 – Specimen Preparation

PLLA granules were dissolved in chloroform (CHCl$_3$, from Sigma - Aldrich) to achieve a polymer concentration of 10 wt% in the solution. The process was conducted at room temperature using an agitator until complete polymer dissolution. Then, the solution was diluted with distilled water - 10 parts of water per 1 part of solution - and stirred for 1 hour. The obtained final feedstock solution - PLLA concentration of 1 wt% in the solution - was kept under stirring while it was plasma sprayed.

3.1.1.2 – Spray Drying Technique

The technique steps take place inside a drying chamber. The solution is sprayed through a nozzle, as ultra-fine droplets, to the drying chamber. The organic solvent is instantly evaporated. The dried microparticles are conducted with dry air flow under low pressure to be collected in the bottom of the drying chamber – Figure 3.1. [11], [65]
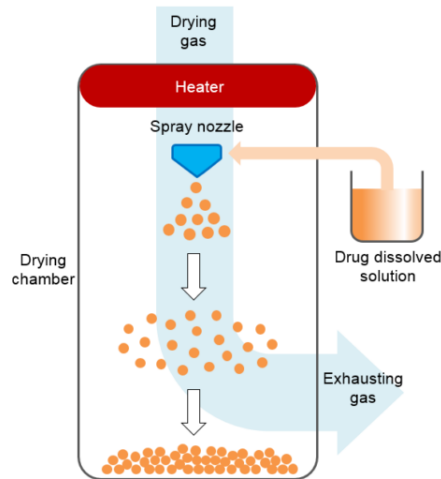
Figure 3.1 – Schematic description of spray drying technique [65]

Characteristics of the studied material were analysed conducting tests by Scanning Electron Microscopy (SEM), Fourier Transform Infrared Spectroscopy (FTIR), Differential Scanning Calorimetry (DSC) and Thermogravimetric Analysis (TGA).

3.1.2 – Chitosan-based Hydrogel Production

The reagents were obtained from Sigma-Aldrich - Chitosan from shrimp shells ($\geq 75\%$ deacetylation), Acetic acid (analytical standart), (3- Glycedyloxypropyl) trimethoxysilane ($\geq 96\%$) and $\boldsymbol{\beta}$-Glycerophosphate disodium salt hydrate ($\geq 99\%$ tritation).

Upon the analysis of the state of the art about chitosan-based thermosensitive hydrogels, the production of the chitosan hydrogel is founded on Yuki Shirosaki's works. [23] [25]

The process starts by adding 2% (w/v) of chitosan in acetic acid solution (0.25M) and stirring until complete dissolution – Figure 4.3.A). Then, GPTMS is added in the molar ratio of $\boldsymbol{0.5{:}1}$ (GPTMS: Chitosan) and the solution is stirred at ambient temperature for two hours, to allow the reticulation process to occur. Afterwards, the chitosan and $\boldsymbol{\beta}$-GP (2.5M) solutions is placed in an ice-bath until its temperature reaches 4ºC. Furthermore, maintaining this temperature, $\boldsymbol{\beta}$-GP is added drop by drop to the chitosan solution and stirred until it is neutralized at a pH=7.3. The resulting fluid gel is stirred in an ice bath (T=4ºC) for 10 minutes, to allow further reticulation with $\boldsymbol{\beta}$-GP.

3.1.2.1 – PLLA Microparticles loading into hydrogel

The pretended ratio of microparticles are added to the hydrogel after its neutralization with $\boldsymbol{\beta}$-GP. For instance, for a chitosan-based hydrogel sample of 30mL in volume, 0.045g of

PLLA MPs are gradually added to the sample while stirring in a magnetic agitator, to obtain a sample with 1.5% (w/v) of MPs. Afterwards, the solution is placed in the ultrasound bath and the magnetic agitator alternately, until the microparticles are evenly disperse. The whole process is performed with the sample continuously immersed in 4°C ice bath.

After synthesis, the samples, regardless of being loaded with MPs or not, can be maintained at its liquid state or allow to transit into gel. For the first, the samples are kept inside a thermo-isolating container at a temperature range between 5°C to 15°C, whereas to transit to gel state, the samples are placed in an incubator at physiological temperature – 36.5°C – overnight.

The hydrogel synthetized in this work will be composed by chitosan, GPTMS and β-GP as the active agents, with the expectation that it possesses the ability to promote proliferation of human gingival fibroblasts. The PLLA microparticles will be within incorporated to potentialize the hydrogel's effect, due to their tissue forming promoting properties. The best method to administrate the hydrogel *in situ* is thought to be through an injectable system. In this work, the hydrogel's fluidity will be preliminarily tested by the material's extrusion through a syringe.

3.2 – Materials Characterization

3.2.1 - PLLA Microparticles Characterization

3.2.1.1 – Scanning Electron Microscopy Analysis

SEM analyses the topography, morphology and chemical elements of a sample. PLLA microparticles were coated with a Gold (Au) and Palladium (Pd) thin film, by sputtering, using the SPI Module Sputter Coater equipment. Then, araldite was applied and left to dry overnight to adhere the microparticles into the sample holder, since they did not adhere with the traditional method - conductive tape. The first SEM / EDS (Energy Dispersive X-Ray Spectroscopy) exam was performed using Quanta 400 FEG ESEM / EDAX Genesis X4M, whereas the second was performed using - JEOL JSM 6301F/ Oxford INCA Energy 350 -, since the first was unavailable. For the first SEM analysis, the implemented accelerating voltage was 15kV and in each image, the specific remain analysis conditions are described in the databar. The second SEM analysis contemplated a range of accelerating voltages which will be described within the legend of each image as well as the remaining analysis conditions. Microparticles average diameter was measured by the SEM equipment as well as by Image J software of the obtained images. [66]

4.2.1.1 – Microparticle's Purification Method

The drying chamber had a tantalum contamination, which was only detected after the microparticles processing. That justifies the tantalum contamination detected in the first SEM analysis of the microparticles. Therefore, the tantalum moieties had to be withdrawn, to purify the sample.

The process started with two tubes, containing 1 g of PLLA microparticles each. Each tube content was poured into a 50 mL falcon tube and made up with ultra-pure water until the 25 mL mark. The tubes were shaken until complete dispersion of the PLLA microparticle's agglomerates and dissociation of the tantalum moieties from the specimen. Hereafter, the solutions were centrifugated at 4000 rpm for 8 minutes. The tantalum possesses different density when compared with PLLA, so, it was discarded in the supernatant. This process was repeated three times. By the end, the samples were left to dry in a desiccator for two days.

Afterwards, a similar washing process was performed to make sure that all the tantalum moieties were withdrawn. This time, in a 50 mL falcon tube, ultra-pure water made up until the 50 mL mark and the tubes were left in an ultrasound bath for 1 hour, prior to centrifugation at 4000 rpm for 5 minutes. The supernatant was discarded, and the tubes were left to dry in a desiccator for 10 days, before new SEM analysis. As it can be demonstrated in the SEM-EDS results in this report, the tantalum was successfully removed from the sample.

3.2.1.2 – Fourier Transform Infrared Spectroscopy

FTIR was performed using the system from Shimadzu IRAffinity-1S apparatus in the attenuated total reflectance (ATR) mode from 600 to 4000 cm^{-1}. The infrared spectra was collected with 32 scans and a resolution of 1 cm^{-1}, at room temperature.

3.2.1.3 – Differential Scanning Calorimetry

The thermal behaviour of the PLLA microparticles were analysed by differential scanning calorimetry measurements (DSC) with a DSC 214 Polyma (Netzsch) apparatus. The samples were placed into 40 µL aluminium pans and heated between 0 and 200 ºC at a heating rate of 10 ºC.min^{-1}. The glass transition temperature (T_g), cold crystallization temperature (T_c), melting temperature (T_m), and melting enthalpy (ΔH_m) of the PLLA microparticles were obtained through the analysis of the respective spectra.

3.2.1.4 – Thermogravimetric Analysis

The thermal degradation kinetics of the samples was characterized by thermogravimetric analysis (TGA) in a TGA4000 apparatus from Perkin-Elmer at different heating rate scans - 10 ºC/min, 20 ºC/min, 30 ºC/min and 40 ºC/min. The derivative of each process was also obtained in the differential degradation curves (DTG). The temperature range between 30 and 700 ºC, being all measurements performed under a nitrogen atmosphere.

3.2.2 - PLLA Microparticles loaded Hydrogel Characterization

3.2.2.1 – Scanning Electron Microscopy Analysis

In order to optimize the concentration of microparticles loaded into the hydrogel, samples with different (weight/volume) ratios – 0.5%, 1.0% and 1.5% - of loaded MPs were observed in SEM. After it's synthesis, the samples were placed in an incubator at 55℃ until dried.

Before being observed, the samples were coated with a Gold (Au) and Palladium (Pd) thin film for 100 seconds, by sputtering, using the SPI Module Sputter Coater equipment. Quanta 400 FEG ESEM / EDAX Genesis X4M was the equipment used to observe their morphology. The implemented accelerating voltage was 15kV and in each image, the specific remain analysis conditions are described in the databar.

3.2.2.2 – Fourier Transform Infrared Spectroscopy – Attenuated Total Reflectance

To prepare for the test, a synthetized 0% MPs sample and a 1.5% MPs sample were left in the incubator at $36.5\,℃$ overnight to transit from a liquid state to a gel state. Then, the samples were frozen at $-80\,℃$ before being lyophilized over the course of 2 days. Figure 3.2 shows the resulting lyophilized samples.
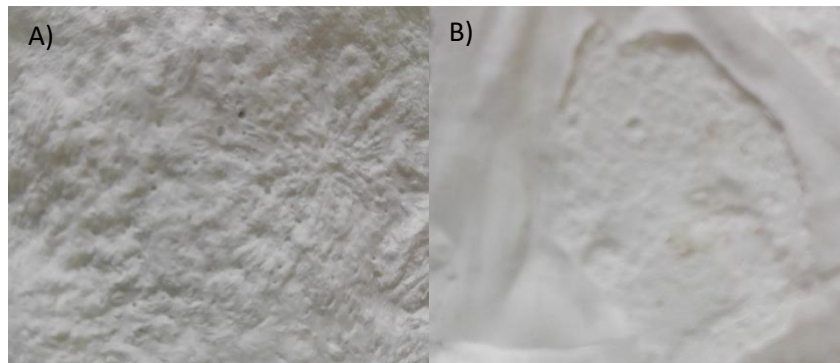
Figure 3.2 – Hydrogel after lyophilization. A) 0% MPs sample. B) 1.5% MPs sample

Fourier transform infrared spectroscopy was performed using the system from Perkin Elmer Spectrometer, Frontier model in the attenuated total reflectance (ATR) mode from 400 to 4000 cm^{-1}. The infrared spectra were collected with 32 scans and a resolution of 1 cm^{-1}, at room temperature.

3.2.2.3 – Swelling and Degradation studies

In order to place the hydrogel in an environment close to the physiological one, the degradation tests were performed with artificial saliva solution, which was synthetized based on the work of D.H. Pashley, et al. [67] The succeeding reagents were added one at a time, until complete dissolution, into ultra-pure water, according to the order: calcium chloride ($CaCl_2$), magnesium chloride hexahydrate ($MgCl_2.6H_2O$), monopotassium phosphate (KH_2PO_4),

potassium chloride (KCl), sodium azide (NaN$_3$) and HEPES, at the following concentrations (mM/L): 0.7, 0.2, 4.0, 30.0, 0.3, 20.0, respectively.

The resultant pH was adjusted to the required. For representative damaged oral areas, the saliva's pH was lowered until 5.00 with chloric acid (HCl), whereas to characterize healthy tissues, the artificial saliva's pH was increased to 7.3 with sodium hydroxide (NaOH). [68]

3.2.2.3.1 – Hydrolytic

To analyse the hydrogel's hydrolytic degradation, the samples were firstly incubated at $36.5\,°C$ to transit from a liquid state to a gel state. Then, 1.5% MPs and 0% MPs samples were immersed in only artificial saliva solution at the two different referred pH's – 3 test samples in pH=7.3, 3 test samples at pH=5, 3 control samples at pH=7.3 and 3 control samples at pH=5.

3.2.2.3.2 – Enzymatic

Lysozyme is an antibacterial oral enzyme that is present at a range of concentrations $[0.412, 30.03]\,\mu g/mL$ at nonperiodontal tissues, due to the different oral physiology of each person, since the quantities of saliva produced vary accordingly. [69], [70], [71], [72]

Thus, to analyse the hydrogel's enzymatic degradation in healthy tissue, the samples were immersed in artificial saliva at pH=7.3 with $20\,\mu g/mL$ of lysozyme. Whereas, to mimic the conditions of damaged tissue, samples were immersed in artificial saliva at pH=5.00 with $16\,\mu g/mL$ of lysozyme. [68], [71]

The test conditions were the same has performed in the hydrolytic degradation assay, except in this case, the saliva contained the previous referred concentrations of lysozyme.

The test process started by weight in the different nylon bags and assigning them to each flask. The samples were placed inside the net to further allow complete immersion in artificial saliva in the proportion of 1:100 (weight of the sample: volume of artificial saliva) inside a sealed container – Figure 3.3. Visually, the samples maintained the shape at which transited from liquid to gel state inside Eppendorf's and presented some flexibility, which allowed to easily transfer them into the nylon bags.

Both enzymatic and hydrolytic degradation tests were performed according to the Standard Test Method for in vitro Degradation Testing of Hydrolytically Degradable Polymer Resins and Fabricated Forms for Surgical Implants. [73] Thus, the immersed specimens with the same start weight, were kept in an incubator at $36.5\,°C$ and weighted periodically – 5 min; 15 min; 30 min; 45 min; 60 min; 3 days; 6 days; 11 days.

The rapid process of each weight in started by drying the nylon bag with filter paper, to remove all the excess saliva, before being weighted in a balance of ± 0.0001 sensibility. Then, the left artificial saliva in the container was measured for its pH, before being discarded. Lastly, fresh saliva, also kept at 36.5ºC, was poured with a measuring pipette in accordance with the sample's weight at the time, to maintain the above referred proportion of 1:100.
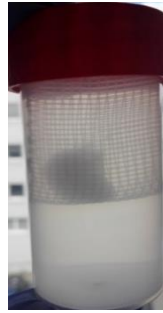
Figure 3.3 – Sample's preparation for degradation and swelling tests. Nylon net with the sample immersed in artificial saliva inside a sealed container.

3.2.2.4 – Rheological Properties

In order to enable the hydrogel's successful administration by an injectable system, its viscoelastic properties need to be studied, since it is important to acknowledge the stress and range of temperatures that the material is in its liquid and gel form. Therefore, the rheological properties of the hydrogel with – 1.5 % (w/v) - and without loaded microparticles were analysed to understand if the microparticles influence the overall viscoelasticity of the material.

Rheology is the study of the flux and deformation of a material under an applied stress, as a function of its force, time and spatial orientation (piston geometry). The strain of a material measures its degree of deformation, subsequent of the applied stress parameters. [74]

Dynamic rheologic equipment screens the material's microstructural changes during liquid to gel form transition, since it allows the monitorization of its properties during the test, in rest conditions, which prevents interferences with the microstructure. Moreover, it simplifies the analysis of the material's viscoelastic functions – storage modulus (G'), loss modulus (G'') and loss tangent (tan (δ)), equated as follows:

$$G' = \frac{\sigma_0 \cos(\delta)}{\gamma_0} \qquad\qquad \text{(Eq. 1)}$$

$$G'' = \frac{\sigma_0 \sin(\delta)}{\gamma_0} \qquad\qquad \text{(Eq. 2)}$$

$$\tan(\delta) = \frac{G''}{G'} \qquad\qquad \text{(Eq. 3)}$$

where δ is the phase angle between stress and strain, γ_0 is the strain's amplitude, $\cos(\sigma_0)$ is the stress's amplitude in phase with the strain and $\text{sen}(\sigma_0)$ is the stress's amplitude in quadrature with the strain (90º). [75], [76]

The storage modulus predicts the amount of elastic deformation that a material experiences when a force is applied, as well as the way that it returns to its initial form, when the force is removed. When a such amount of stress applied to a material hinders it to return to its initial state, the energy dissipated during the deformation is measured through the loss modulus. The

loss tangent indicates the overall viscoelasticity (viscous portion and elastic portion) of the material. [75], [76]

Most of the liquid materials are viscoelastic and can be divided into Newtonian and non-Newtonian liquids. Newtonian liquids – Figure 3.4.A) - possess the same viscosity, regarding the force, time and spatial orientation of the stress applied to it, whereas non-Newtonian fluids alter their viscosity in function of the stress's parameters. The last type is sorted into three classes: pseudo-plastic, dilatant and thixotropic. [77]
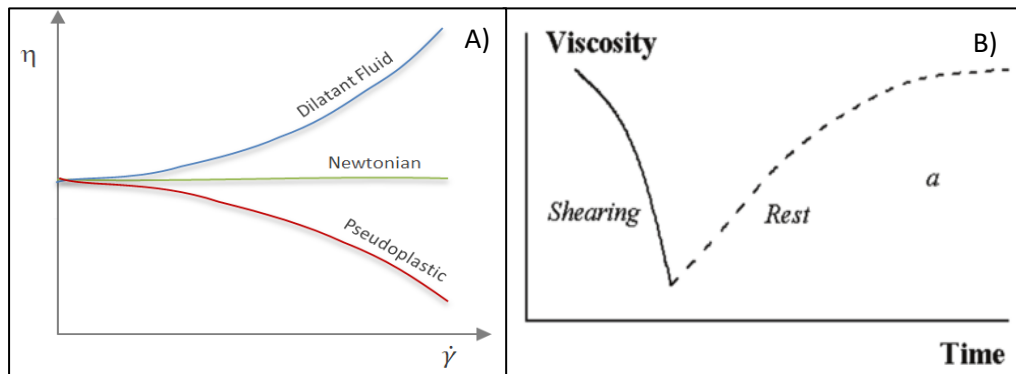
Figure 3.4 – Viscous behaviour of fluids in function of shear stress rate. A) Newtonian and non-Newtonian (Pseudo-plastic and Dilatant). B) non-Newtonian (Thixotropic). [77], [78]

Pseudo-plastic materials decrease its viscosity with the augment of shear stress frequency and rapidly return to its initial viscosity when the applied stress is cessed - Figure 3.4.A). Contrarily, a dilatant fluid augments its viscosity as the shear stress frequency is also increased and returns to its initial viscosity short after the stress is withdrawn – Figure 3.4.A). On the other hand, the viscosity of thixotropic fluids is affected by the shear stress time, which influences the time that the material takes to return to its initial viscosity, which is longer compared with the other two classes – Figure 3.4.B). [77]

By acknowledging the theory, several studies can be performed on the material. A thixotropic test is performed to determine if the material is thixotropic. An amplitude sweep test monitors the storage and loss modulus and phase angle in function of the shear strain, which determines the Linear Viscoelastic Region (LVER) of a material. Furthermore, a frequency sweep with strain-controlled test screens the viscosity of the material during time, as the shear frequency is progressively decreased, which withdrawn the pseudo-plastic or dilatant properties of the material. Additionally, a temperature sweep strain-controlled test monitors the storage and loss modulus as the temperature is progressively increased at a specific heating rate, which determines the instant temperature that the material transits from liquid to gel state.

Kinexus lab+ rheometer from Malvern Instruments was the equipment used with a geometry piston being a cone of 4 cm of diameter. The tests performed were the following: thixotropic test, amplitude sweep test, frequency sweep test with strain-controlled and temperature sweep test with strain-controlled. The former two were carried out once only in the sample of the hydrogel without MPs. The last two were performed in triplicate for each hydrogel sample – 0% MPs and 1.5% MPs.

First, the thixotropic test was performed in three phases, at different applied shear frequencies and times according to Table 4.1.

Table 3.1 – Frequency and duration of the phases in the performed thixotropic test

Number of Phase	Frequency (Hz)	Duration (s)
1	0.1	30
2	100	30
3	0.1	120

Following, in the amplitude sweep test, the parameters were inserted according to: Start shear strain – 1%, End shear strain – 500%, Frequency – $1\,Hz$. Furthermore, the frequency sweep strain-controlled tests were carried out at 25^oC, with a Start to End Frequency from $10\,Hz$ to $0.1\,Hz$ and shear strain value obtained from the amplitude sweep test. Lastly, the temperature sweep tests were performed with a temperature ramp from 15^oC to 50^oC, heating rate of $1^oC/min$ and shear strain determined in the amplitude test. In all tests, the samples per decade parameter was kept at 10.

3.3 – PLLA Microparticles *In Vitro* Study with hGFs

3.3.1 – Cell Culture and Seeding

A primary cell line of human gingival fibroblasts (hGFs) was cultured in alpha modification minimum essential medium ($\alpha - $ MEM), supplemented with 10% fetal bovine serum (FBS), 1% Penicillin and 1% Fungizone. Culture flasks were maintained in a humidified atmosphere of 95% air and 5% carbon dioxide (CO_2) at 37 °C.

Cells were passaged when cell density reached 70 to 80% of confluence. During this procedure, cells were rinsed twice with phosphate buffered saline (PBS) and detached from the culture flasks with trypsin solution at 37 °C for 5 min. Cell content was then subjected to centrifugation at 1200 rpm for 5 min. The supernatant was withdrawn, and cell pellet was mixed with fresh cell culture medium, followed by resuspension into two new T75 flasks.

PLLA microparticles were suspended into simple $\alpha - $ MEM. Afterwards, the solution was diluted with $\alpha - $ MEM, supplemented with 20% fetal bovine serum (FBS), 2% Penicillin and 2% Fungizone, into 6 different concentrations – $\mathbf{1000}\,\mu\mathbf{g/mL}$, $\mathbf{500}\,\mu\mathbf{g/mL}$, $\mathbf{100}\,\mu\mathbf{g/mL}$, $\mathbf{50}\,\mu\mathbf{g/mL}$, $\mathbf{10}\,\mu\mathbf{g/mL}$ and $\mathbf{1}\,\mu\mathbf{g/mL}$.

Figure 3.5 represents a template of a 96-well plate utilized for this experiment. Firstly, $\mathbf{50}\,\mu\mathbf{L}$ of cells with density of $\mathbf{0,3 \times 10^4}$ cells/mL were seeded into the following wells: Lines A to G and columns 1 to 8. In the next day, $\mathbf{50}\,\mu\mathbf{L}$ of PLLA Microparticle's solution was seeded on top of the cells – Lines A to F and columns 1 to 10 – having each line, one of the concentrations prepared. Line G was the positive control (Ctr+) – hGFs - and columns 9 and 10 were the negative control (Ctr-) - PLLA microparticles. The plates were kept at 37°C in a humidified atmosphere with 95% of air and 5% of CO_2. Four plates were used in this experiment. Three of which comply with this configuration, whereas the remnant lacked the collagen test columns.
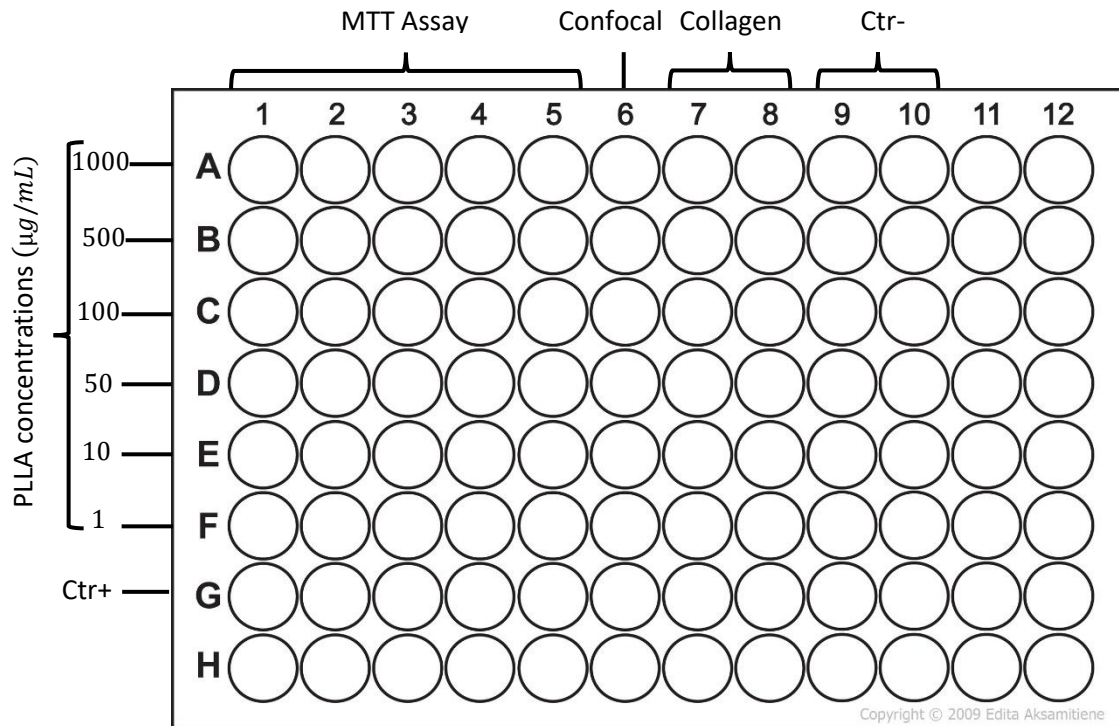
Figure 3.5 – Template of one of the 94-well plates used for the hGFs *in vitro* study with PLLA microparticles.

3.3.2 – MTT assay

The cell viability and proliferation were assessed in days 2, 6, 9 and 13 with the substrate 3-(4,5-di-methylthiazol-2-yl)-2,5-diphenyl tetrazolium bromide (MTT; Sigma). The metabolic activity of the cell reduces this yellow coloured salt into blue formazan, which accumulates within the viable cell's cytoplasm. [79]

For this propose, **10**% of MTT solution relatively to the wells content were added to each well and incubated at **37°C** in a humidified atmosphere of 95% air and 5% CO_2, for 3 hours. Afterwards, **100μL** of dimethylsulphoxide (DMSO) were added to each well to dissolve the formazan salts and the absorbance was measured at 550 nm on a plate reader (Power Wave XS2 spectrophotometer, Biotek).

3.3.3 – Collagen assay

Collagen production was monitored on days 6, 9 and 13 of hGFs seeded with PLLA microparticles. Firstly, glutaraldehyde was added to the wells and maintained at **4°C** with **100μL** of sodium cacodylate trihydrate. Then, the cultures were stained with Sirius Red and observed in the microscope.

3.3.4 – Morphology assay

Fluorescence microscopy was used to observe the morphology of the hGF's cytoskeleton and nucleus after two days of incubation with PLLA microparticles. This test was not performed on the remaining days, since the cells had proliferated in a way that it would be challenging to visualize their morphology in a correct form.

The process starts by fixating the cells to the wells with formaldehyde and then maintain the plate at $4°C$ with $100 \mu L$ of PBS. At the day preceding observation day, the cells are stained with 4',6-diamidino-2-phenylindole (DAPI) and Alexa Fluor $488\,nm$. DAPI strongly binds with the A-T regions of DNA, which absorbs at a maximum of $358\,nm$ (ultraviolet) and is detected through an emission peak of $461\,nm$ (blue/cyan). Concerning Alexa Fluor $488nm$, this dye binds with the cytoskeleton's laminin, absorbs at a maximum of $495\,nm$ (visible) and is detected through an emission peak of $519\,nm$ (green). [80] [81]

3.4 – Statistical Analysis

Throughout the manuscript, all quantitative data is presented as mean $\pm$ stardard deviation. Statistical analysis was performed using GraphPad Prism 7.00 software. The significant differences were found when alpha is minor than 0.05 (p<0.05), using one-way ANOVA test with Tukey's multiple comparisons test. [82]

Chapter 4

Results and Discussion

4.1 – Materials Production

4.1.1 - PLLA Microparticles Production

The microparticles were agglomerated in large pieces as shown in Figure 4.1. The more the particle's size is decreased, the more the attractive forces between the specimen's molecules augment while they are maintained in the bottom of the drying chamber after production. Additionally, the obtained particles possessed a characteristic polystyrene texture, due to its polymeric plastic nature.

Figure 4.1 – Neat PLLA microparticle's agglomerates after production.

4.1.2 – PLLA Microparticles loaded into Hydrogel Production

In the preliminary study of loading MPs into the hydrogel, 20% (w/v) of PLLA microparticles were added. It was observed that most of the microparticles sited in the bottom of the container, separated from the remaining loaded sample, which indicates an overfill. Therefore, since the hydrogel behaves as the microparticles vehicle, the further synthetized samples would

require a much lower concentration of microparticles, which would only fill the interspace of its network.

The further tested hydrogel samples contained different amounts of microparticles loaded within – 0.5%, 1.0% and 1.5%. Subsequent SEM analysis of the samples would conclude that the sample loaded with 1.5% (w/v) of PLLA microparticles presented the suited morphology – chitosan-based hydrogel packed with MPs in its network - to be further characterized and compared with a sample without microparticles.

In Figure 4.2, it is observed a 0% MPs sample and 1.5% MPs sample. Visually, the samples could be distinguished, since the first presented transparency, whereas the second possessed an opaque white colour.
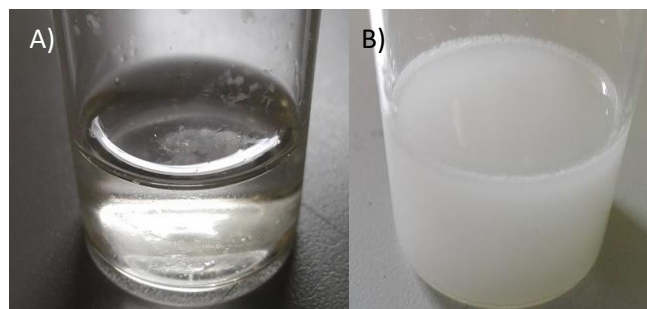
Figure 4.2 – Synthetized hydrogel maintained in liquid state. A) Resultant hydrogel without PLLA microparticles; B) Resultant hydrogel loaded with 1.5% of PLLA microparticles.

The material's injectability was preliminary tested by extrusion through a syringe. In the images of Figure 4.3, it is possible to observe its fluid passage through the syringe to the metallic support as well as the its gel like nature adhering to the referred support. Rheological tests are required to understand the material's behaviour when exposed to different shear stress frequencies as well as temperatures, since it may ultimately influence its injectability.

Figure 4.3 – Preliminary injectability of a 1.5% MPs sample through a syringe

4.2 – Materials Characterization

4.2.1 - PLLA Microparticles Characterization

4.2.1.1 – Scanning Electron Microscopy Analysis

At a first analysis, different portions of the studied specimen presented variable topography as it may be seen in Figure 4.4. With secondary electrons detector mode, it is possible to verify that one of the regions contains a dense spider like network, whereas in the other, that mesh is almost undetectable. This can be due to the high temperature inside the heat chamber during the solution's synthesis through the spray drying technique. The effect of polymeric chain's movement and reorganization is higher, with the increase of the temperature at which are exposed during time. Thus, when withdrawn from the heat chamber, the microparticles were starting a reorganization process at the surface of the collected stack. The particle's reorganization probably justifies the different topology of the regions observed in Figure 4.4, where Figure 4.4.A) is the surface of the stack and Figure 4.4.B) is its interior.
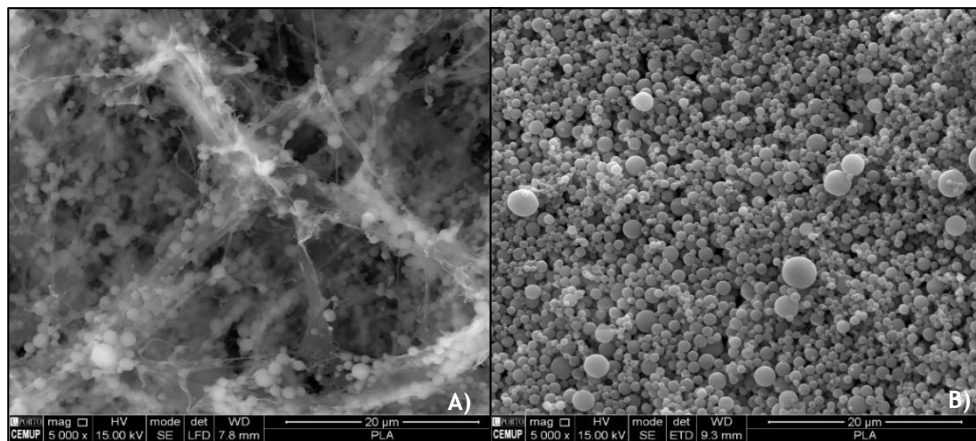
Figure 4.4 – SEM Analysis 1: Topography of the different facets of the specimen. A) Collected stack surface region. B) Collected stack interior region. Scale bar shows 20 μm magnification in both images

Furthermore, at the same magnification as the previous images, in Figure 4.5.A) it is possible to detect some collapsed and quite a few particles show no spherical shape as well. Moreover, the unevenness of the microparticles diameter size is observed in both images of Figure 5.3, in which the average calculated diameter was $(976 \pm 1084)\ nm$. The high standard deviation value reflects the unevenness of size, which could be caused at the time of the dissolution process of the PLLA pellets with the chloroform, where the granules complete dissolution was unsuccessful. Thus, a few particles became larger than others when drying in the heat chamber during the spray drying process

Figure 4.5 – SEM Analysis 1: Details of PLLA microparticles observed at a magnification of 20 μm. A) Collapsed and no spherical microparticles. B) Range of Microparticle's diameter sizes

As the analysis proceeded, an unusual contamination was detected with the backscattered electrons mode. In Figure 4.6.A), is possible to observe some moieties brighter than the regular specimen, which concludes that the highlighted component possesses a higher atomic number than the remaining chemical elements. Through the respective (EDS) analysis – Figure 4.6.B) -, tantalum (Ta) was identified, apart from the common chemical elements of the PLLA microparticles – Carbon (C) and Oxygen (O) - and the coating films – Au and Pd. Tantalum may have incorporated the sample through the drying process performed with a metallic device that contained Ta in its constitution.

Figure 4.6 – SEM Analysis 1: A) Detection of tantalum contamination through backscattered electron's mode observed at a magnification of 10 μm. B) Respective EDS spectrum.

4.2.1.1.1 – Microparticles Purification Method

In a visual analysis – Figure 4.7.A), the microparticle are dispersed, when compared with the agglomerates observed before the tantalum washing process. Additionally, the specimen possessed the textured of a polymeric powder.

A second SEM analysis was performed after the tantalum washing process, to verify if the PLLA particles were finally purified. At a half magnification as the anterior SEM analysis, in Figure 4.7.B), the size of the microparticles diameter is more consistent relatively to the sample before the washing process. Moreover, the average diameter is $(1.718 \pm 1.898)\ \mu m$, which is higher than the anterior. Moreover, since mainly the higher diameter ones were maintained, it is suspected that a same proportion of smaller microparticles were discarded in the supernatant upon centrifugation of the samples. Another feature that can be observed in Figure 4.7.B) is the absence of the dense network attained in the images prior the tantalum washing process. This is consistent with the visual image, in which the power is no longer aggregated. Instead, the microparticles are only interconnected and aggregated by a small link between them. The explanation is straightforward. Since in the centrifugation process, the particles were not exposed to high temperatures, the polymer chains did not go through another reorganization process.
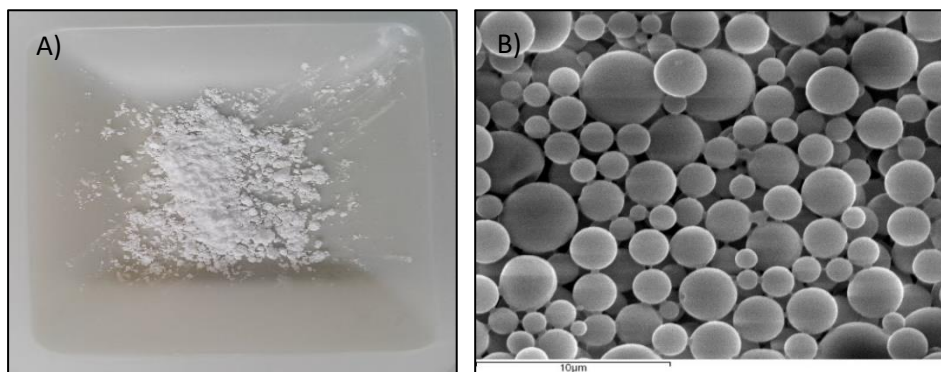
Figure 4.7 – A) Visible aspect of PLLA MPs after washing process. B) SEM analysis 2: Secondary electron's mode after Ta washing process. The scale bar shows 10 μm of magnification. The accelerating voltage is 15 kV and the working distance (WD) is 15 mm.

In figure 4.8, it was observed that the tantalum was completely washed away from the specimen which became completely purified. It can be verified in backscattered electron's mode – Figure 4.8.A) -, the inexistence of moieties brighter than the remaining sample. The respective EDS – Figure 4.8.B) - assures that the sample contains PLLA microparticles coated with Gold and Palladium.
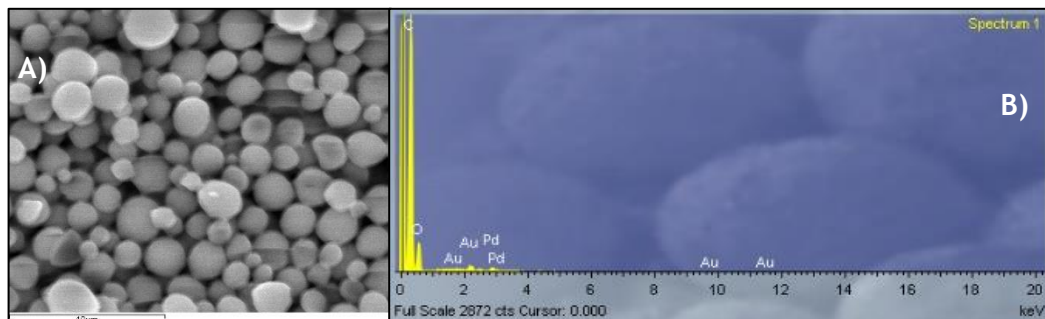
Figure 4.8 – A) SEM analysis 2: Backscattered electron's mode. Scale bar shows 10 μm of magnification. The accelerating voltage is 15 kV and the working distance (WD) is 15 mm. B) Respective EDS spectrum.

The conditions in which the PLLA microparticles were synthetized, its molecular weight and purity, for instance, influence its crystallinity degree, crystallization and thermal properties. [48] Thus, it is important to attain those properties to understand the biopolymer's effect on cells.

4.2.1.2 – Fourier Transform Infrared Spectroscopy

PLLA is the most common stereoisomer of PLA and can crystallize in the $\alpha-$, $\beta-$ or $\gamma-$ form, depending on its preparation conditions. The most common and stable polymorph is the $\alpha-$crystal PLLA. [49]

For every infrared wavelength value of the light beam hitting the sample, there is a respective characteristic energy value of transmittance. The downwards peaks correspond to an associated molecular group vibration in the specimen, with a type of crystallinity phase form. This infrared frequency (IR) peak values are unique for each material. Therefore, this analysis provides the specific fingerprint of a specimen. [83] FTIR analysis the crystallinity of a material's structure to denote if it is amorphous, or if it is crystalized in one of the three forms mentioned above.

Table 4.1 – Literature wavelengths and respective phase forms and vibrations of neat Poly (L- Lactide Acid). [83]

Wavelength (cm^{-1})	Phase Form	Vibration Assignment
860	Amorphous	
871	α	
908	β	
921	α	Coupling of the C-C backbone stretching with the CH$_3$ rocking mode
955	Amorphous	
1044	Amorphous, α' and α	ν(C-CH$_3$)
1053	α	ν(C-CH$_3$)
1092	α' and α	ν_s(C-O-C)
1107	α' and α	
1134	Amorphous, α' and α	r_s(CH$_3$)
1183	Amorphous, α' and α	ν_{as}(C-O-C) + r_{as}(CH$_3$)
1213	α' and α	ν_{as}(C-O-C) + r_{as}(CH$_3$)
1222	α	ν_{as}(C-O-C) + r_{as}(CH$_3$)
1268	Amorphous + semycrystalline	ν(CH) + ν(C-O-C)
1302	Amorphous	C-H stretching
1360	Semicrystalline	δ(CH), CH wagging (bending)
1363	Amorphous	δ(CH), CH wagging (bending)
1368	Semicrystalline	δ(CH), CH wagging (bending)
1382	α	δ_s(CH$_3$)
1386	α' and α	δ_s(CH$_3$)
1387	Amorphous	δ_s(CH$_3$)
1444	α	δ_{as}(CH$_3$)
1454	Amorphous	δ_{as}(CH$_3$)
1457	α' and α	δ_{as}(CH$_3$)
1749	α	ν(C=O)
1757	Amorphous	ν(C=O)
1759	α	ν(C=O)
1761	α'	ν(C=O)
2945	Amorphous	ν_s(CH$_3$)
2946	α' and α	ν_s(CH$_3$)
2964	α	ν_s(CH$_3$)
2995	Amorphous	ν_s(CH$_3$)
2997	α' and α	ν_{as}(CH$_3$)
3006	α	ν_{as}(CH$_3$)

By relating the downwards peaks of the infrared spectra obtained – Figure 4.9 - with the literature wavelength values and respective phase and vibration assignment listed in Table 4.1, a study of the PLLA crystalline development can be conducted.
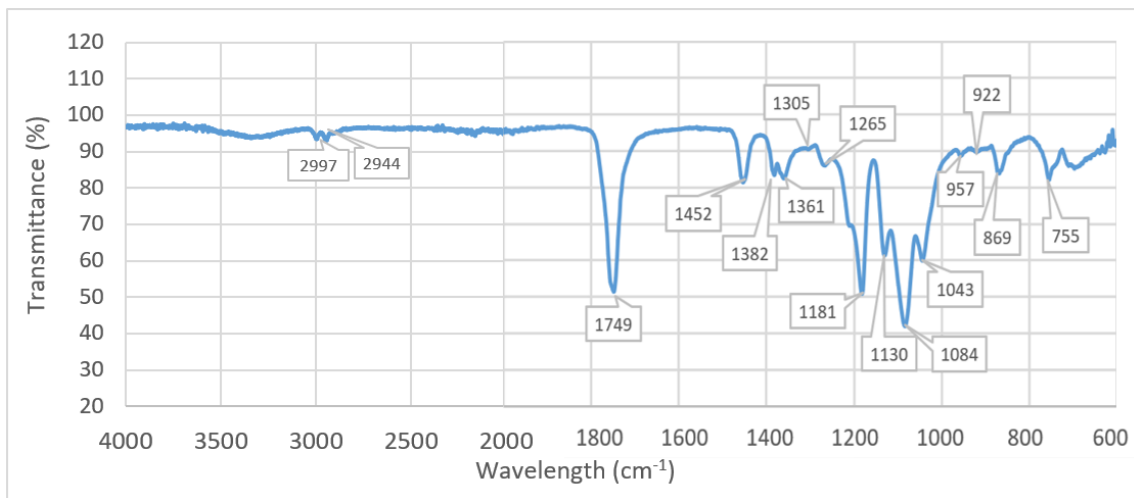
Figure 4.9 – Infrared spectra of correspondent transmittance percentage to every IR frequency. The characteristic downward peaks are marked with the respective wavelength value in cm^{-1}.

Firstly, analysing the spectrum from right to left, it is possible to denote that the characteristic $\beta -$ form PLLA crystal band at 908 cm^{-1} is absent, which indicates that the polymer does not crystallize in this form when the microparticles are being synthetized through the spray drying technique. Instead, the specimen appears to be primarily amorphous since most of the peak values obtained in the spectrum are relatively close to the literature values of this form. For a better comparison, Table 4.2 lists the obtained IR values with the coinciding literature wavelength peak values of Table 4.1, that only belong to the amorphous phase form.

Table 4.2 – Comparison between the obtained wavelength values on IR spectra and literature ones for the amorphous phase form, and respective vibrational assignment.

Obtained Wavelength value (cm^{-1})	Literature wavelength value (cm^{-1})	Phase form	Vibrational Assignment
957	955	Amorphous	
1043	1044	Amorphous, α' and α	$\nu(C\text{-}CH_3)$
1130	1134	Amorphous, α' and α	$r_s(CH_3)$
1181	1183	Amorphous, α' and α	$\nu_{as}(C\text{-}O\text{-}C) + r_{as}(CH_3)$
1265	1268	Amorphous + semycrystalline	$\nu(CH) + \nu(C\text{-}O\text{-}C)$
1305	1302	Amorphous	C-H stretching
1361	1363	Amorphous	$\delta_s(CH_3)$
1452	1454	Amorphous	$\delta_{as}(CH_3)$
2944	2945	Amorphous	$\nu_s(CH_3)$

Lastly, by analysing the remaining highlighted peaks, it is detected a 922 cm^{-1} IR frequency peak, which is approximated to the 921 cm^{-1} characteristic peak assigned to the coupling of C-C backbone stretching with the CH_3 rocking mode of PLLA $\alpha -$ crystals. However, it is almost indistinct, since it has broad width and non-steep height. Contrarily, within the IR frequency

range from 840 cm^{-1} to 880 cm^{-1}, the 869 cm^{-1} peak was is clearly observed in the spectra, and is approximated to the peak at 871 cm^{-1}, characteristic of $\alpha -$ crystals. [83] Additionally, other $\alpha -$ form characteristic peaks can be distinctively observed which cause vibration and stretching of the polymer's functional groups. The wavelength values that trigger the vibrations of -C-O-C symmetric, -C=O and -CH$_3$ asymmetric are 1084 cm^{-1}, 1749 cm^{-1} and 2997 cm^{-1}, respectively. Whereas the only IR frequency that causes stretching is 1382 cm^{-1}, being symmetric in the functional group -CH$_3$. Concluding, the crystallinity of the used PLLA is very low, but not inexistence, since it also possesses a relatively small percentage of $\alpha -$ form crystals complementing the main amorphous characteristic crystals. It is stated that the permeability of gases in a polymer decreases with crystallinity. [45] So, since the PLLA Microparticle's crystallinity is very low, this polymer possesses a high permeability towards gases. Thus, the studied biomaterial possesses a beneficial characteristic to allow gas exchanges through cells, which enhances their proliferation.

4.2.1.3 – Differential Scanning Calorimetry

DSC allows the knowledge of the material's stability to heat by attaining its transition temperatures, such as glass, cold crystallization and melt. [84]
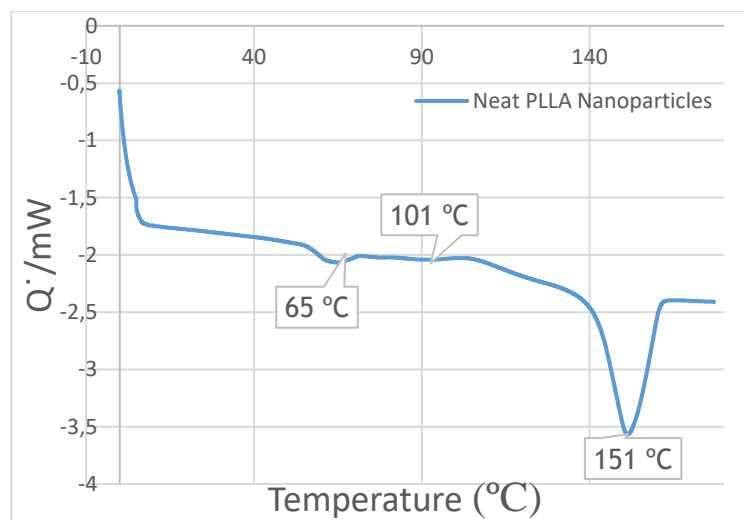
Figure 4.10 – DSC normalized thermogram of employed neat PLLA microparticles.

The three points labelled in the thermogram above correspond to the state's transitions. The endotherm peaks coincide to glass (T_g) and melt (T_m) transition temperatures at $65\,°C$ and $151\,°C$, respectively. In literature, PLLA fibres with similar molecular weight obtained a $T_g = 65\,°C$ and a $T_m \approx 180\,°C$. [85] Thus, the obtained glass transition temperature was close to the reported one, whereas the obtained melting temperature was about 30°C lower than the stated. [8] Although the obtained value is very low, the synthesis conditions were not equal, which can influence the overall properties of the final product. Therefore, the melting temperature can differ from one material to another, since it is related with its specific production conditions as well as molecular weight.

The broad exotherm peak represents the cold crystallization transition temperature (T_c) at $101\,°C$. T_c transition state corresponds to a broad peak on the thermogram, perchance due to the studied biopolymer's high molecular weight. In literature, Migliaresi C., *et al,* reports a possible relation between the molecular weight of PLLA and T_c transition state. By comparing polymers with diverse molecular weights, they notice that higher molecular weight PLLA's - $M_w = 2.3\,\times 10^5\,Da$ -, presented a higher range of temperatures in the T_c transition. This occurs, since higher molecular weight polymers possess longer chains, which decrease the molecular mobility. The feasible motion of the molecules is required for faster crystallization to occur. Thus, while a low molecular weight amorphous polymer – $M_w = 8.5\,\times 10^4\,Da$ - is able to rapidly crystallize, longer chained polymers, representative of the higher molecular weight property, require a higher T_c transition phase. Bearing in mind that the studied PLLA's molecular weight is between $2.17\,\times 10^5\,Da$ and $2.25\,\times 10^5\,Da$, this theory is highly conceivable to demonstrate the used polyester's kinetics in the T_c transition phase. [8]

Another property that can be retreated from the DSC thermograph is the melting enthalpy (ΔH_m), which is related to the crystalline form of the polymers. By computing the area above the curve of the melt transition event – Figure 4.11 -, the obtained value is $2.3\,J/g$. Taking into consideration that the enthalpy of melting for a 100% crystalline PLA sample is $93\,J/g$. [8] Thus, the small cold crystallization transition obtained in the DSC outcomes, corroborates the mainly amorphous state of the PLLA particles concluded by the FTIR analysis.
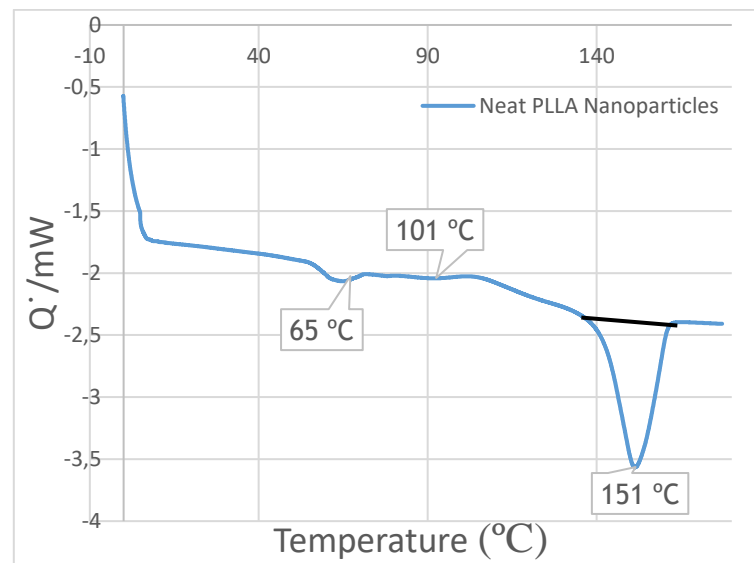
Figure 4.11 – The area delimited by the curve of the melt transition event and the black line was considered to compute the melting enthalpy through the OriginLab software

4.2.1.4 – Thermogravimetric Analysis

The kinetics of the different decomposition processes through various heating rates may facilitate the recognition of the thermal degradation mechanisms of the polymer in study. [85] Figure 4.12.A) shows TGA data obtained for the neat PLLA microparticles at various heating

rates. Their respective differential degradation curves (DTG) are plotted in the graph of Figure 4.12.B).

On both graphs, a characteristic is noticeable. The TGA and DTG curves translate towards higher temperatures as the heating rate tests are increased from $10°C/min$ to $40°C/min$.
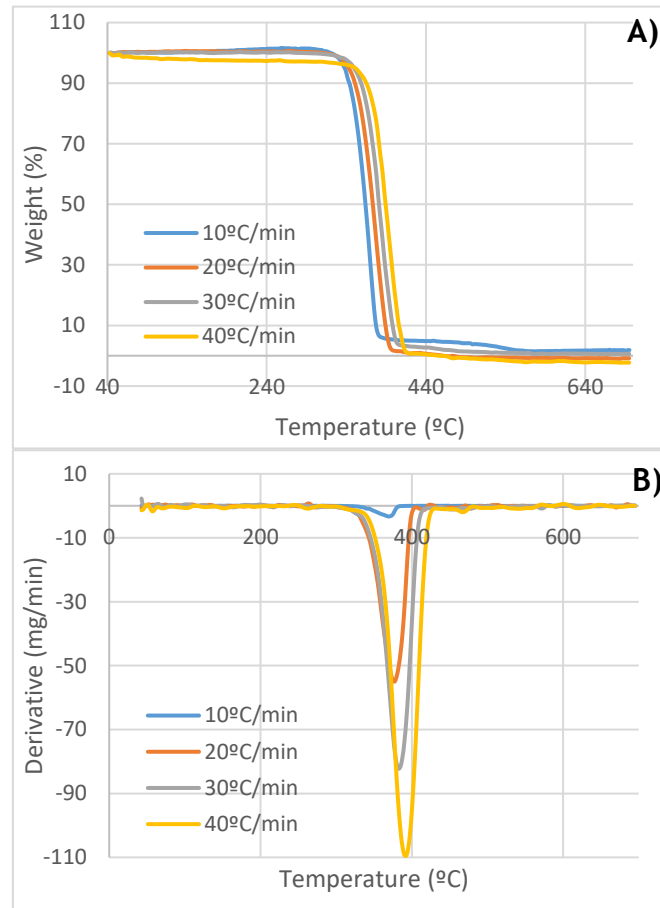
Figure 4.12 – [A] TGA and [B] DTG results of neat PLLA microparticles at various heating rates.

Moreover, it is noticeable that the weight of PLLA microparticles steeply decline when temperatures exceed approximately $350°C$, until $420°C$. At $10°C/min$ and $20°C/min$, only the slightest amount of undecomposed material is observed when temperatures exceed $420ºC$. At higher heating rates, the weight percentage reaches negative values.

Two temperature values were retrieved from the TGA curves for each heating rate: the initial temperature (T_i) and the onset temperature (T_o). The first is the temperature at which the experimental curve deviates from the tangent line that the mass evolution follows before degradation. The latter is the computed temperature by extending the pre-degradation portion of the curve to the point of the interception with a line drawn as a tangent of the steepest portion of the mass curve occurring during degradation. [85] The DTG curves allow the retrieval of the temperature on the inflection point of the thermogram (T_p). The last is the temperature that corresponds to the maximum degradation point of the microparticles. The mentioned retrieved temperatures for each heating rate are listed in Table 4.3.

Table 4.3 - T_i, T_o and T_p for each heating rate of the TGA experiment of neat PLLA microparticles.

Heating Rate	T_i ($^{\circ}C$)	T_o ($^{\circ}C$)	T_p ($^{\circ}C$)
10 $^{\circ}C/min$	324	381	369
20 $^{\circ}C/min$	337	395	378
30 $^{\circ}C/min$	345	402	383
40 $^{\circ}C/min$	353	415	393

4.2.1.4.1 – Material's thermal kinetics

TGA monitors a polymer's decomposition during increase of temperature in a specific heating rate. In theory, the general expression applied in all kinetic studies is described by the fundamental rate equation:

$$\frac{\partial \alpha(t)}{\partial t} = k(T) \times f[\alpha(t)],$$ (Eq.4)

where α is the reactant concentration loss and k is the rate constant. Thus, Eq. 4 expresses the conversion rate - $\frac{\partial \alpha(t)}{\partial t}$ – over time, at a stable temperature, as a function of the reactant concentration loss and rate constant [64]. α is defined by:

$$\alpha = \frac{w_o - w_t}{w_o - w_c},$$ (Eq.5)

where w_o, w_t and w_c are the sample weights before degradation, at a given time t and after complete degradation, respectively. [86] Rate constant - k – changes in function of absolute temperature - T – and is expressed by the Arrhenius equation:

$$k(T) = A \exp\left(-\frac{E_{aa}}{R \times T}\right),$$ (Eq.6)

where A (min^{-1}) is the pre-exponential factor, E_{aa} (kJ/mol) is the apparent activation energy, $R = 8.314$ [$J/(k.mol)$] is the gas constant and T ($Kelvin$) is the absolute temperature. [64] The differential conversion function - $f[\alpha(t)]$ – for solid state reactions may present various functional forms. The most commonly used form is expressed as:

$$f[\alpha(t)] = (1 - \alpha)^n,$$ (Eq.7)

where n is the reaction order, which remains constant during the entire degradation process. [87] By combining Eq. 4 and Eq.6, Eq. 8 is obtained.

$$\frac{\partial \alpha(t)}{\partial t} = A \exp\left(-\frac{E_{aa}}{R \times T}\right) . f[\alpha(t)]$$ (Eq.8)

The performed TGA was dynamic, so the heating rate – β (Eq.9) - needs to be a part of the thermal kinetics expression. Thus, combining Eq.8 and Eq.9 in Eq.5, Eq.10 is obtained:

$$\beta = \frac{\partial T}{\partial t} \tag{Eq.9}$$

$$\frac{\partial \alpha}{\partial T} = \frac{A}{\beta} exp\left(-\frac{E_{aa}}{R \times T}\right).(1-\alpha)^n \tag{Eq.10}$$

Equations 5 and 7 are the fundamental expressions of analytical methods to compute kinetic parameters on the basis of TGA data results. [87] The method applied in this work to evaluate the activation energy was the Kissinger method, which is expressed by the equation:

$$ln\left(\frac{\beta}{T_p^2}\right) = \frac{ln(A \times E_{aa})}{R} + ln\left[n\left(1-\alpha_p\right)^{1-n}\right] - \frac{E_{aa}}{R \times T_p}, \tag{Eq.11}$$

where T_p is the absolute peak temperate of each heating rate obtained from the differential degradation curves and α_p is the reactant concentration loss at the maximum weight lost rate. Thus, T_p is the absolute temperature at the α_p point. [64]

Kissinger's method is fast, easy to use and the most reliable within similar methods. Since the thermal degradation of PLLA is a first-order reaction, the apparent activation energy is determined from a simple plot. $ln\left[\beta/(T_p)^2\right]$ versus $(1000/T_p)$ is plotted for each peak temperature from a series of tests at different heating rates. The slope of the function (Eq.12), is obtained – Figure 5.11 - and the apparent activation energy can be calculated. Therefore, bearing in mind that the tests in this work were performed in different heating rates (10 ℃/min⁻¹, 20 ℃/min⁻¹, 30 ℃/min⁻¹ and 40 ℃/min⁻¹), this method is the most indicated to determine the kinetic parameters of the data results. [64], [88]

$$m = -\frac{E_{aa}}{R}, \tag{Eq.12}$$

where R is the gas constant with the value of 8.314 $[J/(k.mol)]$. Figure 4.13 shows the plot with the linear tendency line and its respective equation.
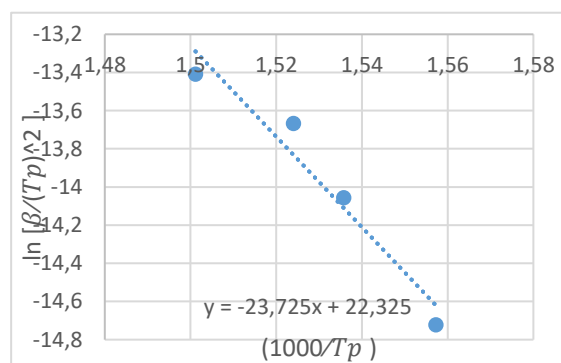
Figure 4.13 – Linear tendency line and its respective equation obtained with Kissinger's method for neat PLLA microparticles.

Thus, after computing, the obtained value for the apparent activation energy is 197 Kj/mol. In literature, through Kissinger's method, a few studies reported neat PLLA fibres, which possess the same molecular weight as the microparticles, sea exhibited lower E_{aa}. Sencadas V., *et all* and Santos D., *et all* analysed neat PLLA fibres, being the resultant apparent

activation energy $157\ kJ/mol$ and $134\ kJ/mol$, respectively. [64] [89] Taking into consideration that these composites were moulded into different structures and synthesized with a dissimilar method – electrospinning -, the overall thermal properties of the same material can vary. Thus, the apparent activation energy can be influenced by the material's morphology.

4.2.2 – PLLA Microparticles loaded Hydrogel Characterization

4.2.2.1 – Scanning Electron Microscopy Analysis

Hydrogel samples loaded with 0.5%, 1% and 1.5% of PLLA microparticles were morphologically analysed through scanning electron microscopy to select the one to be further characterized as a test sample and compare to the control one.

Overall, in the images below – Figure 4.14 -, it is possible to observe irregularities in the overall material. This is due to the high voltage of the electron beam at which the samples were exposed for long periods after dehydration in the incubator, which consequently disturbed the hydrogel's morphology.

Figure 4.14 - SEM images of chitosan hydrogel loaded with different ratios of PLLA microparticles. A) 0.5% (w/v); B) 1% (w/v), C) 1.5% (w/v). The accelerating voltage is 15 kV and magnification at 50 μm.

The three hydrogels present the same concentration of matrix components, since they were synthetized from the same sample before being loaded with different ratios of microparticles. In the images above, an unsmooth morphology is observed, which is due to the reticulation process characteristic of both chitosan/GPTMS and chitosan/β-GP hydrogels, as also reported in literature. Moreover, a skin layer is formed at the surface due to the dehydration of the hydrogel during its incubation at 55ºC overnight. [23], [90]

At Figure 4.14.A), the microparticles cannot be distinguished from the hydrogel matrix, since the dense network of reticulating bonds between the components predominates throughout the sample. In Figure 4.14.B), it is possible to observe a few spherically shaped structures, that can possibly represent PLLA MPs. Here, the network is less dense, showing some porosity, which indicates higher length bonds between the matrix's components. The hydrogel loaded with 1.5% of MPs – Figure 4.14.C) - presents more uniformity throughout particle distribution and the less dense network connecting the matrix components. Since in this sample is denoted a greater particle distribution in the hydrogel's matrix and less dense morphology, this sample was chosen as the test sample to be further compared with a matrix solely hydrogel, to understand if the microparticles influence the reticulating activity that GPTMS and β-GP exert on chitosan.

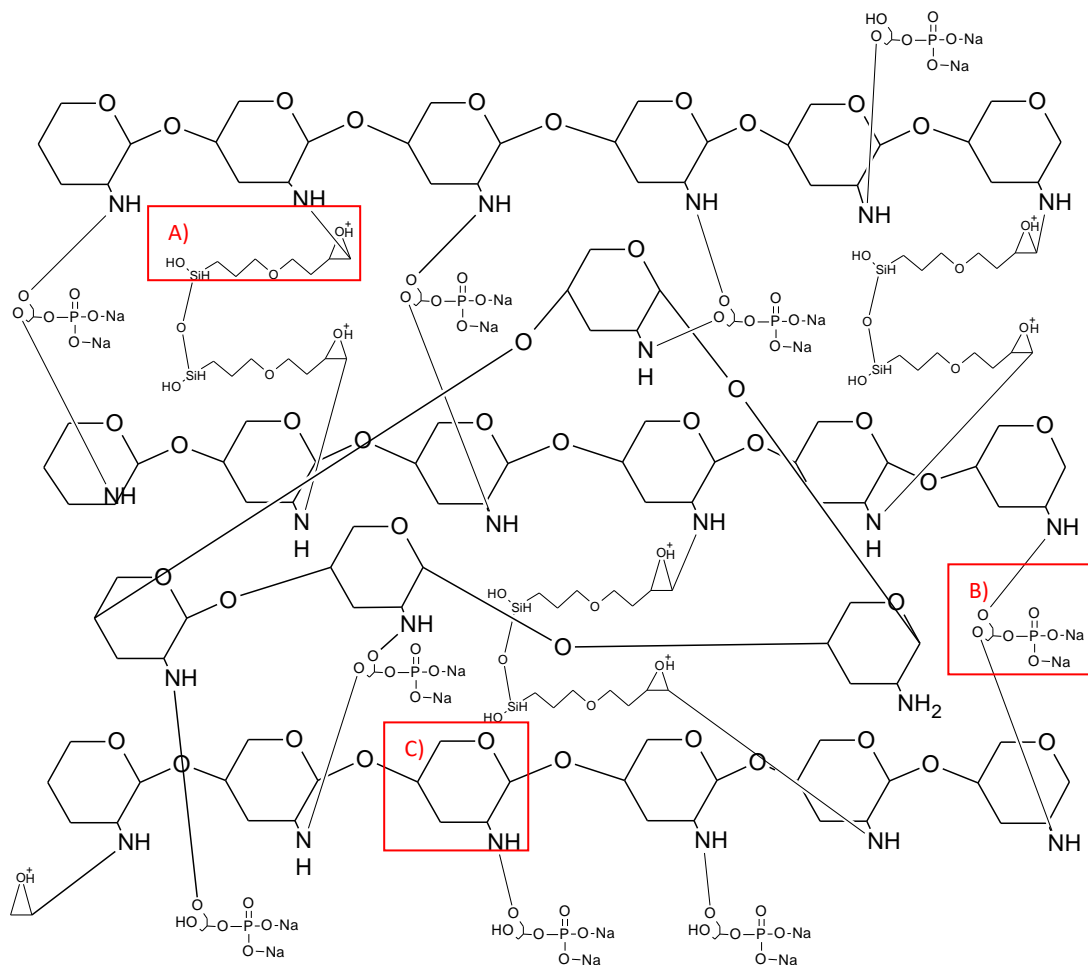## 4.2.2.2 – Fourier Transform Infrared Spectroscopy – Attenuated Total Reflectance

Figure 4.15 – Possible chemical structure of the synthetized chitosan/GPTMS/ β-GP hydrogel without PLLA microparticles. A) GPTMS; B) β-GP; C) Chitosan

In order to acknowledge the existent chemical bonds between the chitosan and the reticulating agents – GPTMS and β-GP –, FTIR was performed to attain the functional groups present in the 0% MPs sample, as well as in the 1.5% MPs sample. Their possible chemical structure was illustrated with ACD/Labs software and is represented in Figures 4.15 And 4.17, respectively. [91]

Table 4.4 presents the characteristic wavelength of the functional group's vibration that are assigned to the different compounds of the hydrogel. Relating this literature values with the FTIR spectra obtained – Figure 4.16, it is possible to confirm the present functional group bonds between the molecules, which provide information about the reticulating process between the components of the hydrogel.

Table 4.4 - Functional group vibrations and corresponding literature wavelength bands of each compound. [92]

Wavelength Band (cm^{-1})	Peak Characterization	Functional Group Vibration Assignment	Assigned Compound
3700-3200	M	O-H str	Silicon
3580-3200	m; br	O-H str	Hydroxy
3550-3100	M	$N-H^+$ str	Amine
3500-3300	M	>N-H str	Amine
3300-2500	W	O-H str	Carboxylic Acid
$\simeq$1680	Br	P=O def	Phosphorous
1475-1400	W	$Si-O-CH_3$ rock	Silicon
1280-1150	W	NH_3^+ rock	Amine
1250-1175	W	$SiCH_2R$ def	Silicon
1090-1010	Vs	Si-O str	Silicon
$\simeq$1100	m-s	Ch_2-O-Ch_2 str	Ether
$\simeq$1050	Vs	OH-C	Hydroxy
1040-910	m-s; br	P-O str	Phosphorous
995-945	m-s	$ROPO_3^{2-}$	Phosphorous
985-800	m-s	Si-H def	Silicon
880-775	m-s	G_1-O-G_2 ring	Ether
710-570	w-m	O-H out of plane def	Hydroxy
660-600	m; br	O-H out of plane def	Hydroxy
610-480	Vs	Si-O-Si symmetric str	Silicon
570-390	w-m	C-O def	Hydroxy
500-450	w-m	C-O in plane def	Hydroxy

Caption words - Peak intensity: w - weak; m - medium; s - strong; vs - very strong
                          Peak width: br - broad
                          Type of vibration: str – stretching; def – deformation, rock - rocking

By analysing the FTIR spectra – Figure 4.16 -, the first peak observed from left to right can be assigned to multiple functional groups, which possess characteristic wavelengths overlapped in this section – (3700-2500 cm^{-1}). Takes part in this region, characteristic peaks of O-H and N-H^+ stretching of GPTMS and chitosan's molecules, respectively. Additionally, it contains the >N-H stretching vibration, which indicates the bond between GPTMS and chitosan, and O-H stretching of hydroxy groups, which can be assigned to the bond between chitosan and a β-GP, as observed in Figure 4.15.

Concerning the peak situated amid the spectra – 1663 cm^{-1} -, it is confirmed from the literature that it corresponds to the characteristic deformation vibration of the phosphorous group – P=O – of β-GP. The two weak intensity peaks – (1475-1400 cm^{-1}) and (1250-1175 cm^{-1}) - are characteristic of the $Si-O-CH_3$ rocking and $Si-CH_2$R deformation vibrations occurring in the GPTMS's molecule. The peak in between – (1280-1150 cm^{-1}) – corresponds to the rocking vibration oh the functional group NH_3^+ of chitosan.

After this point, the spectrum acquires medium to strong intensity peaks, being the first related to the Si-O functional group stretching of GPTMS and the following – $\simeq 1100$ cm^{-1} –, characteristic of the CH$_2$-O-CH$_2$ stretching bond that connects two chitosan molecules, as it can be observed in Figure 4.15. The last is overlapped with the highly absorbed hydroxyl group peak of the bond between a carbon and a hydroxy group - $\simeq 1050$ cm^{-1} – present within chitosan and β-GP molecular structure.

The following peak is an overlap of three functional groups characteristic wavelengths – (1040-910 cm^{-1}), (995-945 cm^{-1}) and 985 and 800 cm^{-1}. The first two correspond to the phosphorous components of β-GP. More specifically, the first corresponds to a stretch of the P-O functional group and the second is representative of the symmetric stretching between the OPO$_3$$^{2-}$ and Na groups. The last is the characteristic peak of Si-H functional group deformation of GPTMS.

It is denoted that the higher intensity peaks (lower % of transmittance) are characteristic of the phosphorous components of β-GP, or its bond with chitosan. This is justified by the higher quantity of β-GP incorporated within the matrix, relatively to the remain compounds.

Figure 4.16 – FTIR spectra of the synthetized chitosan/GPTMS/ β-GP hydrogel without PLLA microparticles.

Furthermore, the ether characteristic peak between 880-775 cm^{-1} is specific to the ring deformation between the chitosan molecules in the G$_1$-O-G$_2$ bond. The broad medium peak between 660-600 cm^{-1} corresponds to the O-H out of plane deformation between the hydroxy group in the different components of the hydrogel – chitosan, GPTMS and β-GP. The following low transmittance peak – (610-480 cm^{-1}) corresponds to the connection between two molecules of GPTMS, representing the symmetric stretching between Si-O-Si. This one is overlapped with a medium intensity one in the wavelength band of 570-490 cm^{-1}, which is characteristic of a C-O deformation of hydroxy groups present in chitosan and GPTMS. The last peak centred at 455 cm^{-1} also corresponds to a C-O deformation of the same compounds, but this specific vibration is in plane with the molecule.

Thus, it is possible to confirm that GPTMS and β-GP bonded with chitosan, since the characteristic peaks of the functional groups that interconnect their structures are observed in the resultant FTIR spectra. Moreover, the bond between chitosan molecules is also evident, as

well as the assemble between two GPTMS structures, which allows the connection between two chitosan molecules.

The microparticles were incorporated within the hydrogel – Figure 4.17, with the purpose to potentialize its regenerative promoting properties, since it was previously demonstrated that PLLA is able to accelerate the tissue formation process of gingiva.

Figure 4.17 – Possible chemical structure of the synthetized chitosan/GPTMS/ β-GP hydrogel loaded with PLLA microparticles. A) PLLA.

A FTIR spectra of the hydrogel sample loaded with 1.5% (w/v) of PLLA MPs was also obtained and compared with the FTIR spectra of solely matrix and only PLLA microparticles – Figure 4.18 -, to perceive if the incorporation of the MPs disrupted the reticulation process previously achieved. At a first glimpse of the test sample's FTIR spectra, it is denoted that the peaks are roughly in the same wavelengths as in the spectra of the control sample. Thus, it can be presumed that the reticulating bonds observed between the hydrogel matrix components were not cleaved. However, it is noticed that the mentioned peaks are comparatively lower in absorbance intensity. As it can be observed in the illustrated chemical structures of the samples, the solely matrix hydrogel contains higher concentrations of chitosan and reticulating agents, whereas the loaded MPs hydrogel, by containing 1.5% (w/v) within its structure, decreases the molecules concentration ratio of the matrix in the overall gel. To better understand the concentration ratios between the matrix and the MPS, the weight to volume ratio can be converted to volume/volume ratio, as follows:

$$\rho_{PLLA} = 1.27 \ g/cm^3 \qquad \text{(Eq.13)}$$

$$1.5\% \ (w_{PLLA}/v_{matrix}) \rightarrow 1.5 \ g \ of \ PLLA \ to \ 100 \ mL \ of \ matrix \qquad \text{(Eq.14)}$$

$$\rho_{PLLA} = \frac{m_{PLLA}}{v_{PLLA}} \leftrightarrow v_{PLLA} = m_{PLLA} \times \rho_{PLLA} \leftrightarrow v_{PLLA} = 1.5 \times 1.27 \leftrightarrow v_{PLLA} = 1.905 \ mL \ \text{(Eq.15)}$$

$$\frac{\% \ (v_{PLLA}/v_{matrix})}{100} \times 100 = 1.905 \ \leftrightarrow \% \ (v_{PLLA}/v_{matrix}) = 1.905 \qquad \text{(Eq.16)}$$

For the pure 0% MPs sample, the concentration of the matrix is at its maximum – 100% -, whereas for the samples that contains PLLA MPs – the concentration of the matrix decreases to 98.095%. Thus, the diminishing of the peaks intensity is due to relatively lower matrix concentration within the hydrogel. [93]
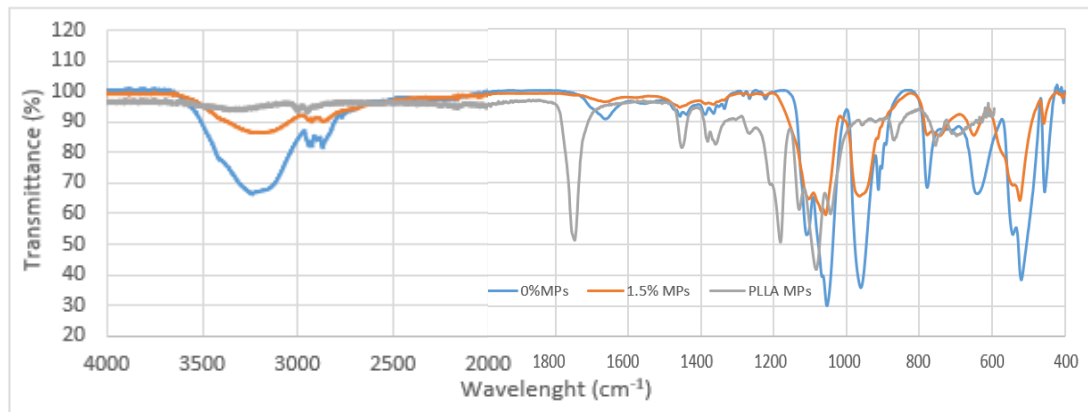

Figure 4.18 – Comparison between the FTIR spectra of both hydrogel samples as well as only PLLA MPs.

Comparing the FTIR spectra of the test sample with the solely MPs one, almost none of the peaks coincide. As described previously, right after the microparticle's synthesis, these ones are highly agglomerated and microscopically possess a dense network interconnecting them, due to the reorganization process suffered during its production in the heat chamber of the spray dryer. The solely MPs FTIR spectra was performed at that point, being also a different batch of microparticles than the ones obtained for the hydrogel's synthesis, free of tantalum contamination. Moreover, the washing process performed to remove the tantalum from the obtained microparticles cleaved and withdrawn the previous dense network, dispersing the MPs in a thin dust. Additionally, only the larger in diameter microparticles remained, since the smaller ones were withdrawn with the less dense tantalum particles. Therefore, the PLLA MPs highly intensity peaks observed in its spectra are characteristic of the strong and short bond between the molecules, since they were agglomerated and densely packed by the surrounding network. Contrarily, since the MPs incorporated into the hydrogel were dispersed throughout the matrix, its characteristic peaks are much more complex to identify. Furthermore, concerning the matrix in the test sample, the concentration of the PLLA MPs is relatively minor – 1.905% (v/v) – and thus, the matrix characteristic peaks predominate in the spectra.

As mentioned previously, the reticulation process increases the material's mechanical properties, which consequently can decrease its gelation time at physiological temperatures. Moreover, it also diminishes its degradation time, which is relevant for applications in acidic environments, characteristic of gingival lesion areas. [71] The conclusion of the FTIR spectra provided information about the reticulating crosslinks between the hydrogels components, that are strongly present within the network, due to the high intensity of its characteristic peaks.

4.2.2.3 – Swelling and Degradation Studies

The swelling test attained the swelling degree at each time point, which was calculated following the norm:

$$S\ (\%) = \frac{W_t - W_i}{W_i} \times 100, \tag{Eq.17}$$

where W_i is the weight of the dried sample before being immersed in artificial saliva and W_t is the weight of the sample upon immersion in artificial saliva at the time interval considered. [94]

The degradation test attained the weight percentage at each time point, which was calculated following the norm:

$$Weight\ (\%) = \frac{W_t}{W_i} \times 100, \tag{Eq.18}$$

where W_i is the initial weight of the sample and W_t is the weight of the sample after being immersed in artificial saliva at the time interval considered. [73]

At a first glimpse of both tests in the following images – Figure 4.19 and Figure 4.20-, it is denoted a mild progressive weight gain in the swelling phase for both samples – 0% MPs and 1.5% MPs - regarding the saliva's pH at which were immersed during 15 min. This behaviour is denominated as swelling and it is expected in these type of polymers, since hydrogels are networks that expand within aqueous solutions, as previously explained. Thus, in these conditions, the samples attained the artificial saliva's molecules in its bulk and consequently expanded, which is reflected on their weight gain. A statistical analysis of the samples in the swelling stage, concludes that there were significant differences between the hydrolytic and enzymatic tests, which corresponds to a 3.74% higher increase in weight by the samples in the hydrolytic test relatively to the ones in the enzymatic test.

Figure 4.19 – Hydrolytic Swelling and Degradation test of samples without MPs and with 1.5% of MPs at pH values 7.3 and 5 immersed in neat artificial saliva.

Concerning the degradation graph of Figure 4.19 of the hydrolytic test, the samples immersed in saliva's pH of 7.3 progressively degrade, whereas the ones immersed at pH=5 had a dissimilar result. The statistical analysis between 0%MPs and 1.5% MPs samples immersed in the acidic pH did not show significant differences. The high values of standard deviation

observed, demonstrate the errors associated in those measurements. Thus, it can be concluded that the weight did not augment, instead the samples maintained maximum swelling observed in the 15 minutes of the swelling test. This can be explained by the results of some previous swelling studies performed on chitosan hydrogels. It is reported that the pH values of the environment where these specimens are placed, influences its weight. Specifically, at acidic pH values, chitosan hydrogels reach maximum swelling, whereas at basic pH, the hydrogel reduces in size. This is explained by protonation, which is the formation of conjugated acids between its amino groups. This phenomenon only occurs at pH values below the chitosan's acid dissociation constant – pKa - of about 6.5. Therefore, in acidic conditions, the formation of conjugated acids leads to repulsion between the polymer chains, which allows the network to expand in size and consequently attain solution within. Contrarily, in basic conditions, the deprotonation predominates, which leads to the reduction of repulsion between the polymer chains, and thus, the hydrogel shrinks in size and withdraws its own water to the surrounding solution. Thus, at pH of 5, the weight was maintained, since the repulsive forces are still present within the chitosan hydrogel's network, which attains in its interior the molecules of the surrounding solution. Contrarily, in basic pH conditions, the decrease in weight is due to the removal of the polymeric network's own solution to the medium as well as its own degradation. [95], [96]
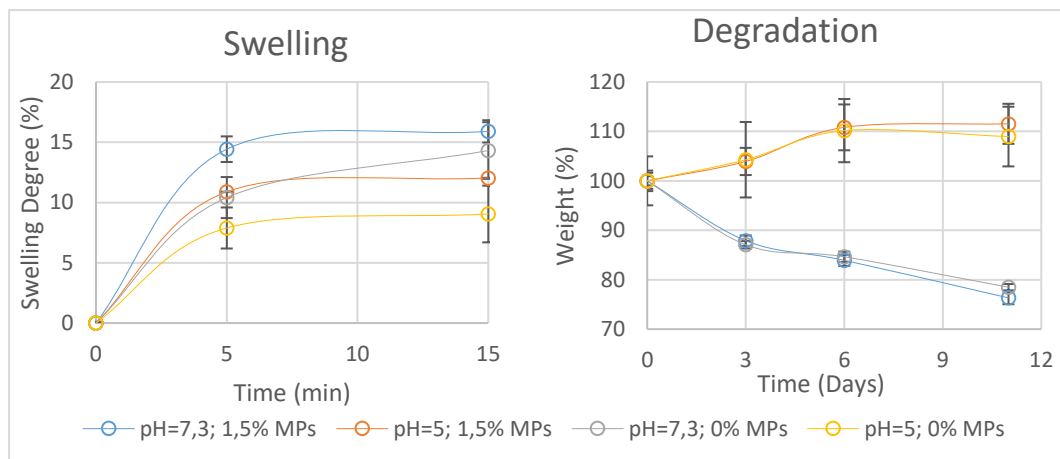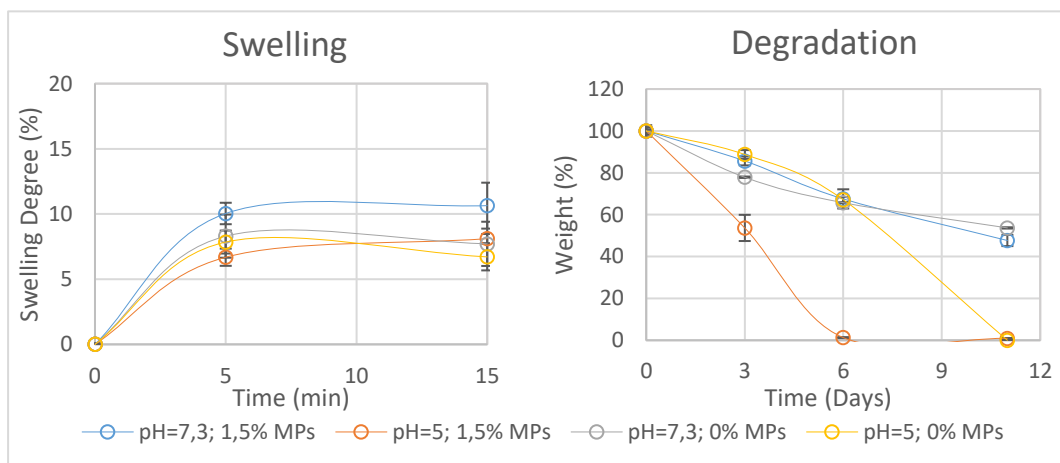

Figure 4.20 - Enzymatic Swelling and Degradation test of samples without MPs and with 1.5% of MPs at pH values 7.3 and 5 immersed in artificial saliva with lysozyme concentration of 20 mg/mL and 16 mg/mL, respectively.

In the right placed graph of the enzymatic degradation test, the degradation of samples immersed in a pH of 5 is accentuated. As previously explained, the samples immersed at acidic pH values, attains the surrounding solution in its bulk, which facilitates its access to the crosslink chains between the different composites of the hydrogel. In the enzymatic test, there is addition of an oral mucosa enzyme, denominated as lysozyme, which cleaves the matrix's crosslinks. Therefore, by attaining the lysozyme containing solution in its bulk, the hydrogel's links are more prone to be degraded, comparably to the hydrolytic test. Thus, the accentuated decrease in weight at day 3 is explained by the disruption of the hydrogel's microstructure, and part of the sample was degraded by the enzymatic action of the solution. In the hydrolytic test, this effect was not observed at pH of 5, since the only hydrolytic degradation was in action, which was not enough to disrupt the hydrogel's microstructure. At day 6 of the enzymatic test, the 1.5% MPs sample lost all the chitosan matrix weight and maintained the microparticles

weight, whereas the 0% MPs samples decreased its weight to the initial values. The higher degradation rate of the hydrogel matrix loaded with MPs is due to its network being expanded by the addition of polymeric particles in its bulk, and so, the crosslinks are more disperse, lengthy and consequently weaker, comparing to the 0% MPs samples. This facilitates the action of the lysozyme, as previously explained. [96] At day 11, the 1.5% MPs samples only maintained the microparticles weight, whereas the samples without microparticles were completely degraded. This is explained by the difference between the degradation rates of the hydrogel and the microparticles, since PLLA takes 6 to 12 months to degrade completely, whereas the synthetized chitosan-based hydrogel only takes 28 days to lose 80% of its initial weight hydrolytically, as reported by Shirosaky. Thus, the weight of the non-degraded microparticles continues to be acquired in the samples containing 1.5% MPs. [25], [33]

Additionally, in the enzymatic test of the samples immersed on pH of 7.3, these ones decreased its weight most intensely relatively to the samples in the hydrolytic test. This is explained by the presence of lysozyme in the artificial saliva's solution, since it degrades the polymer in an enzymatic manner apart from hydrolytic, by cleaving its subunits, which degrades it in a faster rate than the saliva's solution without lysozyme.

The pH changes that a biomaterial can induce once in direct contact with the human body, are a very important factor to consider, since the diminishing of the pH of the affected region can augment its probability to become inflamed. Thus, a monitoring of the saliva's pH was performed at each weight in of the samples – Figure 4.21.
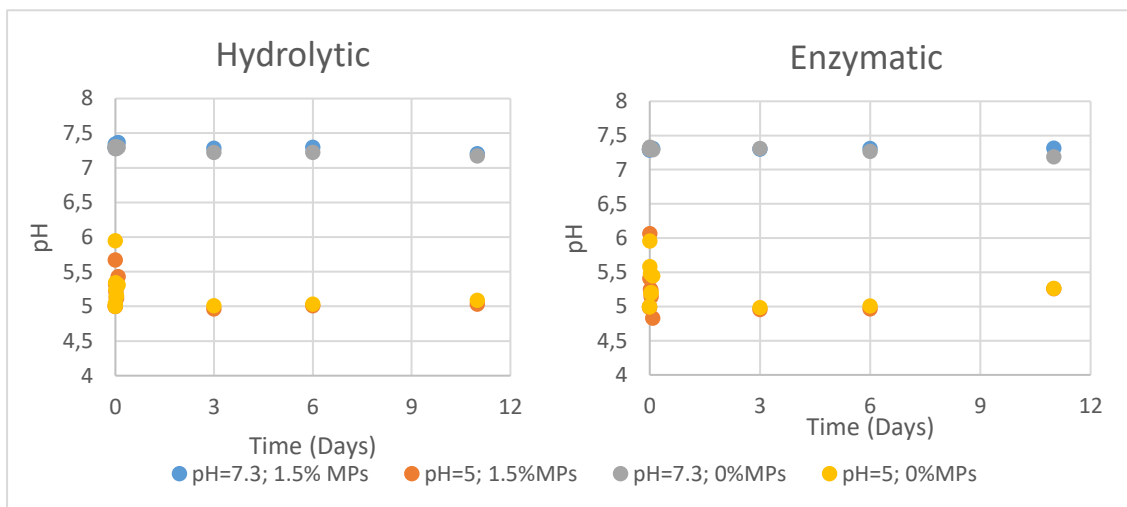
Figure 4.21 – Artificial saliva's pH after immersion with the samples at the time points of their weight in. Enzymatic saliva with pH=7.3 and pH=5 contains 20mg/mL and 16mg/mL of lysozyme, respectively.

As it can be observed in the graphs of the pH monitoring outcomes, in both hydrolytic and enzymatic tests, the saliva's pH of 7.3 roughly maintained the same values throughout all measurements of the test. However, observing the graphical results of the saliva with pH of 5, it is denoted an augment to nearly neutral pH values, and then a gradual decrease to the initial acidic pH value. Bearing in mind that the hydrogel samples final pH was 7.3, it is expected that when immersed in a solution at pH of 5, the water molecules in its bulk would merge with the solution molecules attained inside as well, and so the pH inside the hydrogel, as well as within the solution balance each other. Further fresh artificial saliva with a pH of 5 immerses the same

sample with progressively decreased pH, at different time points. Thus, it is expected, by the same line of thought that the sample's and solution's pH would ultimately equalize, which is observed within 3 days after sample's immersion in artificial saliva with pH of 5. This is indicative that the hydrogel samples, regardless of being loaded with PLLA MPs or not, do not influence the artificial saliva's pH, which is a good indicative for possible future *in vivo* studies.

The following images in Figure 4.22 demonstrate the visible volume of the samples at day 14, which is in accordance with the weight values previously obtained.
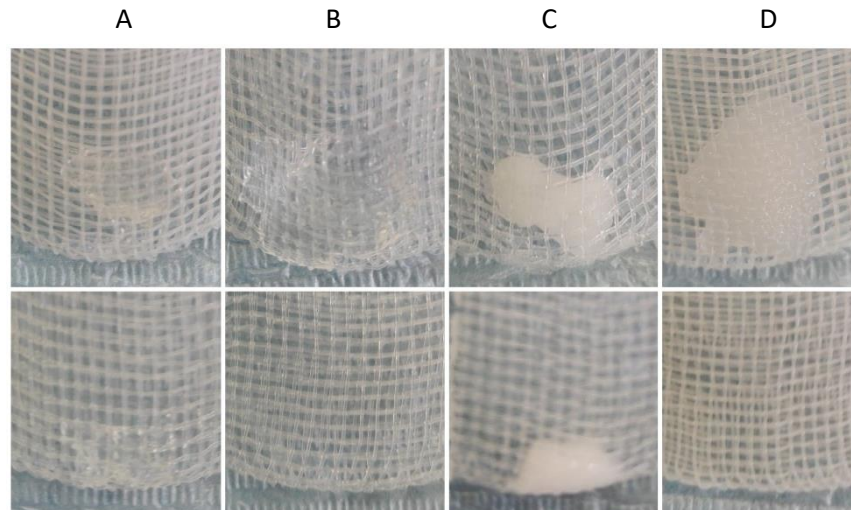

Figure 4.22- Samples inside nylon bags post 14 days of swelling and degradation test. Top row–Hydrolytic Test, Bottom row–Enzymatic Test. Columns: A – 0% MPs samples at pH of 7.3; B – 0% MPs samples at pH of 5; C – 1.5% MPs samples at pH of 7.3; C – 1.5% MPs samples at pH of 5.

As it can be seen, the 1.5% MPs samples as well as the 0% MPs samples immersed in saliva with a pH of 7.3 presented similar volume, In the enzymatic test, both possessed lower weight relatively to the ones tested in hydrolytic degradation. Concerning the samples immersed in saliva with pH of 5, it can be observed that the 1.5% MPs and 0% MPs samples degraded completely in the enzymatic test, contrarily to the ones tested hydrolytically, which maintained their structure at maximum swelling.

4.2.2.4 – Rheological Properties

Rheology tests were performed to study the materials viscosity evolution in function of different applied shear stress frequencies as well as in function of the temperature. This is relevant to understand, in order to acknowledge at which conditions the material can be easily extruded through an injectable system to only be administrated *in situ*.

The thixotropy properties of a material are essential to acknowledge at the first stage of its rheological study. Its test monitors the material's viscosity in function of different shear frequencies imposed on the sample for a certain amount of time. The performed test to the 0% MPs sample – Figure 4.23 – started by applying a low constant shear frequency of 0.1 Hz for 30 seconds, and right after, increasing the shear frequency by 1000 times at 100 Hz for 30 seconds. Lastly, the shear frequency was lowered to the initial value – 0.1 Hz, and the viscosity was monitored for further 2 minutes. As it can be observed in the graph below, the initial viscosity is maintained at constant values until the shear frequency is increased. Under the applied higher stress, the sample presents lower viscosity, which means that the material's structure

was disrupted. However, the material's viscosity rapidly returns to its normal values, when the high shear stress is removed. This almost instantaneous action concludes that the material does not present thixotropy behaviour. [76]
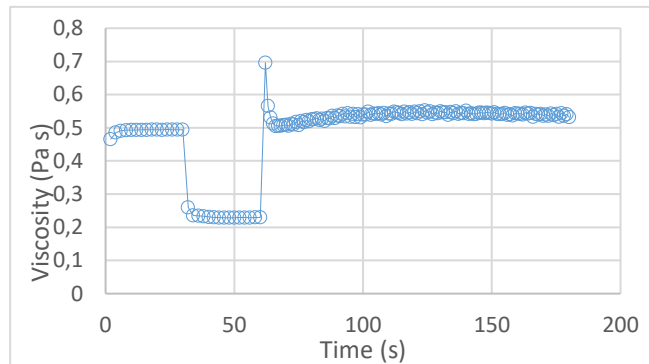

Figure 4.23 – Thixotropy test of sample without PLLA microparticles.

An amplitude sweep test determines the applied shear strain at which the material cannot elastically revert the suffered strain, starting to deform in a viscous manner. In a graph that plots the storage modulus (G') in function of the shear strain percentage - $\gamma(\%)$- applied – Figure 4.24, that value corresponds to the shear strain percentage at which the storage modulus decreases. By analysing the graph below, the value of the shear strain at which G' starts to decrease is 19.9%. This is a value important to attain, since it limits the following characterization tests to only be performed at the Linear Viscoelastic Region (LVER) of the material, in which its properties are monitored without disrupting its microstructure. Otherwise, the characterization tests would result in inconclusive data. [77]
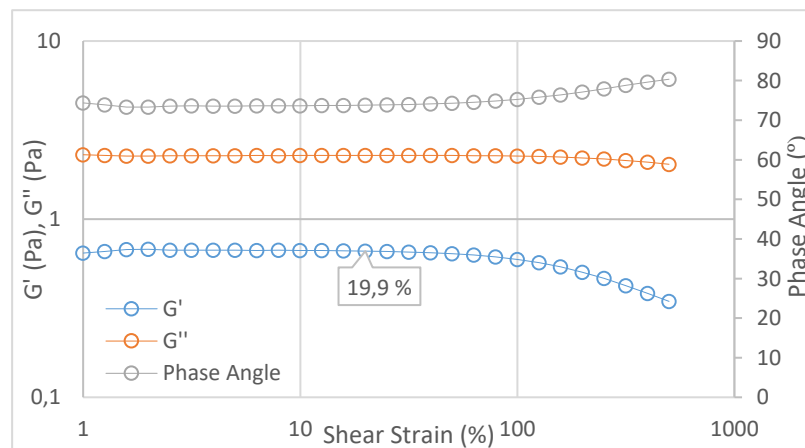

Figure 4.24 – Amplitude sweep test of the 0% MPs hydrogel. Graph plots storage modulus (G'), loss modulus (G'') and phase angle in function of the shear strain.

In frequency sweep tests, diverse characteristics of the material in study can be extrapolated from the different data obtained. The shear strain applied was 19%, to keep the material in the LVER region.

A graph that plots the complex viscosity of a material in function of the angular frequency – Figure 4.25 - imparts information about its class. Observing the graph below, the complex viscosity decreases as the angular frequency increases, which indicates that the material is pseudo-plastic. Comparing the control and test samples, it is denoted that the control sample presents higher viscosity, regarding the augment of the shear stress frequency applied. [74]
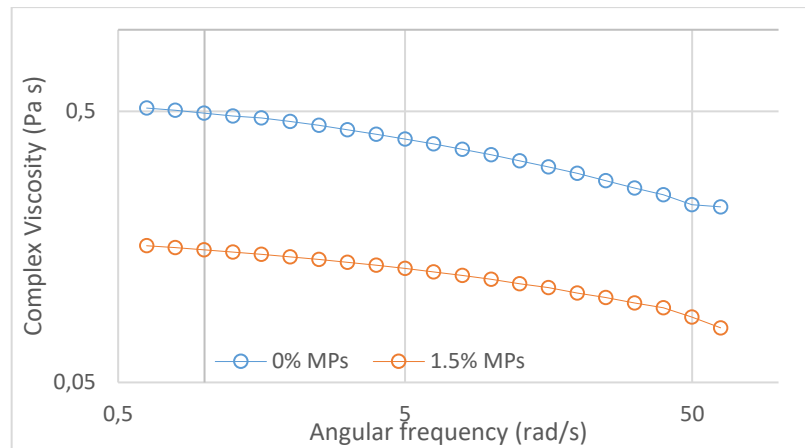

Figure 4.25 – Frequency sweep strain-controlled test. Graph plots complex viscosity in function of angular frequency.

A plot between both modulus (storage and loss) and the angular frequency provides information about the number of crosslinks between the different composites that constitute the hydrogel. It is stated in literature that the higher the storage modulus of a material, the higher is the number of crosslinks present. This is logic, since a higher number of crosslinks enables the sample to elastically deform at higher amounts of strain without disrupting its microstructure in a viscous manner. Therefore, observing the graphs of Figure 4.26, it is possible to denote that the 0% MPs sample possesses slightly higher storage modulus, which indicates its higher amount of crosslinks between the hydrogel's components, in relation to the 1.5% MPs sample. [75]

The analysis of this graph correlated in an equivalent manner with the anterior, since the loss modulus of the 1.5% MPs sample observed in the following graph is lower, relatively to the 0% MPs sample. It is acknowledged that the loss modulus measures the viscous portion of the material. So, this graph – Figure 4.26 - confirms the conclusion withdrawn from the graph of Figure 4.25, that the 1.5% MPs sample presents lower viscosity when compared to the 0% MPs sample.

The results previously commented of the swelling and degradation tests, can be related with the ones obtained in the frequency sweep tests of the rheological characterization. It was observed that the 1.5% MPs samples, degraded at a faster rate than the 0% MPs samples, in the enzymatic degradation test. Since the rheological results conclude that the 1.5% MPs samples contained a minor number of crosslinks between the hydrogel's components, it is possible to denote that, apart from the long length crosslinks due to the incorporation of the microparticles, those bonds are in a minor quantity as well. Thus, it is expected that this network degrades faster than the 0% MPs one.
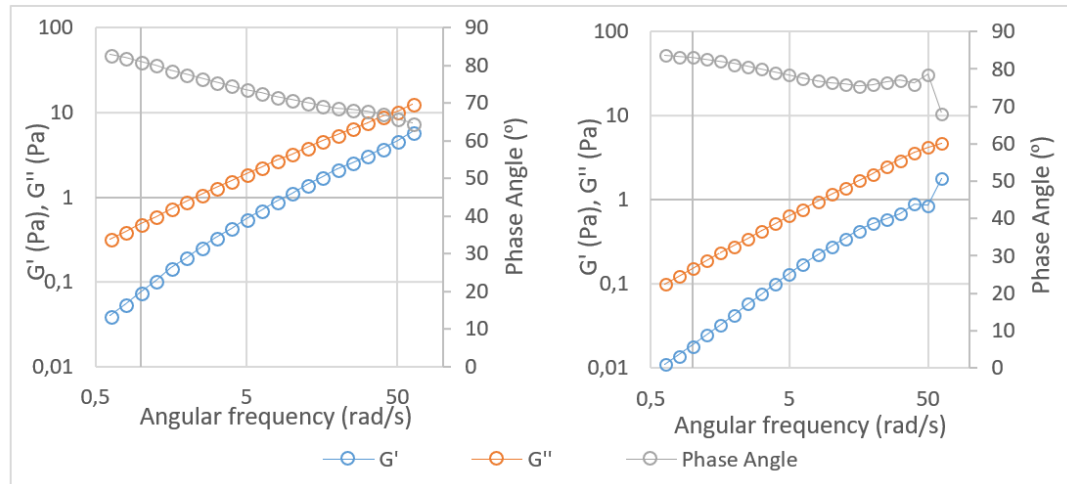
Figure 4.26 – Frequency sweep strain-controlled test. Graph plots storage modulus (G'), loss modulus (G'') and phase angle in function of angular frequency. Left – 0% MPs Sample; Right – 1.5% MPs Sample.

The phase angle indicates whether the sample presents a liquid state or transited to a gel like state. In literature, it is reported that a pure elastic solid has a phase angle of 0°, whereas a pure viscous liquid possesses a phase angle of 90°. Thus, it is assumed that when the phase angle value is above 45°, the material is in its liquid state, whereas in lower values, the material presents a solid like state. [97] Therefore, by analysing the phase angle monitored on the thixotropy as well as frequency sweep tests, it can be concluded that all the samples tested were at its liquid state.

The following temperature sweep tests provide an analyse of the material's transition from liquid to gel state in function of the temperature. These tests were also performed in the LVER region, with the shear strain limited to 19%.

It is known that during heating, the water sheaths that conceal the chitosan chains are removed, and thus, the heat reaches the crosslink bonds of chitosan and β-GP, occurring protons transfer between the protonated groups. This causes the formation of hydrophilic interactions, that possess higher energy, as higher amounts of water molecules are evaporated from the material. These interactions decrease the viscous part of a material and increase its elastic modulus. Thus, there will be a point at which the material transits from a liquid to a gel like state which is rheologically represented by the storage and loss modulus crossover in the temperature sweep graphs. [75]

In Figure 4.27, the temperatures at which the hydrogel samples transit to a gel state at a heating rate of 1°C/min are presented. The 0% MPs sample reported a transition temperature similar to the one observed for the 1.5% MPs sample. Statistical analysis concludes that there were not encountered significant differences between the variables of both tests. It is also denoted that, for both samples, the phase angle starts at values close to 80° and terminates the test at values close to 0°. This indicates that the hydrogels were in a viscous liquid state and transited to an almost pure elastic solid state, confirming its total transition from liquid to gel like state.
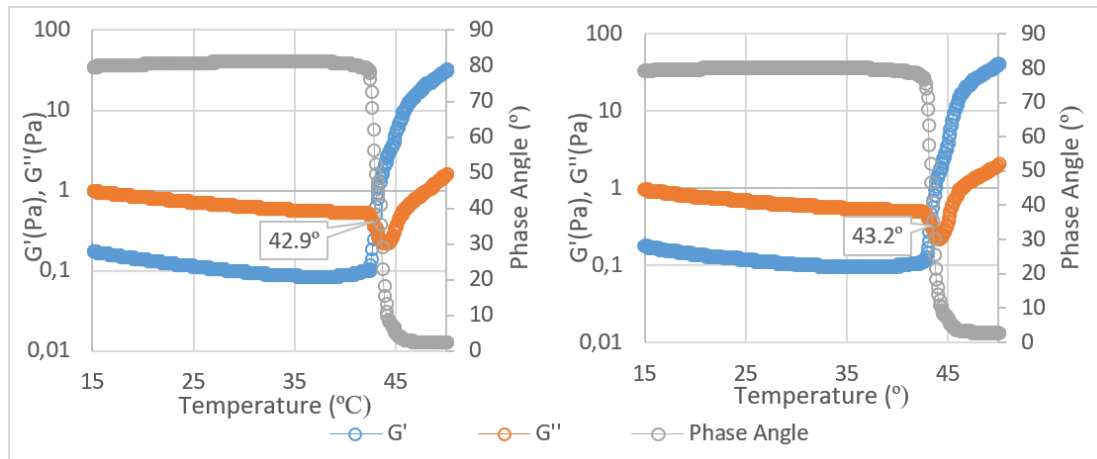
Figure 4.27 – Temperature sweep strain-controlled test. Graph plots storage modulus (G'), loss modulus (G'') and phase angle in function of temperature. Left – 0% MPs Sample; Right – 1.5% MPs Sample.

However, the verified transition instantaneous temperature is not feasible for practical application *in vivo*, in which the temperature that the hydrogel takes to solidify in the oral mucosa, must be lower, at around 36ºC. Additionally, as previously mentioned in the results of the hydrogel's synthesis, the time that it takes for the hydrogel to become solid at physiological temperatures is not feasible either, since it takes at least 5 hours for the chitosan-based hydrogel to completely transit to a gel like state at those conditions.

4.3 – PLLA Microparticle's *In Vitro* Study

4.3.1 - MTT Assay

At days 2 and 6, the absorbance values of some wells containing only PLLA MPs solution – blank values - were higher than expected. As it can be observed in Figure 4.28, the negative control wells containing PLLA MPs at concentrations of $1000\,\mu g/mL$, $500\,\mu g/mL$ and $100\,\mu g/mL$ also synthetized some of the salt into blue formazan, which was then dissolved in DMSO and posteriorly scanned. Thus, the absorbance outcome of this wells will not be considered in the posterior statistical analysis, since it cannot be compared with the remaining absorbance values.
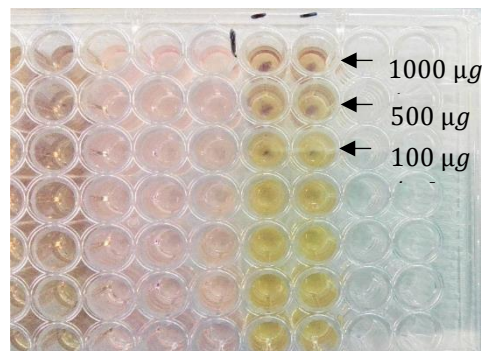

Figure 4.28 – Salt synthetized into blue formazan in negative control wells containing only PLLA MPs at concentrations of $1000\,\mu g/mL$, $500\,\mu g/mL$ and $100\,\mu g/mL$.

The initial cell density was $0,3 \times 10^4 \ cells/mL$. Thus, an overall analysis of the graph on Figure 4.29 indicates that cell density increased with time of culture, regarding the concentration of PLLA MPs with which were incubated.

Statistical analysis of all data was performed to denote significant differences between the absorbance values of cells cultured with different concentrations of PLLA MPs, for each day. For instance, at day 9, statistical analysis shows significant differences between the absorbance values of cells cultured with 1000 µg/mL and 1 µg/mL of PLLA MPs concentration as well as between 1000 µg/mL and control. By observing the graph, it is denoted that at this day, the absorbance values of MPs_1 and MPs_control were higher than the MPs_1000. Moreover, at day 13, statistical analysis shows significant differences between the absorbance values of cells cultured with 100 µg/mL and 10 µg/mL of PLLA MPs concentration as well as between 100 µg/mL and control. However, at days 2 and 6, no significant differences were encountered between the various PLLA MPs concentration wells. However, these results can be due to the MPs synthetization of the MTT salt, as mentioned previously, since the outcomes could not be properly examined through statistical analysis.
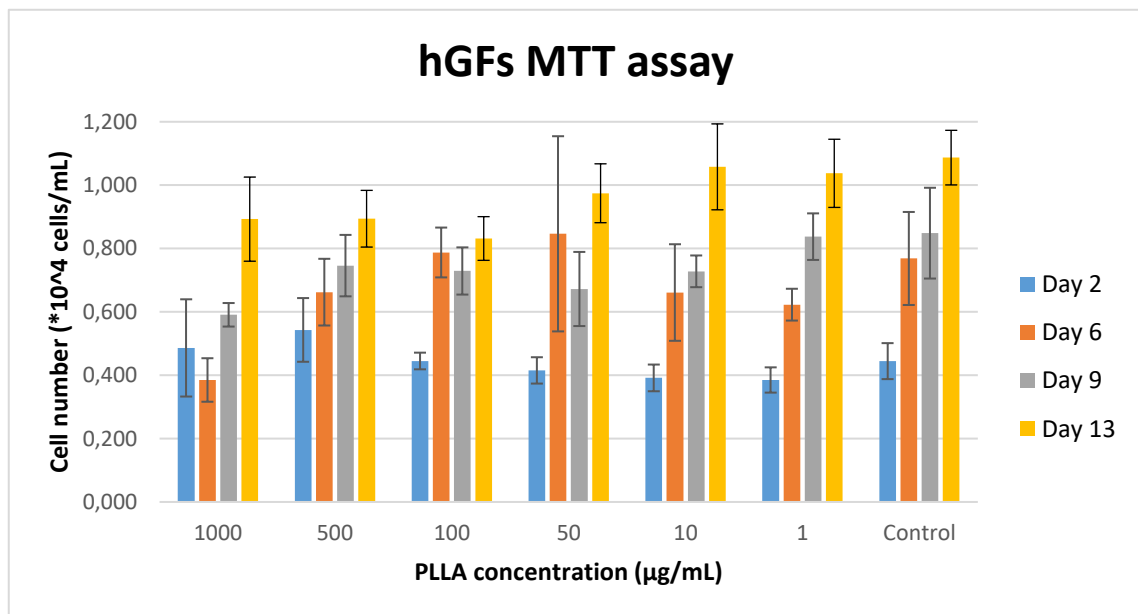
Figure 4.29 – Statistical Analysis of hGFs proliferation 2, 6, 9 and 13 days post-seeded with neat PLLA microparticles.

Additional statistical analysis was performed to compare the absorbance values between the culture days. Significant differences were found between all the days, except between days 6 and 9. This means that the growth between 3 days – Days 6 and 9 - is minor than the growth between 4 days – Days 2 and 6; Days 9 and 13, which is logically expected.

Overall, this assay concludes that neat PLLA microparticles are biocompatible with human gingival fibroblasts, regarding the concentration at which are cultured with, and possess the potential to promote their proliferation.

4.3.2 - Collagen Assay

Within the human body, fibroblasts secrete collagen fibres to synthetize extra-cellular matrix and promote their proliferation, development and tissue maintenance. [98] [99]

In figures 4.30, 4.31 and 4.32, it is presented the results of the hGF's collagen assay after 6, 9 and 13 of culture with neat PLLA MPs at different concentrations. The outcome of this test lacks some accuracy, since the PLLA MPs absorbed most of the Sirius Red die. Thus, the collagen is scarcely spotted in wells with high concentration of PLLA MPs – $500 \mu g/mL$ and $1000 \mu g/mL$. This could be due to the microparticles being seeded above the cell culture. Taking into consideration that poly l-lactic acid can absorb Sirius Red, the die was firstly absorbed by the MPs and minor amounts of stain were absorbed by the cell's collagen.

As it can be observed in Figure 4.30, 6 days after culture, at control, the collagen is being synthetized by the cell in a uniform manner. Along the increase of the MPs concentration, the collagen is most rapidly secreted, and fibres start to form in the cell's extra-cellular matrix.

Figure 4.30 – Collagen assay of hGFs after 6 days of being cultured with neat PLLA microparticles in the following concentrations: A) $0\,\mu g/mL$, B) $1\,\mu g/mL$, C) $10\,\mu g/mL$, D) $50\,\mu g/mL$, E) $100\,\mu g/mL$, F) $500\,\mu g/mL$, G) $1000\,\mu g/mL$

In a distinct manner, at day 9, collagen fibres are already secreted in all wells with different MPs concentrations. At Figure 4.31.C) and 4.31.D), it is possible to observe that the fibres are reaching for the neighbour cells, and thus, the cell to cell contact augments.

Figure 4.31 – Collagen assay of hGFs after 9 days of being cultured with neat PLLA microparticles in the following concentrations: A) $0\,\mu g/mL$, B) $1\,\mu g/mL$, C) $10\,\mu g/mL$, D) $50\,\mu g/mL$, E) $100\,\mu g/mL$, F) $500\,\mu g/mL$, G) $1000\,\mu g/mL$

Contrarily, at day 13, a higher density of collagen fibres is observed between the higher number of cells proliferated, relatively to the previous days. In Figures 4.32.B), 4.32.C) and 4.32.D) it is denoted that the fibres are interconnecting the cells through their extracellular matrix, which leads to superior organization and orientation of the cell's bed. Some fibres are also denoted in the wells with higher concentrations of MPs in a more arranged manner, which can be an indicative of primal formation of gingival tissue.

In conclusion, it can be denoted that the augment of microparticles concentration during cell proliferation, accelerates the secretion process of collagen fibres. Moreover, along the days, the amount of fibres augments, which indicates continuous biocompatibility of the MPs, regarding the time at which are in direct contact with the cells.
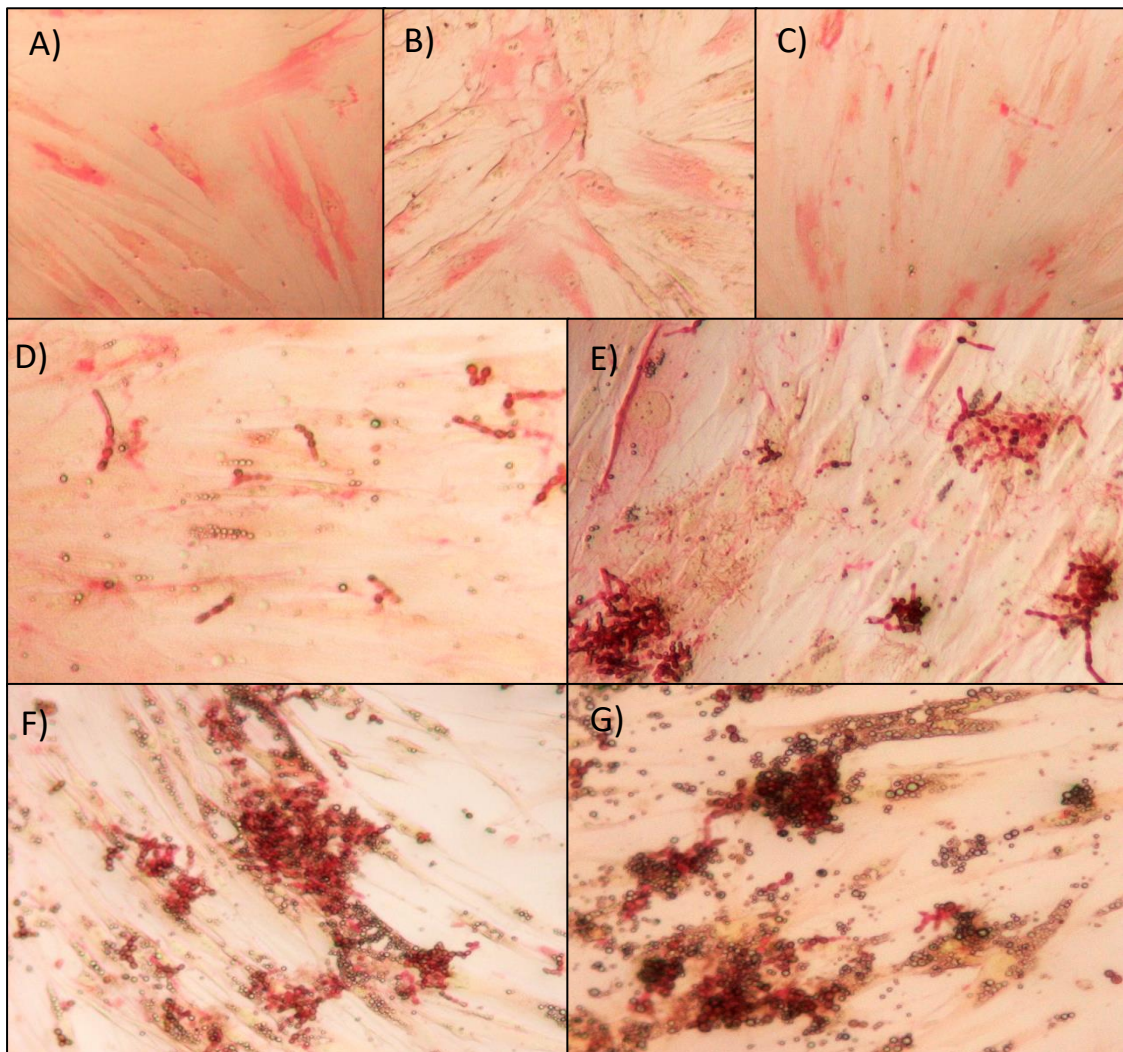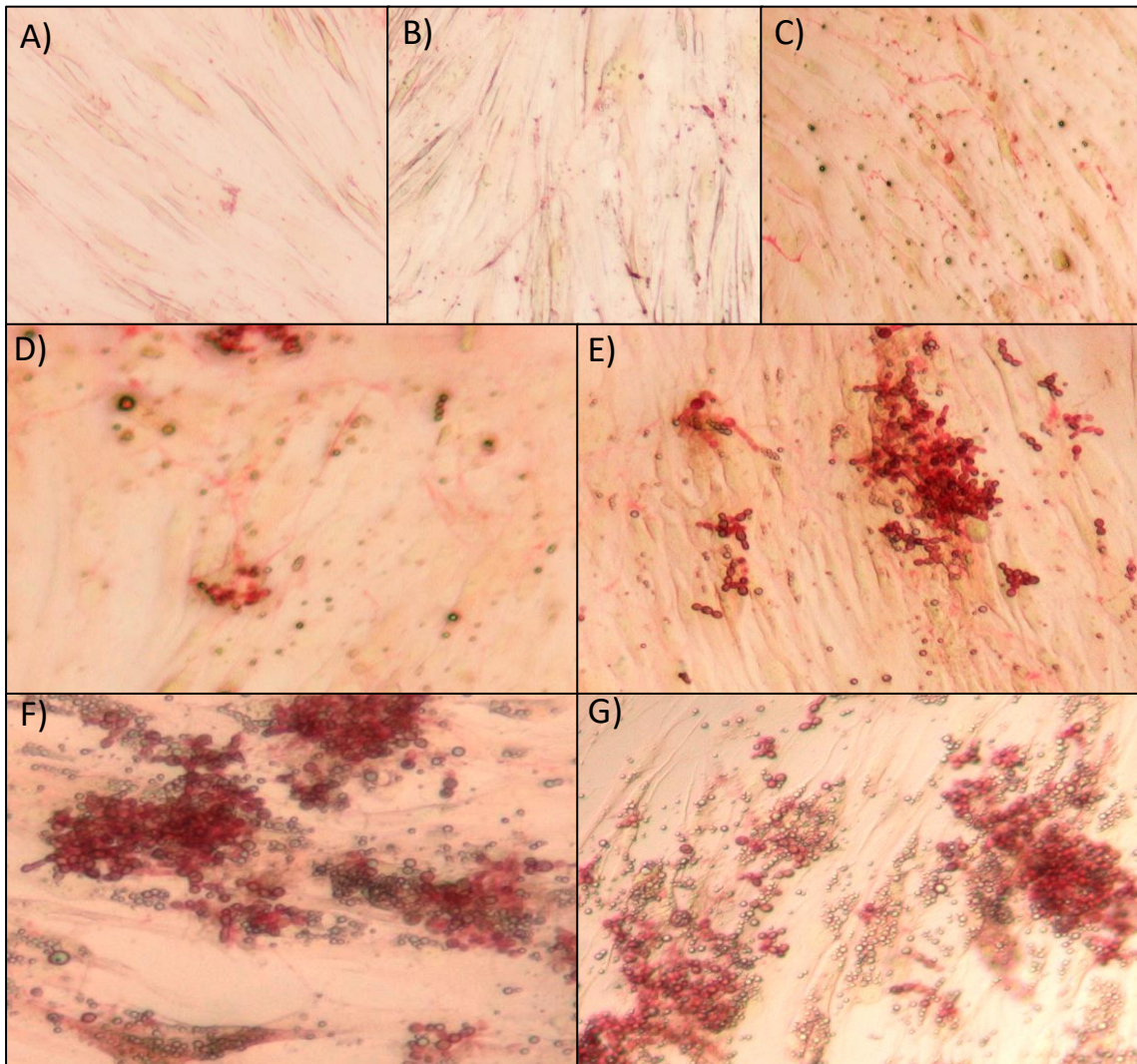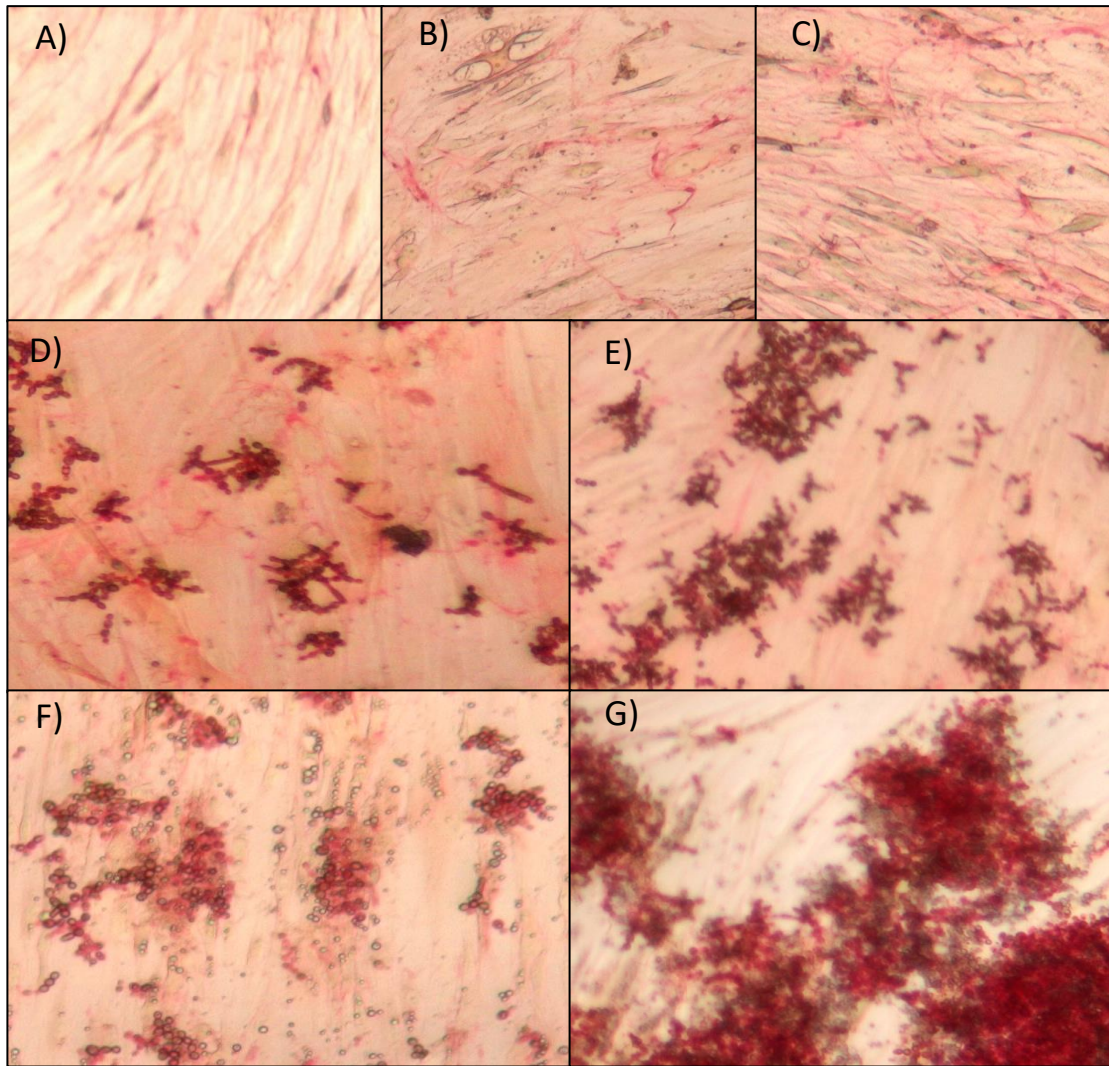
Figure 4.32 – Collagen assay of hGFs after 13 days of being cultured with neat PLLA microparticles in the following concentrations: A) $0\,\mu g/mL$, B) $1\,\mu g/mL$, C) $10\,\mu g/mL$, D) $50\,\mu g/mL$, E) $100\,\mu g/mL$, F) $500\,\mu g/mL$, G) $1000\,\mu g/mL$

4.3.3 - Morphology Assay

The morphology of the cell's cytoskeleton and nucleus give us information about its cycle stage and viability. Additionally, the stained laminin allows to observe the cell's rearrangement, which can indicate the beginning of formation of primal tissue.

As it can be observed in the images below – Figure 4.33 -, the cell's viability is high regarding the PLLA MPs concentration at which were cultured with. So, this corroborates the results of the MTT assay, that the microparticles are cytologically compatible with the cells.

In a deeper analysis, with the increase of PLLA MPs concentration, it is possible to observe a crescent elongation of the cell's morphology and an increase in the inter-cell contact. The last is superior in the presence of collagen fibres that connect the cells through their extracellular matrix. Thus, although the collagen test's outcome was not accurate, it can be denoted from the morphology results, that the collagen fibres were present in the wells with

higher concentrations of MPs. Accordingly, cells develop inter rearrangement, which is higher in the spots that the microparticles agglomerate – the blue distortion lodged above the cells denoted in Figure 4.33.F) and 4.33.G).
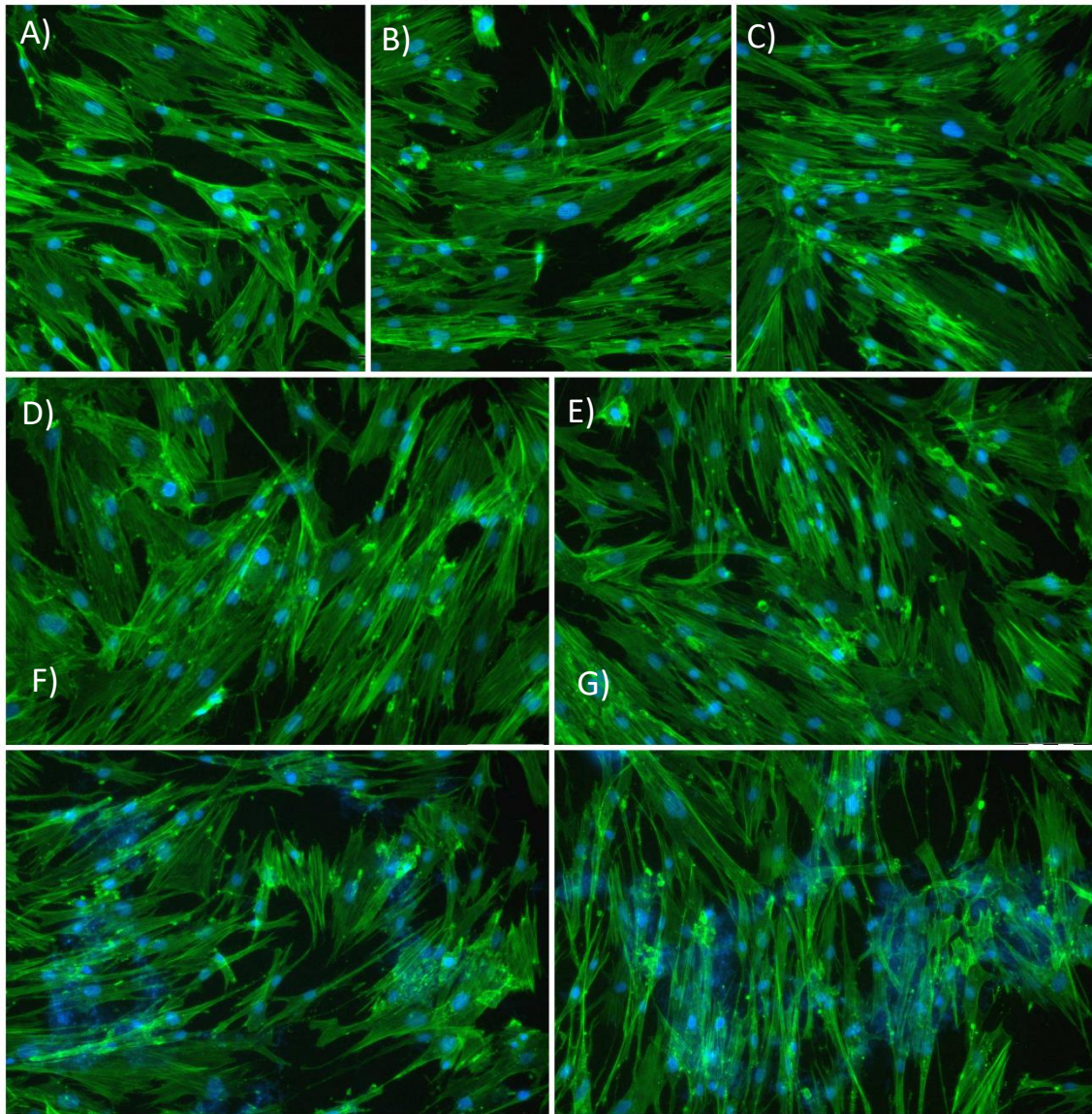
Figure 4.33 – Fluorescent microscopy -DAPI and AlexaFluor stain - of hGFs, 2 days after being cultured with neat PLLA microparticles in the following concentrations: A) $0\,\mu g/mL$, B) $1\,\mu g/mL$, C) $10\,\mu g/mL$, D) $50\,\mu g/mL$, E) $100\,\mu g/mL$, F) $500\,\mu g/mL$, G) $1000\,\mu g/mL$

Thus, the results from the morphology assay corroborate with the collagen ones. Therefore, the combination of both outcomes concludes that the neat Poly L-Lactic Acid microparticles may promote an accelerated primal formation of gingival tissue from human gingival fibroblasts.

Chapter 5

Conclusions

The aim of this work was to synthetize and characterize a chitosan-based hydrogel loaded with Poly (L-Lactic Acid) microparticles to promote gingival repair, as well as study the feasibility of PLLA MPs *in vitro* cultured with human gingival fibroblasts.

In the primer part of the dissertation, the Poly (L - Lactic Acid) microparticles, previously produced by spray drying technique, were characterized. The resultant MPs visually presented a highly agglomerated structure. By analysing the SEM results, it was denoted that the microparticles were contaminated with tantalum. Henceforth, the polymeric material was purified by a washing process, which successfully removed all the tantalum moieties. Moreover, the microparticles dispersed into a viewable powder and presented an even diameter size of about $(1.718 \pm 1.89)\mu m$. Relatively to the FTIR analysis, it was concluded that the analysed material is primarily amorphous, containing some α-form crystals within its structure. Additionally, DSC analysis confirmed the mainly amorphous state of the PLLA microparticles also validated by the results of the FTIR analysis. Relatively to the TGA results, the apparent activation energy was calculated $197 \, kJ/mol$. This value indicates the required energy that the microparticles need to absorb within their microstructure to trigger their degradation.

In a second laboratory practice, samples of chitosan-based hydrogel matrix – 0% MPs sample - and with PLLA MPs loaded in its interior were successfully synthetized. The resultant hydrogels presented high fluidity and could be visually distinguished, since 0% MPs samples were completely transparent, whereas samples with loaded MPs presented an opaque white colour, due to the uniform microparticles distribution in the hydrogel matrix. Thereafter, SEM analysis was used to compare morphologically, three samples loaded with different concentrations of PLLA MPs. The sample with the morphological outcome, which was characteristic of a hydrogel network with its interspace completely packed with microparticles – 1.5% (w/v) sample - was chosen to be further compared with the 0% MPs sample. FTIR analysis of both samples confirmed the reticulation process between chitosan/GPTMS and chitosan/β-GP, as well as the ionic bonds between chitosan monomers. Moreover, since the sample loaded with MPs possessed a portion of microparticles in its interior, the concentration of hydrogel matrix is lower in this sample, whereas in the 0% MPs sample, the concentration of chitosan-based matrix is 100%, as expected. The following swelling and degradation *in vitro* studies concluded that in the swelling phase,

both samples, regarding the pH value at which were immersed and the test - hydrolytic or enzymatic, swelled until its maximum. In the degradation tests, at pH values characteristic of periodontal lesions – around 5 -, in the hydrolytic test, the samples maintain their maximum swelling until the termination of the study at day 11. Contrarily, in these pH values, in the enzymatic test, the samples significantly lose weight until complete degradation of the chitosan-based hydrogel matrix is verified at day 11. At pH values of 7.3, both samples in both hydrolytic and enzymatic tests, progressively degraded, being the degradation rate of the enzymatic test higher. It is advantageous that the swelling effect is prolonged at lesion characteristic pH values, since it allows for a faster release of the repair promoting MPs and creates space in its bulk to accommodate proliferating cells. Lastly, the rheological tests concluded that the material does not present thixotropic behaviour, instead, is it classified as a non-Newtonian pseudo-plastic fluid, since its viscosity diminishes, with the increase of the shear stress applied. Moreover, the 0% MPs samples present a higher storage modulus, which indicates its higher elasticity, due to the higher number of crosslinks present in its network, when compared to 1.5% MPs samples. Additionally, the instantaneous temperature at which both hydrogel samples transit from liquid to a gel like state was about 43ºC, since at physiological temperatures, it requires at least 5 hours. The instantaneous temperature as well as the long time required for a physiological environment is not feasible for *in situ* administration of the hydrogel.

The PLLA microparticles trials *in vitro* with human gingival fibroblasts were described and reported. The MTT assay concluded that the microparticles are biocompatible with the human cells, regarding the concentration in which are cultured with, and potentially promote their proliferation. Regarding the collagen assay results, it was denoted that the augment of microparticles concentration during cell proliferation, accelerates the secretion process of collagen fibres. Moreover, along the days, the amount of fibres augments, which indicates continuous biocompatibility of the MPs, regarding the time at which are in direct contact with the cells. At last, the morphology test with DAPI and Alexa Fluor fluorescent colourants, indicated that the cells develop inter rearrangement, which is higher in the spots that the microparticles agglomerate. Therefore, since the PLLA microparticles increase the organization between the cells, it is feasible to state that they can potentiate the formation of primal gingival tissue from human gingival fibroblasts.

5.1 – Future Work

To augment the degradation time in enzymatic acidic environments and to diminish the temperature at which the synthetized hydrogel transits from a liquid to a gel like state, its synthesis requires some improvements. In my opinion, the addition of the reticulating agent β-GP in a less diluted solution would improve the mechanical properties of the material, since it wouldn't add too much liquid into the chitosan/GPTMS hydrogel solution. Consequently, the time as well as temperature for the transition to gel state to occur would probably be minor, since less water molecules need to evaporate. Moreover, the hydrogel's microstructure would possess shorter length crosslinks with higher mechanical strength, since the water ratio inside the network was decreased. Thus, an increased period exposed to enzymes in acidic conditions would likely be required for the disruption of its microstructure, and subsequent degradation.

References

[1]   M. G. Newman, H. H. Takei, P. R. Klokkevold, and F. A. Carranza, *Carranza's Clinical Periodontology*, 12th ed. Elsevier Inc., 2015.

[2]   "World Health Organization: Regional Office for Europe Disease Prevention - Oral Health." [Online]. Available: http://www.euro.who.int/en/health-topics/disease-prevention/oral-health. [Accessed: 08-Dec-2017].

[3]   M. B. Dreifke, N. A. Ebraheim, and A. C. Jayasuriya, "Investigation of potential injectable polymeric biomaterials for bone regeneration," *J. Biomed. Mater. Res. - Part A*, vol. 101 A, no. 8, pp. 2436–2447, 2013.

[4]   M. J. Danesh-meyer and U. M. E. Wikesjo, "Gingival recession defects and guided tissue regeneration : a review," *J. Periodontal Res.*, vol. 36, no. 12, pp. 341–354, 2001.

[5]   S. Sowmya, J. D. Bumgardener, K. P. Chennazhi, S. V. Nair, and R. Jayakumar, "Role of nanostructured biopolymers and bioceramics in enamel, dentin and periodontal tissue regeneration," *Prog. Polym. Sci.*, vol. 38, no. 10–11, pp. 1748–1772, 2013.

[6]   E. Castro-Aguirre, F. Iñiguez-Franco, H. Samsudin, X. Fang, and R. Auras, "Poly(lactic acid)—Mass production, processing, industrial applications, and end of life," *Adv. Drug Deliv. Rev.*, vol. 107, pp. 333–366, 2016.

[7]   M. P. C. M. Soares *et al.*, "Biocompatibility of three bioabsorbable membranes assessed in FGH fibroblasts and human osteoblast like cells culture," *Head Face Med.*, vol. 10, p. 29, 2014.

[8]   C. Migliaresi, D. Cohn, A. De Lollis, and L. Fambri, "Dynamic mechanical and calorimetric analysis of compression-molded PLLA of different molecular weights: Effect of thermal treatments," *J. Appl. Polym. Sci.*, vol. 43, no. 1, pp. 83–95, 1991.

[9]   Lh. Yahia, "History and Applications of Hydrogels," *J. Biomed. Sci.*, vol. 04, no. 02, pp. 1–23, 2015.

[10]   J. A. Yang, J. Yeom, B. W. Hwang, A. S. Hoffman, and S. K. Hahn, "In situ-forming injectable hydrogels for regenerative medicine," *Prog. Polym. Sci.*, vol. 39, no. 12, pp. 1973–1986, 2014.

[11]   I. Armentano *et al.*, "Multifunctional nanostructured PLA materials for packaging and tissue engineering," *Prog. Polym. Sci.*, vol. 38, no. 10–11, pp. 1720–1747, 2013.

[12]   D. Boynueğri *et al.*, "Clinical and radiographic evaluations of chitosan gel in periodontal intraosseous defects: A pilot study," *J. Biomed. Mater. Res. - Part B Appl. Biomater.*,

vol. 90 B, no. 1, pp. 461–466, 2009.

[13] Q. X. Ji *et al.*, "Biocompatibility of a chitosan-based injectable thermosensitive hydrogel and its effects on dog periodontal tissue regeneration," *Carbohydr. Polym.*, vol. 82, no. 4, pp. 1153-1160, 2010.

[14] Y. Pakzad and F. Ganji, "Thermosensitive hydrogel for periodontal application: In vitro drug release, antibacterial activity and toxicity evaluation," *J. Biomater. Appl.*, vol. 30, no. 7, pp. 919-929, 2016.

[15] D. G. Miranda, S. M. Malmonge, D. M. Campos, N. G. Attik, B. Grosgogeat, and K. Gritsch, "A chitosan-hyaluronic acid hydrogel scaffold for periodontal tissue engineering," *J. Biomed. Mater. Res. - Part B Appl. Biomater.*, vol. 104, no. 8, pp. 1691–1702, 2016.

[16] M. Bansal, N. Mittal, S. K. Yadav, G. Khan, B. Mishra, and G. Nath, "Clinical evaluation of thermoresponsive and mucoadhesive chitosanin situ gel containing Levofloxacin and Metronidazole in the treatment of periodontal pockets – A split-mouth, clinical study," *J. Pierre Fauchard Acad. (India Sect.*, pp. 1–9, 2016.

[17] A. S. Gawish and M. M. Bilal, "Smart Liposomal Chitosan - Based Auto Gel with Ofloxacin ; a new Controlled Release Device used for Treatment of Chronic Periodontitis . a Randomized , Double-Blind Controlled Clinical Trials," *Med. Clin. Res.*, vol. 2, no. 3, pp. 1-7, 2017.

[18] H. Ruan, Y. Yu, Y. Liu, X. Ding, X. Guo, and Q. Jiang, "Preparation and characteristics of thermoresponsive gel of minocycline hydrochloride and evaluation of its effect on experimental periodontitis models," *Drug Deliv.*, vol. 23, no. 2, pp. 525-531, 2016.

[19] M. I. A. Echazú, M. V. Tuttolomondo, M. L. Foglia, A. M. Mebert, G. S. Alvarez, and M. F. Desimone, "Advances in collagen, chitosan and silica biomaterials for oral tissue regeneration: from basics to clinical trials," *J. Mater. Chem. B*, vol. 4, no. 43, pp. 6913–6929, 2016.

[20] M.-C. Yu *et al.*, "pH-Responsive Hydrogel With an Anti-Glycation Agent for Modulating Experimental Periodontitis," *J. Periodontol.*, vol. 87, no. 6, pp. 742–748, 2016.

[21] P.-C. Chang *et al.*, "Inhibition of Periodontitis Induction Using a Stimuli-Responsive Hydrogel Carrying Naringin," *J. Periodontol.*, vol. 88, no. 2, pp. 190–196, 2017.

[22] S. Nguyen and M. Hiorth, "Advanced drug delivery systems for local treatment of the oral cavity," *Ther. Deliv.*, vol. 6, no. 5, pp. 595–608, 2015.

[23] Y. Shirosaki, C. M. Botelho, M. A. Lopes, and J. D. Santos, "Synthesis and characterization of chitosan-silicate hydrogel as resorbable vehicle for bonelike-bone graft," *J. Nanosci. Nanotechnol.*, vol. 9, no. 6, pp. 3714-3719, 2009.

[24] Y. Shirosaki, S. Hayakawa, and A. Osaka, "The Effect of Si(IV) Species Derived from Chitosan-Silicate Hydrogels on Osteoblast Behavior," *Key Eng. Mater.*, vol. 493–494, pp. 698-702, 2011.

[25] Y. Shirosaki *et al.*, "Preparation and in vitro cytocompatibility of chitosan-siloxane hybrid hydrogels," *J. Biomed. Mater. Res. - Part A*, vol. 103, no. 1, pp. 289-299, 2015.

[26] "TePe®." [Online]. Available: https://www.tepe.com/products/gingival-gel/. [Accessed: 25-May-2018].

[27] "Oddent®." [Online]. Available: https://www.menarini.es/vademecum/autocuidado-de-la-salud-otc/item/37-oddent-gel-oral-forte.html. [Accessed: 25-May-2018].

[28] "Bexident ®." [Online]. Available: https://www.isdin.com/pt-PT/produto/bexident/gengivas-sob-tratam-gel-dentifrico. [Accessed: 25-May-2018].

[29] "Gengigel®." [Online]. Available: https://www.gengigel.pt/produtos/produto/gengigel-gel/. [Accessed: 25-May-2018].

[30] A. H. Rabiya, "Treatment of periodontal disease with High Functional Paste made from Nanoemulsion Gel 'NBF,'" *Guident*, vol. 12, pp. 70–71, 2013.

[31] M. Roccuzzo, G. Corrente, and S. Gandolfo, "Comparative Study of a Bioresorbable and a Non-Resorbable Membrane in the Treatment of Human Buccal Gingival Recessions*," *J. Periodontol.*, no. 67, pp. 7–14, 1996.

[32] C. A. Waterman, "Guided Tissue Regeneration Using a Bioabsorbable Membrane in the Treatment of Human Buccal Recession . A Re-Entry Study *," *J. Periodontol.*, vol. 68, pp. 982–989, 1997.

[33] H.-P. Muller, M. Stahl, and T. Eger, "Dynamics of mucosal dimensions after root coverage with a bioresorbable membrane," *J. Clin. Periodontol.*, vol. 27, pp. 1–8, 2000.

[34] D. Tatakis and L. Trombelli, "Gingival recession treatment: guided tissue regeneration with bioabsorbable membrane versus connective tissue graft," *J. Periodontol.*, vol. 71, no. 2, pp. 299–307, 2000.

[35] L. Trombelli, A. Scabbia, D. N. Tatakis, L. Checchi, and G. Calura, "Resorbable barrier and envelope flap surgery in the treatment of human gingival recession defects," 1998.

[36] S. Matarasso, "Guided Tissue Regeneration Versus Coronally Repositioned Flap in the Treatment of Recession with Double Papillae," *Int. J. Periodontics Restorative Dent.*, vol. 18, no. 5, pp. 445–453, 1998.

[37] E. S. Amarante, K. N. Leknes, J. Skavland, and T. Lie, "Coronally Positioned Flap Procedures With or Without a Bioabsorbable Membrane in the Treatment of Human Gingival Recession," *J. Periodontol.*, vol. 71, no. June, pp. 989–998, 2000.

[38] T. Von Arx, *Clinical Oral Anatomy: A Comprehensive Review for Dental Practitioners and Researchers*, 1st ed. 2017.

[39] G. Mahon, C. R., Lehman, D. C., & Manuselis, *Illustrated Dental Embryology, Histology and Anatomy*, 4th ed. 2016.

[40] B. L. Pihlstrom, B. S. Michalowicz, and N. W. Johnson, "Periodontal diseases," *Lancet*, vol. 366, no. 9499, pp. 1809–1820, 2005.

[41] D. F. Kinane, P. G. Stathopoulou, and P. N. Papapanou, "Periodontal diseases," *Nat. Rev. Dis. Prim.*, vol. 3, pp. 1–14, 2017.

[42] N. J. Kassebaum *et al.*, "Global, Regional, and National Prevalence, Incidence, and Disability-Adjusted Life Years for Oral Conditions for 195 Countries, 1990–2015: A Systematic Analysis for the Global Burden of Diseases, Injuries, and Risk Factors," *J. Dent. Res.*, vol. 96, no. 4, pp. 380–387, 2017.

[43] N. J. Kassebaum, E. Bernabé, M. Dahiya, B. Bhandari, C. J. L. Murray, and W. Marcenes, "Global Burden of Severe Periodontitis in 1990-2010," *J. Dent. Res.*, vol. 93, no. 11, pp. 1045–1053, 2014.

[44] R. J. ;Borgnakk. Genco W. S., "Risk factors for periodontal disease," *Periodontol. 2000*, vol. 62, no. 1, pp. 59-94, 2013.

[45] H. Tsuji, "Poly (Lactic Acid)," *Bio-Based Plast. -Materials Appl.*, no. ii, pp. 171–239, 2014.

[46] O. Avinc and A. Khoddami, "Overview of poly lactid acid (PLA) fibre part I : Production , properties , performance , environmental impact , and end-use applications of poly (lactic acid) Fibres," *Fibre Chem.*, vol. 41, no. 6, pp. 16–25, 2009.

[47] K. Hamad, M. Kaseem, H. W. Yang, F. Deri, and Y. G. Ko, "Properties and medical applications of polylactic acid: A review," *Express Polym. Lett.*, vol. 9, no. 5, pp. 435–455, 2015.

[48] H. T. Rafael A. Auras, Loong-Tak Lim, Susan E. M. Selke, *Poly(lactic acid): Synthesis,*

Structures, Properties, Processing, and Applications. 2011.

[49]   M. Yasuniwa, S. Tsubakihara, K. Iura, Y. Ono, Y. Dan, and K. Takahashi, "Crystallization behavior of poly(l-lactic acid)," *Polymer (Guildf).*, vol. 47, no. 21, pp. 7554–7563, 2006.

[50]   J. Elisseeff, "Hydrogels: Structure starts to gel," *Nature*, vol. 7, no. April, pp. 271–273, 2008.

[51]   E. M. Ahmed, "Hydrogel: Preparation, characterization, and applications: A review," *J. Adv. Res.*, vol. 6, no. 2, pp. 105–121, 2015.

[52]   B. Balakrishnan and A. Jayakrishnan, "Injectable Hydrogels for Biomedical Applications," *Inject. Hydrogels Regen. Eng.*, no. 15:31, pp. 33–94, 2015.

[53]   F. L. Mi, H. W. Sung, and S. S. Shyu, "Synthesis and characterization of a novel chitosan-based network prepared using naturally occurring crosslinker," *J. Polym. Sci. Part A Polym. Chem.*, vol. 38, no. 15, pp. 2804–2814, 2000.

[54]   L. Xu *et al.*, "Nonionic polymer cross-linked chitosan hydrogel: Preparation and bioevaluation," *J. Biomater. Sci. Polym. Ed.*, vol. 24, no. 13, pp. 1564–1574, 2013.

[55]   I. Younes and M. Rinaudo, "Chitin and chitosan preparation from marine sources. Structure, properties and applications," *Mar. Drugs*, vol. 13, no. 3, pp. 1133–1174, 2015.

[56]   A. Singh, S. S. Narvi, P. K. Dutta, and N. D. Pandey, "External stimuli response on a novel chitosan hydrogel crosslinked with formaldehyde," *Bull. Mater. Sci.*, vol. 29, no. 3, pp. 233–238, 2006.

[57]   J. Xu, S. Strandman, J. X. X. Zhu, J. Barralet, and M. Cerruti, "Genipin-crosslinked catechol-chitosan mucoadhesive hydrogels for buccal drug delivery," *Biomaterials*, vol. 37, pp. 395–404, 2015.

[58]   L. Cui, J. Jia, Y. Guo, Y. Liu, and P. Zhu, "Preparation and characterization of IPN hydrogels composed of chitosan and gelatin cross-linked by genipin," *Carbohydr. Polym.*, vol. 99, pp. 31–38, 2014.

[59]   G. Ramos, J. J. Prieto, and J. Guardiola, "Physico-chemical characterization of sizings for the manufacture of E and AR glasses," *Mater. Lett.*, vol. 20, no. 1-2, pp. 47–49, 1994.

[60]   K. Tsuru *et al.*, "In Vitro Biodegradability of Chitosan-Organosiloxane Hybrid Membrane," *Key Eng. Mater.*, vol. 284-286, pp. 823–826, 2005.

[61]   L. Morelli, M. A. Cappelluti, L. Ricotti, C. Lenardi, and I. Gerges, "An Injectable System for Local and Sustained Release of Antimicrobial Agents in the Periodontal Pocket," *Macromol. Biosci.*, vol. 17, no. 8, pp. 1–11, 2017.

[62]   A. Jain, K. R. Kunduru, A. Basu, B. Mizrahi, A. J. Domb, and W. Khan, "Injectable formulations of poly(lactic acid) and its copolymers in clinical use," *Adv. Drug Deliv. Rev.*, vol. 107, pp. 213–227, 2016.

[63]   Corbian Purac, "Corbion.com, (2015). Product Data Sheet Purasorb® PL 18," 2017. [Online]. Available: http://www.corbion.com/static/downloads/datasheets/45d/PURASORB PL 18.pdf.

[64]   V. Sencadas *et al.*, "Thermal Properties of Electrospun Poly (Lactic Acid) Membranes," *J. Macromol. Sci. Part B*, vol. 51, no. 3, pp. 411–424, 2012.

[65]   B. K. Lee, Y. Yun, and K. Park, "PLA Micro- and Nano-particles," *Adv. Drug Deliv. Rev.*, vol. 107, pp. 176–191, 2016.

[66]   C. A. Schneider, W. S. Rasband, and K. W. Eliceiri, "NIH ImageJ: 25 years of image analysis," *Nature methods*, vol. 9, no. 7. pp. 671–675, 2012.

[67]   D. H. Pashley *et al.*, "Collagen Degradation by Host-derived Enzymes during Aging," *J. Dent. Res.*, vol. 83, no. 3, pp. 216–221, 2004.

[68] S. Baliga, S. Muglikar, and R. Kale, "Salivary pH: A diagnostic biomarker," *J. Indian Soc. Periodontoly*, vol. 17, no. 4, pp. 461–465, 2013.

[69] C. K. Yeh, M. W. J. Dodds, P. Zuo, and D. A. Johnson, "A population-based study of salivary lysozyme concentrations and candidal counts," *Arch. Oral Biol.*, vol. 42, no. 1, pp. 25–31, 1997.

[70] A. Klimiuk, D. Waszkiel, A. Jankowska, and M. Choromańska, "The evaluation of lysozyme concentration and peroxidase activity in non - stimulated saliva of patients infected with HIV," *Adv. Med. Sci.*, vol. 51, no. Suppl. 1, pp. 6–8, 2006.

[71] T. Ito *et al.*, "Relationship Between Antimicrobial Protein Levels in Whole Saliva and Periodontitis," *J. Periodontol.*, vol. 79, no. 2, pp. 316–322, 2008.

[72] N. Rathnayake *et al.*, "Salivary biomarkers of oral health - A cross-sectional study," *J. Clin. Periodontol.*, vol. 40, no. 2, pp. 140–147, 2013.

[73] M. Molinos, V. Carvalho, D. M. Silva, and F. M. Gama, "Development of a hybrid dextrin hydrogel encapsulating dextrin nanogel as protein delivery system," *Biomacromolecules*, vol. 13, no. 2, pp. 517–527, 2012.

[74] P. Janmey and M. Schliwa, "Rheology," *Curr. Biol.*, vol. 18, no. 15, pp. 1–5, 2008.

[75] M. J. Moura, M. M. Figueiredo, and M. H. Gil, "Rheological study of genipin cross-linked chitosan hydrogels," *Biomacromolecules*, vol. 8, no. 12, pp. 3823–3829, 2007.

[76] M. Aliaghaie, H. Mirzadeh, E. Dashtimoghadam, and S. Taranejoo, "Investigation of gelation mechanism of an injectable hydrogel based on chitosan by rheological measurements for a drug delivery application," *Soft Matter*, vol. 8, no. 27, p. 7128, 2012.

[77] A. I. Malkin, Alexander Ya.; Isayev, *Rheology: Concepts, Methods and Applications*. 2012.

[78] "Flow Properties of Polymers." [Online]. Available: http://polymerdatabase.com/polymer physics/Viscosity2.html. [Accessed: 20-May-2018].

[79] M. S. Laranjeira, M. H. Fernandes, and F. J. Monteiro, "Innovative macroporous granules of nanostructured-hydroxyapatite agglomerates: Bioactivity and osteoblast-like cell behaviour," *J. Biomed. Mater. Res. - Part A*, vol. 95, no. 3 A, pp. 891–900, 2010.

[80] J. Kapuscinski, "DAPI: A DMA-Specific fluorescent probe," *Biotech. Histochem.*, vol. 70, no. 5, pp. 220–233, 1995.

[81] H. M. Dick, "Single domain antibodies.," *BMJ*, vol. 300, no. 6730, pp. 659–660, 1990.

[82] G. Sorftware, "GraphPad Prism." LA Jolla California, 2016.

[83] C. Ribeiro, V. Sencadas, C. M. Costa, J. L. Gómez Ribelles, and S. Lanceros-Méndez, "Tailoring the morphology and crystallinity of poly(L-lactide acid) electrospun membranes," *Sci. Technol. Adv. Mater.*, vol. 12, no. 1, p. 015001, 2011.

[84] B. Gupta, N. Revagade, and J. Hilborn, "Poly(lactic acid) fiber: An overview," *Prog. Polym. Sci.*, vol. 32, no. 4, pp. 455–482, 2007.

[85] J. F. Mano, "Thermal stability of side-chain polymer liquid crystals," *e-Polymers*, no. 77, pp. 1–11, 2004.

[86] F. Yao, Q. Wu, Y. Lei, W. Guo, and Y. Xu, "Thermal decomposition kinetics of natural fibers: Activation energy with dynamic thermogravimetric analysis," *Polym. Degrad. Stab.*, vol. 93, no. 1, pp. 90–98, 2008.

[87] J. F. Mano, D. Koniarova, and R. L. Reis, "Thermal properties of thermoplastic starch/synthetic polymer blends with potential biomedical applicability," *J. Mater. Sci. Mater. Med.*, vol. 14, no. 2, pp. 127–135, 2003.

[88] R. L. Blaine and H. E. Kissinger, "Homer Kissinger and the Kissinger equation," *Thermochim. Acta*, vol. 540, pp. 1–6, 2012.

[89] D. Santos, D. M. Silva, P. S. Gomes, M. H. Fernandes, J. D. Santos, and V. Sencadas, "Multifunctional PLLA-ceramic fibre membranes for bone regeneration applications," *J. Colloid Interface Sci.*, vol. 504, pp. 101–110, 2017.

[90] J. Cui *et al.*, "Preparation and characterization of chitosan/ß-GP membranes for guided bone regeneration," *J. Wuhan Univ. Technol. Mater. Sci. Ed.*, vol. 26, no. 2, pp. 241–245, 2011.

[91] A. C. Development, "ACD/Structure Elucidator." Toronto,ON,Canada, 2015.

[92] G. Socrates, *Infrared and Raman characteristic group frequencies*. 2004.

[93] B. Smith, *Infrared Spectral Interpretation: A Systemic Approach*. 1999.

[94] F. M. Goycoolea *et al.*, "Temperature and pH-sensitive chitosan hydrogels: DSC, rheological and swelling evidence of a volume phase transition," *Polym. Bull.*, vol. 58, no. 1, pp. 225–234, 2007.

[95] C. Lim, D. W. Lee, J. N. Israelachvili, Y. Jho, and D. S. Hwang, "Contact time- and pH-dependent adhesion and cohesion of low molecular weight chitosan coated surfaces," *Carbohydr. Polym.*, vol. 117, pp. 887–894, 2015.

[96] A. Altinisik and K. Yurdakoc, "Synthesis, Characterization, and Enzymatic Degradation of Chitosan/PEG Hydrogel Films," *J. Appl. Polym. Sci.*, vol. 122, pp. 1556–1563, 2011.

[97] A. Silva-Weiss, V. Bifani, M. Ihl, P. J. A. Sobral, and M. C. Gómez-Guillén, "Structural properties of films and rheology of film-forming solutions based on chitosan and chitosan-starch blend enriched with murta leaf extract," *Food Hydrocoll.*, vol. 31, no. 2, pp. 458–466, Jun. 2013.

[98] R. Ravichandran, J. R. Venugopal, S. Sundarrajan, S. Mukherjee, R. Sridhar, and S. Ramakrishna, "Composite poly-l-lactic acid/poly-(α,ß)-dl-aspartic acid/collagen nanofibrous scaffolds for dermal tissue regeneration," *Mater. Sci. Eng. C*, vol. 32, no. 6, pp. 1443–1451, 2012.

[99] W. Liao *et al.*, "In vitro human periodontal ligament-like tissue formation with porous poly-l-lactide matrix," *Mater. Sci. Eng. C*, vol. 33, no. 6, pp. 3273–3280, 2013.